DredgDikes

South Baltic Guideline for the

Application of Dredged Materials,
Coal Combustion Products and Geosynthetics
in Dike Construction

ANNEX II

Edited by:
Fokke Saathoff & Stefan Cantré
Universität Rostock, Chair of Geotechnics and Coastal Engineering
Zbigniew Sikora
Gdansk University of Tecnology, Dept. Geotechnics, Geology and Maritime Engineering

South Baltic Guideline for the

Application of Dredged Materials,
Coal Combustion Products and Geosynthetics
in Dike Construction

ANNEX II

Edited by:

Fokke Saathoff & Stefan Cantré
Universität Rostock, Chair of Geotechnics and Coastal Engineering

Zbigniew Sikora
Gdansk University of Technology, Dept. Geotechnics, Geology and Maritime Engineering

South Baltic Guideline for the Application of Dredged Materials, Coal Combustion Products and Geosynthetics in Dike Construction, Annex II

Authors

Dr hab. inż. Lech Bałachowski, prof. PG: 4.1, 4.2, 5.1, 6.3

Dr.-Ing. Stefan Cantré: 1.1 - 1.3, 1.5 - 1.9, 2.1, 2.2, 2.3, 2.5, 2.8, 7.1, 7.2, 7.3, 8

Dr hab. inż. Marcin Cudny: 4.1, 4.3, 6.2

Dr inż. Remigiusz Duszyński: 5.1

Dipl.-Ing. Anne-Katrin Große: 1.1 - 1.6, 7.1, 7.2, 8

Dr. Michael Henneberg: 2.6, 7.4

Dipl.-Ing. Ricarda Neumann: 2.6, 7.4

M.Sc. Elisabeth Nitschke: 2.3, 2.4

M.Sc. Jan Olschewski: 1.9, 2.2, 5.3

Dr inż. Rafal Ossowski: 4.1, 5.1, 5.2, 5.4, 6.1

Prof. Dr.-Ing. Fokke Saathoff: 1.9, 2.1, 2.2, 2.5

Prof. dr hab. inż. Zbigniew Sikora: 4.1, 5.1

CONTENTS

ANNEX II: SCIENTIFIC BACKGROUND

In this document, information is provided about the investigations performed in the DredgDikes project on which the recommendations in the guideline document are based. In particular, information about the geotechnical and hydraulic laboratory and field tests in Rostock and Gdansk, the environmental analysis and the modelling is provided.

1. LABORATORY ANALYSIS OF THE ROSTOCK DREDGED MATERIALS

In this chapter, the laboratory experiments with the dredged materials used in the Rostock investigations are presented. In the first paragraph, the results of the standard DM analysis are summarised. The focus of this chapter is the geotechnical analysis. In the following paragraphs information is provided for those standard laboratory tests that showed peculiarities when performed with fine-grained DMs rich in organic matter as well as additional special laboratory tests not included in the first paragraph.

1.1. Summary of the DM analysis in the DredgDikes project

In the beginning of the project different dredged materials (DMs) were chosen for investigation. For the test dike, the materials M1, M2 and M3 were chosen. They are all ripened DMs from the municipal DM processing plant in Rostock (spoil field Radelsee). While M1 and M2 are fine-grained DMs rich in organic content (ripened sludge), M3 is a mixed soil type material (Table AII.1, Table AII.2, Table AII.3). The main difference between M1 and M2 was the ripening time at the time of the first investigation in 20114: while M1 had been ripened for 5 years, M2 had been ripened for only two years. For retained samples, one lorry load was taken from heaps that were initially characterised as M1, M2 and M3 respectively. However, the characterisation of the materials after homogenisation showed that particularly the "new" materials M2 and M3 contained much more sand than the original samples (pre-investigation, during installation, etc.). Therefore, these retained samples were classified as M1-2, M2-2 and M3-2.

The material chosen for the pilot dike had been ripened on the spoil field Schnatermann of Rostock's municipal DM processing plant. It is indicated as S2 (Table AII.4) and similar to the materials M1 and M2.

The soil mechanical analysis includes the granulometry with different methods (DIN 18123, ISO 11277), Atterberg limits and derived plasticity parameters, proctor tests with different drying methods, the determination of the organic matter content using the TOC (total organic carbon), Loss on Ignition and the carbonate content, shear strength as determined with the laboratory (and field) vane shear tester as well as a direct shear box, the hydraulic conductivity as determined in a triaxial permeability cell with two different operation modes (standard and pressure controlled saturation), densities, oedometric parameters, water absorption (using different sample preparation methods), strength parameters as determined in the triaxial shear test and uniaxial compression tests. In addition to the soil mechanical properties, the geohydraulic properties (soil matrix potential) were determined for materials M1, M2, M3 and MB12 (Table AII.5).

Most of the geotechnical analyses were performed in the geotechnical laboratory of the Chair of Geotechnics and Coastal Engineering at Universität Rostock. The ISO 11277 granulometry and TOC determination were performed by LUFA Rostock, the triaxial shear tests were performed by the geotechnical laboratory of the Technical University of Hamburg-Harburg (Prof. Grabe), and the soil matrix potential was determined by the soil physical laboratory of the Chair of Soil Physics and Resource Protection, Universität Rostock (Prof. Lennartz).

The geochemical analysis of all materials was originally provided by the municipal DM processing plant of Rostock, where a certification system for the DMs demands regular quality control. During the project, the materials were analysed again by the Agricultural Analysis and Research Institute LUFA, Rostock as presented in Table AII.6.

Additionally, the mineralogy was analysed in the soil science laboratory of Universität Halle (Dr. Kühn) and the composition and structure of the organic matter in the materials was analysed in the soil science laboratory of the Chair of Soil Science, Universität Rostock (Prof. Leinweber).

Table AII.1. Laboratory analysis results for dredged material M1

Sample		M1	M1	M1	M1	M1-1	M1
Sample description		2011 RS	2012 Constr.	2012 BackS	2013 Dike	2013 Dike J/F	2014 BackS
Water content	%	61 - 68		58.8		82 - 88	64.6
Granulometry (ISO 11277)							
Sand	%	29 - 34	47			40	
Silt (< 0.063 mm)	%	41 - 44	32			55	
Clay (< 0.002 mm)	%	25 - 28	20			6	
Atterberg etc.							
Liquid limit LL	%	80 - 98		105.3		88.8	111.4
Plastic limit PL	%	75 - 81		74.2		48.8	75
Plasticity index PI	%	4 - 22		31.1		40	36.4
Consistency index IC (use LI!)	-	2 - 5		1.46		0.12	1.27
Liquidity index LI		(-1) - (-4)		-0.46		-0.12	-0.27
Activity A	-	0.15 - 0.88		1.11 - 1.25		6.67	1.35-1.45
Soil state		semi solid		semi solid		plastic	semi solid
Oversize grains (> 0.4 mm)	%	n/a	n/a	2.2	n/a	2.0	1.1
Corrected water content	%	n/a		60.1		84.0	65.3
Shrinkage limit SL	%	58					54 - 56
Shrinkage limit SL comp. from LL and PI	%	70 - 75		66		39	65
Volumetric shrinkage value Vs	%	33 - 35					42 - 43
Proctor test							
Optimal density OD (oven drying 55°C)	g/cm³	1.14 - 1.18				1.091	
Optimal water content wopt	%	40 - 43				45.1	
Optimal density OD (Air drying)	g/cm³	0.939				1.062	
Optimal water content wopt	%	45				46.8	
TOC	%	6 - 7					
Organic matter OM	%	10 - 11					
Loss on ignition LOI	**%**	13 - 14					
Carbonate / Lime	**%**	9 - 10					
Vane shear test cur	kPa	(53) - 132					
Direct shear test (box, 50,100,200 kN/m²)							
Density	g/cm³	1.46 - 1.47					
Dry density	g/cm³	0.85 - 0.90					
Angle of internal friction	°	28 - 30					
Cohesion	-	35 - 47					
Hydraulic conductivity k$_{10}$							
Uncontrolled saturation	m/s	3-5 E-09					
Associated water content	%	61 - 68					
Slow saturation with pressure control	m/s				4-6 E-08	2.6-3.1 E-09	
Associated water content	%				54.2	88.72	
Grain density, specific dens.	g/cm³	2.53 - 2.54					
Porosity n	-	0.65 - 0.66					
Void ratio e	-	1.83 - 1.98					
Oedometer test							
Water content w	%				63.9	78.8 - 88.5	
Max. settlement	mm				1.97	2.04 - 2.94	
Constrained modulus load removal	MN/m²				36.36	7.28 - 8.66	
Constrained modulus max load	MN/m²				3.65	1.14 - 1.32	
Constrained modulus max reloading	MN/m²				6.1	3.47 - 3.54	
Swelling index	-				0.007	0.034 - 0.042	
Creep index max loading	-				0.2315	0.7379 - 0.9004	
Creep index max reloading	-				0.3288	0.6468 - 0.6673	
Water absorption capacity DIN 18132 Enslin/Neff							
wA (oven drying 105°C)	%			87			
Definition	-			high			
wA (oven drying 60°C)	%			90			
Definition	-			high			

Sample description: 2011 RS: Sampling on spoil field Radelsee, material heaps, 2011. 2012 constr.: Sampling during the construction. 2012 BackS: Retained samples from 2012 (construction), full test range. 2013 dike: Samples taken from the test dike 2013 to complement the earlier tests. 2013 Dike J/F: Additional series with samples taken from the dike at the beginning of 2013. 2014 BackS: Re-evaluation of the first retained samples from 2012.

Table AII.2. Laboratory analysis results for dredged material M2

Sample		M2	M2	M2	M2	M2	M2	M2-1	M2
Sample description		2011 RS	2012 Constr.	2012 comp.	2012 comp.	2012 BackS	2013 Dike	2013 Dike J/F	2014 BackS
Water content	%	(55) - 73				38.9		42	68.62
Granulometry (DIN 18123)									
Sand	%			42.8	36.1				
Silt (< 0.063 mm)	%			57.2	60.2				
Clay (< 0.002 mm)	%			0	3.7				
Granulometry (ISO 11277)									
Sand	%	40 - 47	51				58	74	
Silt (< 0.063 mm)	%	32 - 38	28				26	16	
Clay (< 0.002 mm)	%	22 - 25	21				16	10	
Atterberg etc.									
Liquid limit LL	%	64 - 88				63.8		68.1	95.6
Plastic limit PL	%	54 - 67				43.6		37.4	59.6
Plasticity index PI	%	11 - 24				20.2		30.7	36
Consistency index IC (use LI!)	-	0.5 - 0.9				1.1		0.79	0.69
Liquidity index LI		0.5 - 0.1				-0.1		0.21	0.31
Activity A	-	0.44 - 1.09				0.80 - 0.91		3.07	1.45 - 1.60
Soil state		plastic				semi solid		plastic	plastic
Oversize grains (> 0.4 mm)	%					6.6		3.9	2.8
Corrected water content	%	n/a				41.6		43.8	70.6
Shrinkage limit SL	%	42 - 47						39 - 40	39 - 40
Shrinkage limit SL as com. from LL and PI	%	50 - 58				39		30	51
Volumetric shrinkage value Vs	%	23 - 30						39	40
Proctor test									
Optimal density OD (oven drying 55°C)	g/cm³	1.28 - 1.32		1.264	1.203			1.491	
Optimal water content wopt	%	32 - 35		34.3	34.8			24.9	
Optimal density OD (Air drying)	g/cm³	1.128						1.444	
Optimal water content wopt	%	39.5						26.6	
TOC	%	5 - 6							
Organic matter OM	%	9 - 10							
Loss on ignition LOI	%	12 - 14							
Carbonate / Lime	%	8							
Vane shear test cur	kPa	19 - 34							
Direct shear test (box, 50,100,200 kN/m²)									
Density	g/cm³	1.48 - (1.54)							
Dry density	g/cm³	0.87 - (0.97)							
Angle of internal friction	°	28 - 31							
Cohesion	-	13 - 19							
Hydraulic conductivity k$_{10}$									
Uncontrolled saturation	m/s	5-6 E-10							
Associated water content	%	(55) - 73							
Slow saturation with pressure control	m/s						7-8.5 E-10	3.6-4.0 E-09	
Associated water content	%						51	46.76	
Grain density, specific dens.	g/cm³	2.52 - 2.56							
Porosity n	-	0.62 - 0.66							
Void ratio e	-	1.62 - 1.94							
Oedometer test									
Water content w	%						60.038	42.3	
Max. settlement	mm						1.73	2.79	
Constrained modulus load removal	MN/m²						37.36	14.91	
Constrained modulus max load	MN/m²						2.01	1.93	
Constrained modulus max reloading	MN/m²						3.11	4.07	
Swelling index	-						0.007		
Creep index max loading	-						0.3978		
Creep index max reloading	-						0.5947		
Water absorption capacity DIN 18132 Enslin/Neff									
wA (oven drying 105°C)	%					68			
Definition	-					medium			
wA (oven drying 60°C)	%					66			
Definition	-					medium			

Sample description: 2011 RS: Sampling on spoil field Radelsee, material heaps, 2011. 2012 constr.: Sampling during the construction. 2012 comp.: repeated tests with the 2011 samples to compare the granulometry and verify proctor tests. 2012 BackS: Retained samples from 2012 (construction), full test range. 2013 dike: Samples taken from the test dike 2013 to complement the earlier tests. 2013 Dike J/F: Additional series with samples taken from the dike at the beginning of 2013. 2014 BackS: Re-evaluation of the first retained samples from 2012.

Table AII.3. Laboratory analysis results for dredged material M3

Sample		M3	M3	M3	M3	M3-1
Sample description		2011 RS	2012 Constr.	2012 BackS	2013 Dike	2013 Dike J/F
Water content	%	46		39		38
Granulometry (ISO 11277)						
Sand	%	54	73			79
Silt (< 0.063 mm)	%	31	17			11
Clay (< 0.002 mm)	%	15	10			9
Atterberg etc.						
Liquid limit LL	%	52 - 57		63		49
Plastic limit PL	%	49 - 54		45		38.9
Plasticity index PI	%	3 - 4		18		10.1
Consistency index IC (use LI!)	-	2 - 4		1.27		0.93
Liquidity index LI		(-1)-(-3)		-0.27		0.07
Activity A	-	0.25		1.2		1.11
Soil state		semi solid		semi solid		plastic
Oversize grains (> 0.4 mm)	%	n/a		3.3		4.17
Corrected water content	%	n/a		40.3		39.7
Shrinkage limit SL	%	50 - 51				
Shrinkage limit SL as comp. from LL and PI	%	48 - 52		40		36
Volumetric shrinkage value Vs	%	17.6				
Proctor test						
Optimal density OD (oven drying 55°C)	g/cm³	1.36				1.543
Optimal water content wopt	%	31				21.7
Optimal density OD (Air drying)	g/cm³	1.048				1.555 - 1.597
Optimal water content wopt	%	35.8				21.1 - 22.5
Optimal density OD (Air drying to w = 25%)	g/cm³	1.208				
Optimal water content wopt	%	38.2				
Optimal density OD (Air drying to SL<w<PL)	g/cm³					
Optimal water content wopt	%					
TOC	%	3				
Organic matter OM	%	6				
Loss on ignition LOI	%	9				
Carbonate / Lime	%	10				
Vane shear test cur	kPa	120				
Direct shear test (box. 50.100.200 kN/m²)						
Density	g/cm³	1.58				
Dry density	g/cm³	1.09				
Angle of internal friction	°	30				
Cohesion	-	59				
Hydraulic conductivity k$_{10}$						
Uncontrolled saturation	m/s	6E-09 - 1E-08				
Associated water content	%	46				
Slow saturation with pressure control	m/s				2E-09 - 2E-08	5.4-9.8 E-09
Associated water content	%				32.9	36.72
Grain density. specific dens.	g/cm³	2.59				
Porosity n	-	0.58				
Void ratio e	-	1.38				
Oedometer test						
Water content w	%					47.4
Max. settlement	mm					2.34 - 2.69
Constrained modulus load removal	MN/m²					17.67 - 35.64
Constrained modulus max load	MN/m²					1.9 - 2.87
Constrained modulus max reloading	MN/m²					5.53 - 5.68
Swelling index	-					0.012
Creep index max loading	-					0.3587
Creep index max reloading	-					0.283
Water absorption capacity DIN 18132 Enslin/Neff						
wA (oven drying 105°C)	%			67		
Definition	-			medium		
wA (oven drying 60°C)	%			68		
Definition	-			medium		
Triaxial shear test (UU)						
Angle of internal friction	°					25.1
Undrained cohesion	kN/m²					57

Sample description: see Table AII.1.

8

Table AII.4. Laboratory analysis results for dredged material S2 (incl. sub-batches S3 and S4)

Sample		S2-1	S2-2	S3-1	S4-1	S2	S2	S2	S2	S2
Sample description		2011 Pre	2011 Pre	2011 Pre	2011 Pre	2013 KB	2014-KB1	2014-KB2	2014-KB3	2009 Pre
Water content	%	44.01	50.18	50.77	42.13	53.3 - 62.1	76.43 - 77.91	63.63 - 72.99	71.49 - 71.55	72.4
Granulometry (DIN 18123)										
Sand	%	42.5	41.3	47	44.3					
Silt (< 0.063 mm)	%	55.3	55.1	53	55.7					
Clay (< 0.002 mm)	%	0	0	0	0					
Granulometry (ISO 11277)										
Sand	%	36.9	36.9	26.9	34		32	44	39	37
Silt (< 0.063 mm)	%	41.8	41.8	50.2	46		44	41	39	42
Clay (< 0.002 mm)	%	21.3	21.3	22.9	20		24	15	22	21
Atterberg etc.		without consideration of overgrain								
Liquid limit LL	%	72.9	73.9	69.9	66.9		112.1	91.3	102.8	
Plastic limit PL	%	68.9	66.6	65	62.2		69.8	59.6	72.7	
Plasticity index PI	%	4	7.3	4.9	4.7		42.3	31.7	30.1	
Consistency index IC (use LI!)	-	7.2	3.2	3.91	5.21		0.8	0.6	0.9	
Liquidity index LI		-6.2	-2.2	-2.91	-4.21		0.2	0.4	0.1	
Activity A	-	0.18	0.34	0.21	0.25		0.57	0.47	0.73	
Soil state		semi solid	semi solid	semi solid	semi solid		plastic	plastic	plastic	
Oversize grains (> 0.4 mm)	%	n/a	n/a	n/a	n/a		3.5	12.1	4.8	
Corrected water content	%	n/a	n/a	n/a	n/a		76.7	73.0	75.6	
Shrinkage limit SL	%	64.1	53.7	60.1	60.4		51.9	46.3	48.1	
Shrinkage limit SL as computed from LL and PI	%	68	65	64	61		59	52	65	
Volumetric shrinkage value Vs	%						46 - 48	41 - 43	45 - 46	
Proctor test										
							wmin = 45%	wmin = 30%		
Optimal density OD (oven drying 55°C)	g/cm³	1.095	1.128	1.153	1.135		1.062	1.212		
Optimal water content wopt	%	43.1	40.2	38.7	41.5		50.6	39.9		
							wmin = 40%			
Optimal density OD (Air drying to w = 25%)	g/cm³						1.134			
Optimal water content wopt	%						44.5			
TOC	%	5.6	5.6	5.8	5.7		4.36	4.12	4.23	5.63
Organic matter OM	%	9.65	9.65	10	9.83		7.52	7.1	7.29	9.7
Loss on ignition LOI	%	11	11	9.8	9.9		11.1	9.6	10.3	
Carbonate / Lime	%	1.4	1.7	1.8	1.7		2	2.4	1.1	3.6
Vane shear test cur	kPa	51.4 - 66.6		80.7 - 120.7	34.5 - 38.2		28 - 33	17 - 23	23 - 24	
Water content w (cur)	%									
Direct shear test (box. 50.100.200 kN/m²)										
Density	g/cm³	1.463			1.501	1.47 - 1.54		1.49		
Dry density	g/cm³	0.99			1.043	0.94 - 1.0		0.87		
Angle of internal friction	°	31.27			32.64	39.88		30.24		
Cohesion	-	51.18			65.4	9.87		18.91		
Hydraulic conductivity k₁₀										
Uncontrolled saturation	m/s	6E-9		7E-8	1E-7					
Slow saturation with pressure control	m/s						2.50E-09	1.20E-09	2E-9	
Grain density. specific dens.	g/cm³	2.504	2.552	2.534	2.502					
Porosity n	-	0.605			0.583					
Void ratio e	-	1.53			1.4					
Oedometer test										
Max. settlement	mm						2.84		2.41	3.08
Constrained modulus max load	MN/m²						3.61		3.08	3.33

Sample description: Pre: pre-investigation from 2009 or 2011. KB: Samples taken from the material heap on the construction site for the pilot dike at the Körkwitzer Bach 2013 and 2014.

Table AII.5. Soil matrix potential for M1, M2, M3 and MB12

		M1	M2	M3	MB12/13
Sample description		Test Dike	Test Dike	Test Dike	PreInv
Soil matrix potential etc.					
effective field moisture capacity	vol %	31.09	37.51	19.29	41.6
permanent wilting point	vol %	31.58	15.15	23.89	10.8
Porosity n (pv)	vol %	68.3	59.03	50.99	56.5
Dry density	g/cm³	0.84	1.09	1.3	1.15
field moisture capacity FK pf 1.8	vol %	62.68	52.66	43.18	52.4
Air capacity	vol %	5.63	6.37	7.81	4.1

Sample description: Test Dike: Undisturbed samples taken directly from the test dike. PreInv: Pre-investigation from 2009.

Table AII.6. Geochemical characterisation of DMs M1, M2, M3 – solids and eluates [1]

Parameters	Unit	Solids			Unit	Eluates		
Materials		M1	M2	M3		M1	M2	M3
pH value	[-log]	7.4 - 7.7	7.5 - 7.8	6.9 - 7.3				
CaCO3	%	6.2 - 10.0	6.0 - 7.4	5.3 - 8.7				
TOC	%	5.0 - 6.2	4.7 - 6.0	2.2 - 3.2				
Salt contentration	%	1.8 - 2.2	1.5 - 1.7	1.2 - 1.8				
Phosphor	mg/100g	0.8 - 1.1	1.4 - 2.1	1.4 - 2.2				
Nmin	mg/100g	1.4 - 3.2	1.6 - 3.5	0.5 - 1.0				
Lead	mg/kg	36	19	23	µg/l	2.3	< 2	1.6
Cadmium	mg/kg	0.9	0.4	0.6	µg/l	0.1	< 0.2	n.n
Chromium	mg/kg	20	16	13	µg/l	2.3	< 1	0.6
Copper	mg/kg	36	23	22	µg/l	14.7	6.8	9.9
Nickel	mg/kg	14	13	9.5	µg/l	6.4	< 2	4.7
Mercury	mg/kg	0.6	0.3	0.4	µg/l	n.n	< 0.2	n.n
Zinc	mg/kg	179	130	112	µg/l	11	37	4
Arsenic	mg/kg	9	10	6	µg/l	0.7	< 2	0.5
Hydrocarbon	mg/kg	379	115	206				
PAH	mg/kg	1.5	0.9	1.4				
PCB	mg/kg	0.03	0.02	0.01				
El. Conductivity					µS/cm	3930	3340	3300
Chloride					mg/l	404	230	270
Sulfate					mg/l	2162	1600	2036
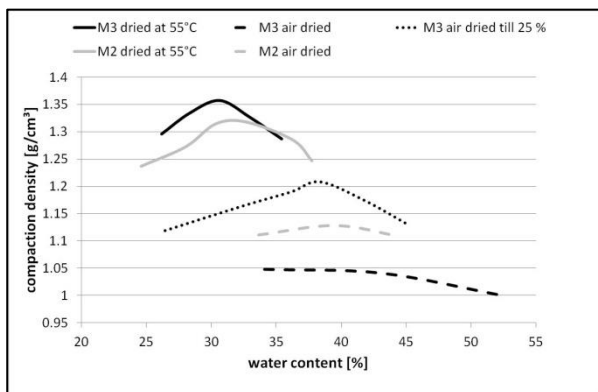
Figure AII.1. Variation of the Proctor comp. test [2]

1.2.   Proctor tests with DM

A comprehensive analysis was performed in the proctor compaction test regarding the drying temperature and drying mode, based on the specification of the German DIN standard, in which a drying process below 60°C for fine-grained and organic soils is demanded. Moreover, the soil has to be dried to a water content between PL and SL. Because of initial problems in determining PL and SL comparable with the difficulties in the proctor test (materials were mostly too wet after the drying to SL), investigations with various drying temperatures (55°C-20°C) and drying modes (full oven drying, full or partial air drying) were examined. The investigations aimed at

determining a general procedure for the proctor test for fine-grained organic dredged material.

Selected results of the proctor compaction tests are presented in Figure AII.1. The figure shows considerable differences between the drying methods. A lower optimal density OD together with a higher optimum water content w_{opt} could be observed with full air drying compared to oven-drying while both w_{opt} and OD for the partial air drying down to of w = 25 % showed values in between.

1.3.   Disintegration tests to determine the erodibility of DMs

To investigate the soil structure stability under static loading, the disintegration tests after Endell [3] and Weißmann [4] were performed for M1, M2, M3, marl and marsh clay. In both tests, cylindrical, Proctor compacted samples with different water contents are placed into a wire mesh basket fixed to an electric scale. During the test, both basket and sample are submerged in water. Due to water immersion the sample starts to crumble, soil particles fall through the basket to the bottom of the water basin and the weight reduction is recorded continuously. A detailed description of the tests, their boundary conditions and their differences are presented in [5].

In the Endell [3] test, the disintegration number $Z(t)$ is determined for every subsample. To compare different materials with different water contents, $Z(8)$ after 8 hrs is used. All samples started to crumble quickly; within $\approx 1,000$ s most of the samples lost 50-70 % of their initial weight. For the rest of the investigation, the residual weight remained more or less constant. The lowest $Z(8)$ value was observed for the samples with natural water content w_n (Table AII.7).

In the test after Weißmann [4], the disintegration time for a liquidity index of $LI = 0.2$ is used to determine the erosion resistance. For each sample the disintegration time t_{30} (time to lose 30 % weight) is determined (with $t_{30} = 24$ h if max. weight loss < 30 %). The function $t_{30,w} = f(w)$ is plotted for three test water contents (oven-dried, w_{opt} and wet). Weißmann proposed an exponential dependency of w and t_{30}. Since the method could not provide repeatable results for the DMs using w_{opt}, replacement samples were prepared with w_n. The results were different to those from the Endell test. The oven-dry samples showed an increase in weight instead of a loss, although soil crumbling was observed, while the wet samples started to crumble after ≈ 3 hrs. with a maximum weight reduction of less than 30 %. The w_n samples showed the largest weight reduction (Table AII.7). In none of the investigations a dependency between w and t_{30} could be determined; consequently, $t_{30,w}$ at $LI = 0.2$ could not be computed for any of the samples. Therefore, t_{30} for w_n was chosen for comparison, in spite of the large variation of w_n among the materials (Table AII.1).

M2 performed best in both tests, followed by M1 (Weißmann test) resp. M3 (Endell test). All DMs bet the marl (larger sand fraction) and showed a lower disintegration resistance than the marsh clay (Table AII.7). The

Table AII.7. Results of disintegration tests with natural water content w_n samples and of the wet sieving method

Parameter	Z(8) at w_n [%]	Ø t_{30} at w_n [s]	As [%]
M1	0.5728	1,320 & 1,600	87.66
M2	0.4714	2,600 & 4,000	87.78
M3	0.5425	1,120	-
Marl	0.6836	482	1.62
Marsh clay	0.2589	60,098	26.09
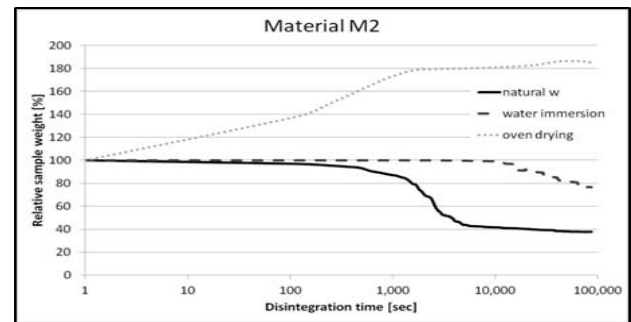
Figure AII.2. Disintegration curves from the Weißmann test

comparison of w_n samples is not fully significant because it only represents a temporary condition of the materials.

In most of the test runs, agglomerates that had already fallen off the sample were caught inside the basket since they exceeded the size of the mesh openings. Also, at the end of each test a cone of soil particles remained in the basket. The choice of mesh size is both important and difficult, since the samples need a stable foundation and at the same time the crumbling agglomerates need to pass through. This is subject for future investigations.

1.4. Aggregate stability

To determine the aggregate stability against water stress, the wet sieving method [6] was performed, in which the stability of air-dried soil aggregates with a size of 1-2 mm is tested. The dry aggregates are put into a sieve diving apparatus with de-ionized water to be moved up and down for 5 min. Instable aggregates crush in the water and fall through the sieve. The weight of the aggregates left on the sieve is determined before they are crushed using a sodium-diphosphate dilution to determine the stable aggregates during a second sieving. Then, the aggregate stability As is computed (Table AII.7).

The results show only minor differences between the DMs which consist of nearly 88 % stable aggregates. The conventional dike cover materials showed considerably lower aggregate stability. This may be explained by the high contents of OM and lime in the DMs, which have a stabilising effect on aggregates [7], with roots and fungal hyphae forming macro-aggregates [8] or hydrophobic properties of clay-humus-complexes in the soil [9].

The small range of analysed aggregates is the major drawback of the wet sieving test. A larger range of aggregate sizes would be preferable.

1.5.　Mineralogy

The mineralogy of the DMs was investigated in the soil science laboratory of the University of Halle, Germany. Materials M1, M2, M3 and S2 were analysed as well as a dredged material from the island of Rugia and a marsh clay from Hamburg for comparison. In a first series in 2013 the mineral composition of the whole samples was determined using x-ray powder diffraction. This showed a very similar composition of all Rostock DMs. In a second series in 2014 the clay (finest) fraction of the samples was separately investigated again in the x-ray powder diffractometer. The main clay minerals of all Rostock DMs were Kaolinite and Illite, with smaller contents of Chlorite and Muscovite. These clay minerals have a low potential of shrinkage and swelling and also a low cation exchange capacity compared to Smektites and Vermikulites.

1.6.　Organic structure analysis

Initially, the difference in undrained shear strength of materials M1 and M2 was extremely distinct, despite their similar grain-size distribution and contents in organic matter and carbonate (see Table AII.1 and Table AII.2). The reason was assumed to be the different types of organic matter in the materials. Therefore, samples of both materials were analysed in the pyrolysis-field ionization mass spectrometer (Py-FIMS) at the University of Rostock's soil science laboratory.

As a result, the main difference between M1 and M2 is that M2 contains more stable carbon compounds, which is a sign for increased hydrophobicity, which was also seen in the disintegration tests where M2 showed lower disintegration numbers than M1. However, the large initial difference in shear strength cannot really be explained with the organic structure. Most possibly the difference was caused by a different consistency state of M2 that was not detected initially because of the problematic determination of Atterberg limits with the materials.

1.7.　Triaxial permeability tests

All tests to determine the hydraulic conductivity (water permeability) of the fine-grained dredged materials were performed in triaxial permeability cells according to DIN 18130-1 [10] under isotropic stress conditions, since the saturation pressure was determined to be generally much more than 50 kPa, which would be possible to achieve in a falling head apparatus in the laboratory (5 m of water). However, some of the investigated DMs showed an influence of the mode of saturation because they are generally compressible due to the contained organic matter. This may lead to a compaction due to the cell pressure when the pore water pressure distribution is not well distributed inside the sample because the trapped air voids are compressible. Therefore, the saturation process should be pressure controlled and a so-called B test should be performed in analogy to triaxial compression tests. The saturation pressure needs to be increased in very small steps and after each step the pressure increase is checked with a pressure gauge on both sides of the sample. This ensures a more reliable result of hydraulic conductivity if there is a fear of compressibility of the materials.

1.8.　Determination of Atterberg limits

Initially, the Atterberg limits of all materials were determined without removing the 5-10 % oversize particles (d > 0.4 mm) contained in the DMs. The brittle effects were so distinct that the roll-out test could not be performed correctly. For samples where a 3 mm thread could be produced, the resulting "plastic limit" was comparably high, leading to a low plasticity index PI. However, since the materials all possess a considerable sand fraction and agglomerates, the idea of this trial was to receive values that are more viable to the real behaviour of the materials. The percussion cup tests are said to be influenced by grains d > 0.4 mm due to friction effects (cf. [11]); however, this could not be confirmed in the tests.

Due to the drawbacks with the thread-rolling method regarding the higher sand fraction, the fall-cone method was chosen as an alternative. There is a long tradition of the fall-cone method to determine the liquid limit (LL) of soils in the UK and in Sweden which became a constituent part of the European standardisation (ISO/TS 17892-12 [12]). On the other hand there has been an international scientific discussion about the applicability of the fall-cone test to determine the plastic limit (PL) for the past 60 years, and the idea seems to have revived during the past decade. The PLs of DMs have been analysed

with this method before (e.g. [13]) and the promising results and good agreement with the standard method were the reasons to use this method in the DredgDikes project as well. For comparison and to analyse the different methods, the tests were also performed after removal of oversize grains.

Critics of the fall-cone method state, that there was neither a justification for the assumption of a 100 kPa strength factor between PL and LL nor a definite strength value for the LLs of all soils [14], [15]. There seems to be a dependency of the actual LL value and the strength at LL, together with additional factors such as clay mineralogy, organic structure, and lime content, while their role remains unidentified [16]. Finally, different authors state that the Casagrande and fall-cone tests are completely different in their mechanical behaviour: While the thread-rolling test determines the brittle behaviour, the fall-cone test specifies the frictional strength at low water contents, and there is no indication that these values correlate in any respect [17]; [15].

Supporters of the fall-cone method claim, that there is a sufficiently good agreement between the results of the LL determined with the fall-cone and percussion cup tests and even between the results of the PL determined with the fall-cone and thread rolling tests, regardless of the theoretical background and the strength and water content hypotheses (e.g. [18]).

To determine the PL from the fall-cone data, different hypotheses about the dependency of water content w and penetration depth d_p are available:

- $f(w; \log(d_p))$ = linear [19]
- $f(\log(w); \log(d_p))$ = linear [18]
- extrapolation from LL to PL using the log-log-linear relationship for $d_p > 4$ mm to determine PI from the inclination m [18]
- $f(w; SR(d_p))$ = linear [20]

In the present study, the values determined with the fall-cone and Casagrande methods correlate well in the samples where the oversize particles (d > 0.4 mm) were removed prior to testing. The agreement was generally above $R^2 = 0.9$. However, the data sets show good agreement regardless of the w-d hypothesis used to determine PL, with the square-root (SR) approach showing the lowest agreement level. The differences between the evaluation methods were small and not

generally explicit. The average best fit among all materials was derived with the linear w-log(d_p) assumption. All results were derived from approx. 12-20 single data points between $d_p = 1.8$ and $d_p = 25$ mm. Selecting a random variation of 4 data points and using the log-log-linear extrapolation from 4 evenly distributed values between $d_p = 4$ mm and $d_p > 20$ mm as suggested by [18] does not work equally well among the investigated materials. The variations of PL are minor for marsh clay and M2-2 while they grow to 10 percent points for M1-2 and S2; using more data points, including those close to $d_p = 2$ mm considerably levels this variability.

The influence of oversize grains was also studied. During the sieving needed to remove oversize grains some of the larger agglomerates, which are very stable, may be removed together with the sand, although they may have an influence on the plastic behaviour of the DMs. To save time with sample preparation and to have the agglomerates included, PL may be determined with the fall-cone method with oversize grains up to 10 % included. The results show only minor differences of PL and LL (exception: S2).

1.9. Small-scale flume experiments

In preparation for the large-scale overflowing field experiments on the Rostock research dike, small-scaled tests were carried out in the laboratories of the Chair of Geotechnics and Coastal Engineering, Universität Rostock. For this a laboratory flume was designed and constructed (Figure AII.3). Aims of the laboratory experiments were to preselect a suitable DM with the highest resistance against erosion, and to find and test different methods for measuring erosion of unvegetated and vegetated soils. The laboratory flume was developed with reference to boundary conditions of the Rostock research dike. Thus, the variable slope was set to 1V:3H for all experiments. Furthermore, four different DMs were used as samples for the experiments, three of which (materials M1 - M3) were also used for the research dike. Both vegetated and unvegetated samples were prepared. Also, samples both with and without an erosion control geomat (GMA) were used. The GMA was installed approximately 2 cm beneath the soil surface. The soil mechanical characterisation is summarised in Table AII.1, Table AII.2 and Table AII.3.

Figure AII.3. Laboratory flume, sample boxes in the front

Figure AII.4. Experimental set-up with laser scanner [21]

1.9.1. Test set-up and measurement techniques

The basic structure of the construction consists of a turbulence tank and the actual flume. It has a width of 0.27 m and an effective length of 2.75 m with a variable slope. The water delivery system includes a basin, a pump, a pipe and the turbulence tank (Figure AII.3, Figure AII.4). The discharge can be regulated with a pipe valve. The maximum possible discharge is about 95 m³h⁻¹ resp. 380 m³h⁻¹m⁻¹ (26 ls⁻¹ resp. 106 ls⁻¹m⁻¹). The flow conditions are usually supercritical.

To determine the soil loss for the whole sample with a pin profiler, the flume is separated lengthwise in ten test sections, each with a size of 0.27 m × 0.27 m.

The flow velocity is measured at several points of the flume with a propeller flow meter. The discharge depth is determined with an ultrasonic sensor at the top of the flume and measured with a scale at each flume test section. The soil surface is measured before and after each flow event to determine the amount of soil loss. Different methods were tested in the course of the test series: (i) determining the surface geometry with a laser scanner, (ii) optical recording of the soil surface by hand and with photos, and (iii) measuring of the soil surface with a pin-profiler.

1.9.2. Test procedure and analysis

Regardless of the way to determine the amount of soil loss, the test procedure is always the same. After installation of a soil sample (Figure AII.5), the initial soil surface geometry has to be measured with one of the mentioned methods (laser scanning, optical recording by hand, pin-profiling). Then the first level of overflowing starts including measuring the discharge depth and flow velocity. Between two overflowing levels and after the last one the soil surface geometry has to be measured again.
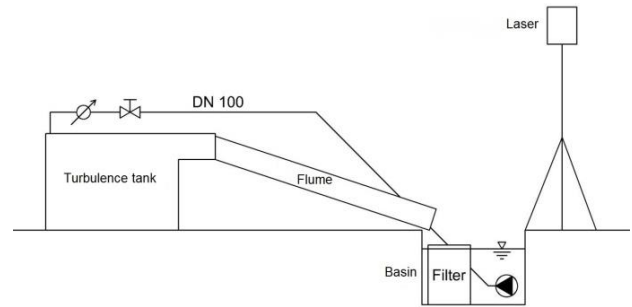
Figure AII.5. Installed samples, unvegetaded (l) and vegetated (r)

For the unvegetated samples, the soil surface has to be scanned before and after each flow event to generate 3D-models of the sample to be able to determine the amount of soil loss with the laser scanning method. The first scan is the reference scan. With the following scans the soil loss can be calculated by computing the difference volume. To describe the amount of soil loss the erosion rate E is defined as follows:

$$E = \frac{V_E}{W} \qquad (1)$$

where V_E = eroded soil volume, W = volume of water.

To determine the amount of erosion with a pin-profiler, the relative height of the slope soil surface is measured in each test section at three points vertical to the flow direction before and after each test. The difference between both values indicates the amount of soil loss (or even soil gain in case of swelling or sedimentation effects).

For each test (unvegetated or vegetated), the minimum discharge has to be chosen. The following tables show the mean minimum and maximum discharge rates and the dependent variables for both unvegetated and vegetated samples (Table AII.8).

The test evaluation includes the calculation of the effective discharges (Q resp. q), the shear stress (τ), and the soil loss resp. soil gain per test-section (SL) and cumulated for the whole flume (CSL).

Table AII.8. Mean unit discharges (q) for unvegetated and vegetated samples, measured and computed hydraulic values (flow velocity (v), discharge depth (h), shear stress (τ)), Froude and Reynolds numbers

	Ø q [ls⁻¹m⁻¹]	Ø v [ms⁻¹]	Ø h [m]	Ø τ [Pa]	Fr[1] [-]	Re[2] [-]
unvegetated						
min	0.3	n.m. [3]	n.m. [3]	n.c. [3]	n.c. [3]	n.c. [3]
max	26	1.4	0.024	80	2.89	19,932
vegetated						
min	0.65	0.07	0.01	32.7	0.22	392
max	106	2.8	0.06	200	3.65	83,804

[1] $Fr < 1$: subcritical, $Fr > 1$: supercritical
[2] $Re \leq 2320$: laminar, $Re \geq 2320$: turbulent
[3] not measurable / not computable

Figure AII.6. Erosion rates of dredged materials (M1-M3) and clay [23]

Figure AII.7. Downstream erosion above the geomat (GMA), originate at a crosswise crack (M2, December 2013)

Figure AII.8. Cumulated soil loss vs. shear stress, single significant case of erosion from the lab tests, vegetated samples (M2, Dec. 2013)

1.9.3. Typical results and evaluation

A total of 44 test series with a total of 127 single overflowing tests were carried out between May 2012 and Oct. 2013. Due to the large amount of data, only typical results are presented here. More information can be found in [21], [22].

For unvegetated soil samples the laser scanning method worked well. The soil loss volume was measured using the laser scanner. From this data, the erosion rates were computed for the different dredged materials and for a reference marsh clay. Figure AII.6 shows the erosion rates for the tested unvegetated soils.

In the laboratory flume experiments material M2 (both with and without GMA) shows results with the best erosion stability among the DMs. The erosion rates of M1 and M3 were up to five times higher. The lowest erosion rate showed was measured with the conventional dike cover material, the marsh clay from Hamburg.

The pin-profiler was used exclusively for vegetated samples. Due to the quite low pump performance no significant erosion was observed in almost non experiment. In the course of installation some cracks occurred crosswise in length direction. Only in these areas a significant amount of soil eroded downstream (Figure AII.7).

Figure AII.8 shows the soil loss versus the hydraulic shear stress. The initial shear stress was between 60 Pa and 80 Pa and the mean maximum soil loss was $CSL \approx 0.019$ m. The mean hydraulic parameters were $\varnothing\,q \approx 64$ ls⁻¹m⁻¹, $\varnothing\,v \approx 2.37$ ms⁻¹, $\varnothing\,\tau \approx 110$ Pa.

2. EXPERIMENTS ON THE GERMAN FULL-SCALE RESEARCH DIKE

2.1. The Rostock research dike

The large-scale research dike in Rostock consists of two parallel dikes (west and east) which are connected with earth dams to form a three-polder system (Figure AII.9). The polders can be filled with water separately for hydraulic loading. There are ten different dike cross-sections, all separated by mineral sealing material to prevent seepage water to spread between the sections. Most of the sections have been realised twice, on the eastern and the western dike respectively.

The water level inside the polders can be regulated to make water flow over the lowered crest areas. The base of the construction is sealed by a geosynthetic clay liner for a defined hydraulic boundary condition to make sure that seepage water only drains on the respective inner slopes. Five different DMs (mainly M1, M2, M3) and four geosynthetic solutions have been installed in the German test dike.

Three general types of cross-sections were realised: The dikes of polder 1 consist of a sand core covered with a layer of fine-grained dredged material with a thickness of 1.5 m on the outer (water side) slope and 1.0 m on the inner (land side) slope and a slope inclination of V1:H2. In polder 2 slopes with an inclination of V1:H3 are realised. The cross-sections consist of a sand core covered with a layer of fine-grained dredged material of 1.0 m thickness. Cross-section H in polder 3 is a homogenous dike made from M3 with a higher sand fraction (Table AII.3).

To reduce shrinkage cracking in the dike cover layer, a geosynthetic reinforcement product was considered in surface parallel layers. Since the tensile stresses at crack development are assumed to be very low compared to the tensile strength of geosynthetic materials and the

friction between soil and reinforcement material needs to be high even for very small displacements, a geosynthetic erosion control grid (Huesker Fortrac 3D) was used. Without reinforcement large cracks were expected that may reach the sand core. With reinforcement installed, a larger number of smaller cracks were expected, not exceeding the reinforcement (Figure AII.10A).

To strengthen the surface of the greened slopes against erosion from wave attack or overflowing / overtopping events, a rolled erosion control product RECP (Colbond Enkamat) was installed on several cross-sections (C, E, F in Figure AII.9), covered by up to 5 cm of DM before greening. The grid was also used as surface erosion control solution on one of the steep cross-sections. The initial idea was that without RECP considerable erosion may occur, particularly in bare or partly vegetated state, while with RECP the surface would be protected (Figure AII.10B).

In the homogenous cross-sections H, innovative drainage solutions using a geosynthetic drainage composite (Colbond Enkadrain) were installed to control the phreatic line inside the dike body. Without installed drainage composite seepage water may soak the whole cross-section, coming out anywhere on the inner slope. With drainage composite, the seepage line should drop to the drainage layer and come out at a defined line along the slope or dike toe (Figure AII.10C).

Table AII.9. Research dike - cross-sections and materials

Section	A	B	C	D	E	F	G	H
Material	M1	M2	M2	M2	M2	M1	M1	M3
RECP	No	no	EW	no	W	W	no	no
Geogrid	no	no	no	no	E	E	no	no
Drainage composite	(W)	(W)	(W)	(W)	(W)	(W)	(W)	EW
Slope (V:H)	1:2	1:2	1:2	1:3	1:3	1:3	1:3	1:2

East: Infiltration and seepage measurement

West: Overflowing experiments
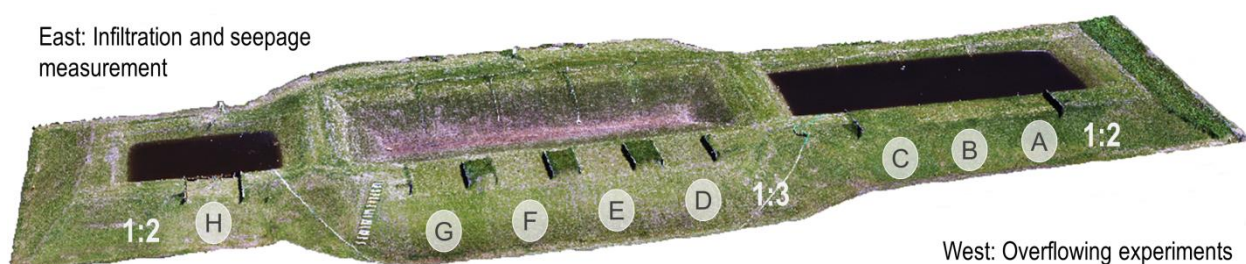
Figure AII.9. Rostock research dike, west view [24].
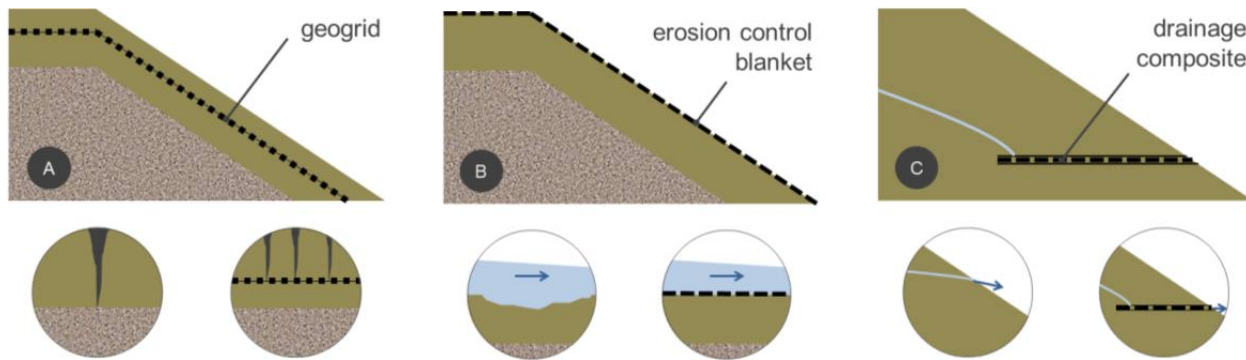
Figure AII.10. Schematic cross-sections: A. Sand core & geogrid reinforced dredged material cover. Without geogrid large cracks. With geogrid more smaller cracks not exceeding the geogrid. B. Sand core & erosion protected dredged material cover. Without erosion control blanket - surface erosion due to overflowing. With erosion control no erosion is expected. C. Homogenous dike with geosynthetic drainage composite. Without composite seepage may occur on the inner slope. With composite defined drainage.

2.2. Overflowing tests

Figure AII.11 schematically illustrates the research dike including all areas relevant for the overflowing experiments. A compilation of information about the sections used for the overflowing tests is given in Table AII.10.

The Rostock experiments were planned resembling a test series of the US National Transportation Product Evaluation Program (NTPEP) [25]. In this programme, a variety of erosion control products have been tested with focus on maximum acceptable shear stresses and flow rates. The overflowing experiments of NTPEP follow the standard ASTM D-6460 [26]. The basic set-up of these experiments consists of three parallel flumes with 40 ft. (~12.2 m) in length and 2 ft. (~0.6 m) in width, installed on a slope. For the flow and erosion measurements a 20 ft. (~6.1 m) long section in the middle of each flume is considered. The slope inclination is 10 % for unvegetated and 20 % for vegetated samples respectively.

Three test series can be performed simultaneously and a high discharge can be realised with reasonable pumping equipment by using only one of the flumes. Each single test is carried out with four levels of discharge with at least one to reach the proposed critical amount of soil loss of 0.5 in. (~1.27 cm) averaged over the entire flume surface. The 20 ft. test section is separated into ten sections. Before and after each flow event, the relative height of the soil surface is measured in each section and a cumulative soil loss index CLS (cf. Paragraph 1.9.2) is determined for each flume. All data is recorded and then analysed focusing on the determination of a critical flow velocity and a critical shear stress.
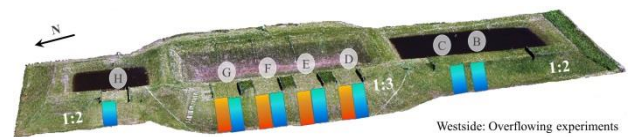
Figure AII.11. Overflowing sections of the 2013 (blue) and 2014 (orange) experiments

Table AII.10. Information about the cross-sections used for overflowing

Section	B	C	D	E	F	G	H
Material	M2	M2	M2	M2	M1	M1	M3
RECP	no	EW	no	W	W	no	no
Slope (V:H)	1:2	1:2	1:3	1:3	1:3	1:3	1:2
Length [m]	6.0	6.0	7.8	7.8	7.8	7.8	5.4
No. test sections*	10	10	13	13	13	13	9
No. short term tests	10	11	23	27	22	25	10
No. 6h-tests	-	1	1	1	-	-	1
No. long-term tests	-	-	2	2	3	2	-

* No. of test sections resp. measuring areas each flume is divided into

2.2.1. Test set-up and measurement techniques

Based on the NTPEP [25] test set-up three parallel flume channels have been installed on each of the slope sections on the research dike. Figure AII.12 shows the basic experimental set-up. Each flume had an inner width of 0.6 m. Depending on the slope inclination a specific length and number of test sections was determined (Table AII.10). The flumes were made out of single walls and each of these was fixed with steel profiles and construction foam into the slope surface. Additional stability was reached with horizontal slats on the top of the walls connecting the three flumes. These wooden slats also served as markings for the single test sections.

Figure AII.12. Basic experimental set-up of the flume system

Figure AII.13. Two pumps deliver water into the polders

Figure AII.14. Filled polder 3, cross-section H

Figure AII.15. Closed water inlets at cross-section H

Figure AII.16. Runoff channel to lead the water back to the basin

The water inlets and the permanent instrumentation for discharge control were placed on the crest. The water delivery system included a basin, two pumps (Figure AII.13), pipes, the dike polders (Figure AII.14), water inlets (Figure AII.15) and a runoff channel (Figure AII.16).

The discharge for the overflowing experiments was regulated on the dike crest with steel shutters. Depending on the water table inside the polders and the opening width of the shutter, a target discharge could be adjusted. During the first test series, the peak discharge was realised with two pumps delivering up to 700 m^3h^{-1}. In 2014 two different pumps were used, delivering a maximum discharge of up to 1300 m^3h^{-1}.

Both the flow velocity and the runoff depth were determined during the experiments. The flow velocity was measured using a permanently installed magnetic-inductive sensor on the dike crest (Figure AII.17) while a mobile inductive sensor was used on the slopes. The run-off depth was measured using ultrasonic sensors on the dike crest (Figure AII.17) and with a ruler on the slopes.

The erosion on the slope surface is determined with a pin-profiler (Figure AII.18). For this, the relative height of the slope soil surface is measured before and after each

Figure AII.17. Ultrasonic sensor to measure runoff depth (left), magnetic-inductive sensor to measure flow velocity (right)

Figure AII.18. Pin profiler to measure the soil loss/ gain and the discharge depth

flow event. The difference between both values indicates the amount of soil loss resp. soil gain. Therefore, the soil surface height is measured at five points in each test section vertical to the flow direction.

Photos of each test section were made before and after each test stage to compare the slope surface conditions, e.g. the vegetation coverage [27].

In addition, the moisture content and the water saturation of the top layer material was determined with TDR-sensors and tensiometers in a depth of 10, 20 and 30 cm below the outer two flumes (Figure AII.19).

Figure AII.19. TDR-sensors and tensiometers under the flumes

Table AII.11. Mean unit discharges (q), measured and computed hydraulic values (flow velocity (v), discharge depth (h), shear stress (τ)), Froude and Reynolds numbers on the dike embankment, September 2013, Stages 3-5 = long-term

Stage	Ø q [ls⁻¹m⁻¹]	Ø v [ms⁻¹]	Ø h [m]	Ø τ [Pa]	Fr[1] [-]	Re[2] [-]
1	60	1.75	0.053	210	2.43	69,203
2	80	2.26	0.060	240	2.95	99,208
3	120	2.62	0.071	260	3.14	132,061
4/5	200	3.28	0.095	340	3.40	207,773

[1] *Fr* < 1: subcritical, *Fr* > 1: supercritical
[2] *Re* ≤ 2320: laminar, *Re* ≥ 2320: turbulent

Table AII.12. Mean unit discharges (q), measured and computed hydraulic values (flow velocity (v), discharge depth (h), shear stress (τ)), Froude and Reynolds numbers on the dike, May 2014

Stage	Ø q [ls⁻¹m⁻¹]	Ø v [ms⁻¹]	Ø h [m]	Ø τ [Pa]	Fr[1] [-]	Re[2] [-]
1	125	2.24	0.057	187	2.99	94,902
2	215	2.97	0.075	245	3.46	156,442
3	264	3.30	0.083	270	3.67	188,000
4	366	3.65	0.105	341	3.60	248,050
5	507	4.32	0.123	402	3.93	330,718
6	553	4.46	0.130	426	3.94	356,067
Long	319	3.67	0.090	295	3.91	223,147

[1] *Fr* < 1: subcritical, *Fr* > 1: supercritical
[2] *Re* ≤ 2320: laminar, *Re* ≥ 2320: turbulent

2.2.2. Test procedure and analysis

Each experiment follows the same procedure:

- Prepare flumes and measuring equipment,
- Record the initial state of the embankment (pin-profiling, photographic and written documentation),
- Increase the discharge slowly by opening the shutter within approximately five minutes to minimise the shock load on soil surface and vegetation,
- 45 minutes overflow with the target discharge,
- Measure the flow velocity and discharge depth in every test section of each flume and on the dike crest,
- Close the shutters and drain the residual water,
- Record the final state of the dike embankment incl. pin-profiling and both photographic and written documentation (initial state for the subsequent flow level or final recording for the whole test series) and
- Transfer of all measured data to a test record sheet.

The "long-term" overflowing tests were performed in a similar way, except that only one or two of the three flumes were used and during the overflowing the amount of erosion was recorded twice during short interruptions.

The target discharges had to be chosen before the start of the test series. The limiting factors are the performance of the pumps and the sizes of both the polder and the reservoir basin. Table AII.11 and Table AII.12 contain compilations of the mean discharge rates and the dependent variables measured and computed for the tests in Sept. 2013 and May 2014 respectively.

The test record sheets have to be analysed after finishing the field experiments. Several values need to be calculated or recalculated to control the target values: (i) soil loss per test section and cumulated for the whole flume, (ii) discharge, (iii) shear stress, and (iv) roughness.

2.2.3. Typical results and evaluation

33 large-scale field test series on 7 dike cross-sections with a total of 141 single overflowing tests were carried out in Sept. 2013 and May 2014, including 128 short-term and 13 long-term tests. Due to the large amount of data, only typical results are presented here. The following tables show the final results of all short-term (2013: Table AII.13; 2014: Table AII.14), 6-hour (Table AII.15) and long-term (Table AII.16) overflowing experiments.

Table AII.13. Summary of max. cumulative soil loss (CSL) and max. hydraulic forces, short-term tests series Sept. 2013

	Max. CSL [cm]	Max. q [ls⁻¹m⁻¹]	Max. v [ms⁻¹]	Max. h [m]	Max. τ [Pa]
B	0.5	180	3.47	0.085	416
C	0	228	3.79	0.095	464
D	0.5	279	3.66	0.101	329
E	0.9	235	3.61	0.110	358
F	0.4	253	3.58	0.094	308
G	0	194	3.46	0.095	311
H	0.2	270	3.48	0.124	606

Table AII.14. Summary of max. cumulative soil loss (CSL) and max. hydraulic forces, short-term tests series May 2014

	Max. CSL [cm]	Max. q [ls⁻¹m⁻¹]	Max. v [ms⁻¹]	Max. h [m]	Max. τ [Pa]
D	0,062	492,25	4,18	0,129	420
E	0,542	542,94	4,40	0,129	421
F	0,097	512,70	4,38	0,122	398
G	0,314	595,90	4,63	0,137	447

Table AII.15. Summary of max. cumulative soil loss (CSL) and max. hydraulic forces (unit discharge (q), flow velocity (v), discharge depth (h), shear stress (τ)), 6h test series, Sept. 2013

	Δt [h]	Max. CSL [cm]	q [ls⁻¹m⁻¹]	v [ms⁻¹]	h [m]	τ [Pa]
C	6	0	190	3.12	0.070	349
D	6	0.5	226	2.80	0.081	264
E	6	1.2	129	2.83	0.076	248
H	6	0	214	2.97	0.070	344

Table AII.16. Summary of max. cumulative soil loss (CSL) and max. hydraulic forces (unit discharge (q), flow velocity (v), discharge depth (h), shear stress (τ)), long-term test series May 2014

	Δt [h]	Max. CSL [cm]	q [ls⁻¹m⁻¹]	v [ms⁻¹]	h [m]	τ [Pa]
D	22,5	0,011	348,95	3,78	0,097	319,99
E	20	0,280	323,88	3,67	0,091	296,82
F	18	0,108	351,50	3,93	0,093	303,10
G	20	0,000	325,35	3,82	0,088	286,75

The soil loss rate was compared with the shear stress τ (Figure AII.20, Figure AII.22) and the flow velocity v (Figure AII.21, Figure AII.23) for each test series. In 2013 the highest amount of soil loss was measured on cross-section E with material M2 and an erosion control product (RECP). On F (same configuration apart from M1) only a small to medium amount of soil loss was determined, just as on D and G. The 2014 results show almost similar

trends: the highest amount of soil loss was determined on cross-section E, however, the total value was lower than in 2013 while the maximum discharge was larger.

The 2013 experiments (Figure AII.20) show the start of erosion at $\tau \approx 200$ Pa for E and F with material M2 and M1, with installed RECP and a slope inclination of 1V:3H. On D with M2 and without RECP the initiation of soil loss was determined at $\tau \approx 280$ Pa. No soil loss could be measured on G with M1 and without RECP. Equivalently, the flow velocities were determined at which erosion starts: For E and F the value is around v = 2.0 ms⁻¹ and for cross-section D around v = 2.6 ms⁻¹ (cf. Figure AII.21).

The experiments which were carried out in May 2014 showed comparable results regarding initial shear stress and flow velocity. The soil loss starts at lower values of the hydraulic parameters ($\tau \approx 170$ Pa, v ≈ 1.8 ms⁻¹), but the total amount of cumulated soil loss is also lower (Figure AII.22 and Figure AII.23).
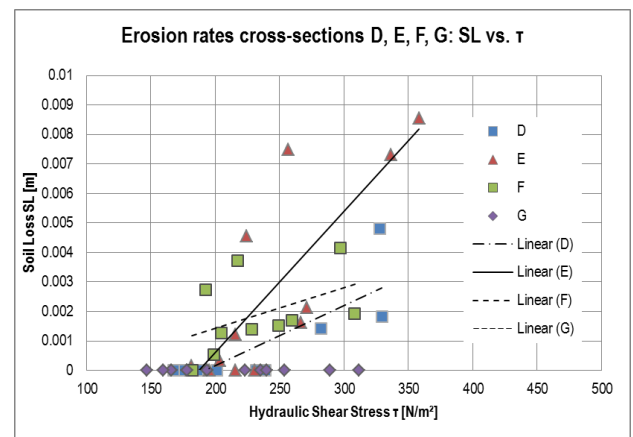
Figure AII.20. Erosion rates in cross-sections D, E, F, G Sept. 2013; the steeper the trend line the higher the erosion rate.
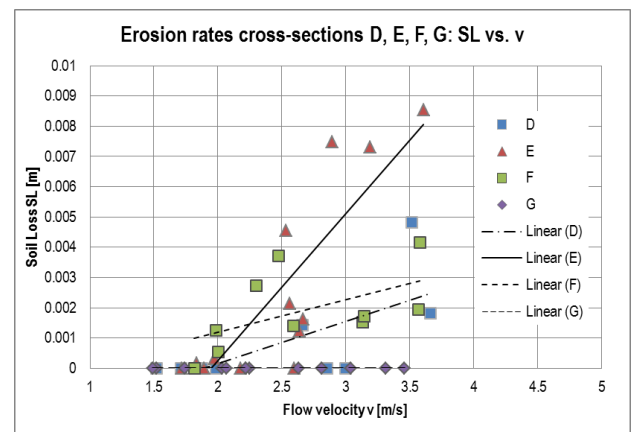
Figure AII.21. Erosion rates in cross-sections D, E, F, G, Sept. 2013; the steeper the trend line the higher the erosion rate.

In all experiments only very low values of cumulated soil loss CLS were determined. None of the results is in the range of the critical soil loss of 1.27 cm as recommended in [26]. The comparably high values of soil loss in cross-section E may be explained by increased erosion in the lower test-sections of the flumes, where soil and vegetation eroded (slid) on top of the installed RECP, where too much uncompacted soil was used to cover it.

Due to the relatively broad distribution of the measurement results, it was not possible to define a "best fit" trend line through the data points. Therefore a linear trend line was chosen for all charts to define the cross-section specific soil loss functions. The slope of the trend line stands for the erosion rate (relationship between soil loss and hydraulic load): the steeper the trend line, the higher is the erosion rate.

In the 6 hour experiments in 2013 section E showed the largest CSL = 0.012 m, while the other sections showed mean CSL-values between 0.005 m (D) and 0.000 m (C and H) after six hours of overflowing. The above explanation applies for the larger soil loss value on E (Figure AII.24). In May 2014, also very low CSL values were determined (Table AII.16).

The moisture and suction pressure measurements underneath the flumes showed that after 15-30 min. the DM was fully saturated down to a depth of at least 20 cm.

In the course of the large-scale field experiments and with respect to all boundary conditions of the Rostock research dike (properties of the DMs and geosynthetics, slope inclination, vegetation, and discharge values) no major erosion failure was caused by the overflowing tests performed on the Rostock research dike.

Cross-section E with a slope inclination of 1V:3H and an installed RECP showed the largest amount of cumulated soil loss (CSL = 0.009 m, 2013 and CSL = 0.0054 m, 2014) after the short-term tests. However, even this value is comparably low. Possible reasons for the larger erosion on E may be explained by insufficient compaction of the soil surface on top of the RECP, a lower interlocking between soil particles and RECP, or a weak connection between plant roots and RECP, among others. All other cross-sections showed CSL-values between 0.005 m and 0.000 m after the experiments.

It should be noted, that all results of the soil loss values are averages of the individual test sections in each flume.
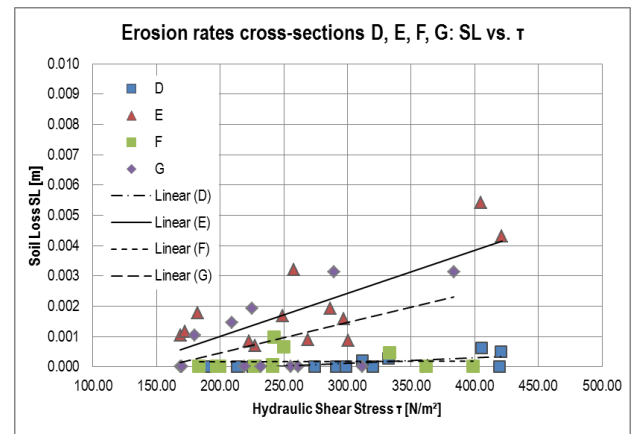
Figure AII.22. Erosion rates in cross-sections D, E, F, G May 2014; the steeper the trend line the higher the erosion rate.
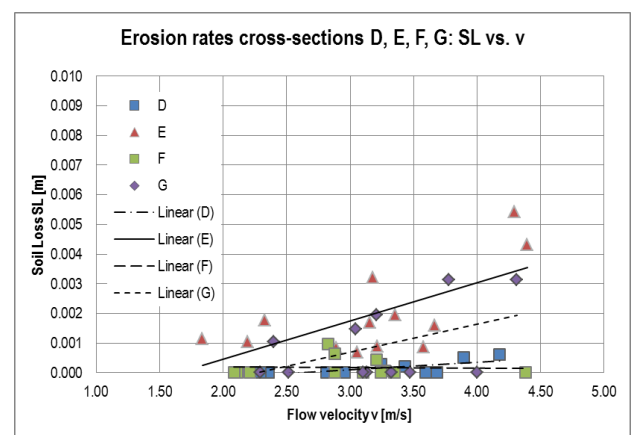
Figure AII.23. Erosion rates in cross-sections D, E, F, G May 2014; the steeper the trend line the higher the erosion rate.
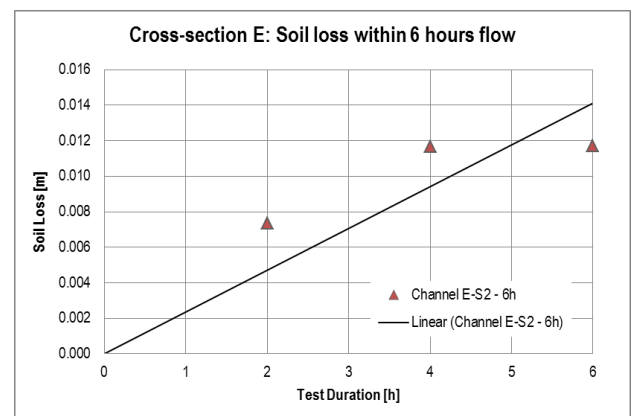
Figure AII.24. Soil loss on cross-section E – 6 h test, Sept. 2013

For example, on E a maximum soil loss SL = 2.0 – 2.4 cm occurred in at least six of the seven lower test sections of the single flumes. Considering the long-term tests on E, soil loss between 2.1 cm and 2.9 cm occurred in test-sections seven to ten.

As yet there are no recommendations for a critical amount of soil loss on a slope regarding overflowing events, except in [26]. All measured amounts of soil loss

of the first DredgDikes overflowing tests are far below the critical values recommended in [26] (CSL = 1.27 cm), although the overflowing discharge of approximately $q = 200$ ls^{-1}m^{-1} (2013) and $q = 550$ ls^{-1}m^{-1} (2014) is much larger than the design discharges e.g. given in [28]. At least four discharge levels are needed to get closer to the critical values of shear stress or flow velocity and the dependent value of CSL step by step.

In the future it should be discussed, whether the definition of soil loss (SL and CSL) is an adequate definition to describe the damage or failure of a dike embankment or the grass cover. An assessment using categories to describe the conditions of grass covers may rather need to be established, e.g. using the categories initial damage, various damage locations, failure and non-failure after testing as in [29]. This method was applied successfully during the Gdansk overflowing experiments in September 2014 (cf. Paragraph 5.3).

There were also difficulties in determining the various hydraulic parameters such as the discharge depth on the dike slope. The determination of the discharge depth in long laminar conditions is generally unproblematic; however, in the test conditions on the dike slopes the flow conditions were highly turbulent with a lot of air entrainment (Figure AII.25). Then it is difficult to decide about the exact water level and how it can be measured accurately. Electronic aids such as ultrasonic sensors usually fail here. The measurement of the flow velocity is equally problematic when it comes to finding the exact point to measure the mean flow velocity. The accuracy of the measurements of discharge depth and flow velocity, however, is basis for the subsequent computations of the effective shear stress and the determination of the critical flow parameters.

Figure AII.25. Turbulent flow conditions in with air entrainment in the lower parts of the flume

It should be noted that the overflowing experiments do not serve as a substitute for overtopping experiments, since wave load may mobilise higher hydraulic loads. However, the particularly high discharge with highly turbulent flow still shows the good performance of the tested DMs, also with respect to loads by wave run-up and overflowing.

2.3.   Infiltration and seepage tests

Infiltration and seepage tests were performed in the DredgDikes project to analyse the performance of the installed DMs regarding the amount and quality of the seepage. In the following, the setup of the tests and the results regarding the seepage line measurements and the measurements of the amount of seepage exiting the dike toe are summarised.

To find a reasonable measurement set up the first results of the laboratory analysis were used to simulate seepage through the constructed dike sections. The water permeability was the decisive parameter for the modelling. Since the permeability in a full-scale construction may be considerably higher than the determined values in the laboratory, the seepage simulations were also performed with a permeability coefficient of ca. 2 orders of magnitude higher than the lab values, to lay out the sensor placement.

The measurement setup was mainly installed at the eastern side of the polder system during and after the construction in the summer of 2012. The instrumentation was installed in the centre of each 8 m wide section. The set-up of the measurement devices was almost similar in each section, with two standpipes on the crest, a tip counter at the toe of the inner slope (only B to G), generally three moisture sensors type EC5 (only in D there are five), one Theta Probe FDR moisture probe at the toe of the outer slope, and five tensiometers on the outer slope (Figure AII.26). This instrumentation setup should account for a theoretical seepage line that enters the sand core somewhere close to the bottom.

The standpipes were installed both on the eastern and the western dike for comparison. Only the western standpipes on the eastern (seepage) dike (EW in Figure AII.26) that are near to the outer slope are equipped with an electronic piezometer to log the seepage water table while on side the water level inside the other standpipes
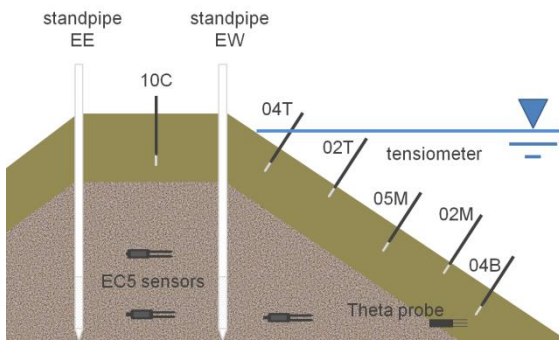
Figure AII.26. Schematic view of an instrumented cross-section.

(EE, WW, WE) was manually measured with an electric contact gauge. These simple set up ensures the comparison between the eastern side and the western side.

Two different kinds of sensors based on frequency domain reflectometry (FDR) are used to measure the moisture in the sand core and the cover layer. Both sensors are recording mV signals and were calibrated in the laboratory to be able to compute the volumetric water content from the mV signals. The EH20-EC5 (EC5) sensors are comparably small and low-cost and were installed during the construction works of the research dike inside the sand core. When a sand layer of 0.5 m thickness was installed and compacted, a 0.4 m deep hole was dug and the EC5 sensor was installed at the bottom of the hole. The cavity was then closed, using the excavated sand, and compacted by hand. Afterwards, the construction machinery was able to move on the sand core without causing any damages to the sensors. The second type of FDR sensors used are Theta Probes from DeltaT which were installed after completion of the construction in the cover material at the toe of the outer slope.

To collect and record the volume of the seepage water tipping counters were installed at each toe of the inner slopes of sections B-G (east) after completion of the research dike. Therefore, a system of drainage pipes was installed during the construction to collect the seepage water ca. 1 m inside the dike core and leading it out of the dike through PVC pipes at the inner dike toe.

Tensiometers (UGT TENSIO 152) were installed for the long-term monitoring of the dike cover materials. The sensors were used to measure both excess water pressure and suction pressure of the DM (-30 kPa to 100 kPa). In every section tensiometers were installed vertically to the slope in a depth of 0.4 m (three sensors)

and in the depth of 0.2 m (two sensors, Figure AII.26). The tensiometers were referred to according to their position in the dike slope (B=bottom, M=middle, T=top, C=crest). The number in the nomenclature indicates the installation depth (02 = 0.2 m depth, 04 = 0.4 m depth, 10 = 1.0 m depth). To work with a closed system for the analysis, the geosynthetic clay liner underneath the construction is defined as the reference plane. All sensors were surveyed with a tachymeter to define the relative level above this plane. Each polder is equipped with a data logger which can be accessed by a network computer. During the filling experiments, the recording interval for all sensors was set to 1 min. to log the min., max. and average values every 15 min.

2.3.1. Evaluation by the percent bias method

Different approaches are known to evaluate the results of simulated data [30], [31]. "The slope and y-intercept of the best-fit regression line can indicate how well simulated data match measured data" ([30] p. 887). The approach of using a function fitting with a high coefficient of determination (R^2) is also commonly used. The value describes the degree of colinearity between simulated and measured data [30].

The percent bias (PBIAS) method, on the other hand, is a tool to compute the deviation of computer generated data (sim) of the actually measured values (obs) [30]. A value of 0.0 describes perfect agreement between measured and simulated data. If the model is underestimated the PBIAS indicates positive values while negative values indicate model overestimation. PBIAS values can be calculated with equation 2.

$$PBIAS = \frac{\sum_{i=1}^{n}(Y_i^{obs} - Y_i^{sim}) * 100}{\sum_{i=1}^{n}(Y_i^{obs})} \quad (2)$$

In this paper, the PBIAS method was not used to compare between simulated and observed data but to compare the measured data of different cross-sections. Positive PBIAS values indicate that the first mentioned section tends to be more permeable than the second section which it is compared with. At first, materials M1 and M2 are compared by using equation 3.

$$PBIAS = \frac{\sum_{i=1}^{n}(Y_i^{M2} - Y_i^{M1}) * 100}{\sum_{i=1}^{n}(Y_i^{M2})} \quad (3)$$

To detect differences between the sections with and without a geosynthetic solution equation 4 was used. In this case sections with the same material but with different cross-sections were compared.

$$PBIAS = \frac{\sum_{i=1}^{n}(Y_i{}^{without} - Y_i{}^{with}) * 100}{\sum_{i=1}^{n}(Y_i{}^{without})} \quad (4)$$

2.3.2. Filling tests in 2013 (F1 toF4)

In polder 2, three filling experiments were performed in 2013. The filling of the polder during overflowing experiments was defined as the fourth (long-term) test. In polder 1, only the first two experiments were performed as filling tests while filling 3 and 4 were performed during the overflowing experiments (cf. above). The general process for the experiments was to fill a polder in approx. one to three days. Afterwards, the water level was kept on the same level (+/- 0.1 m) for seven days. The polder was emptied within a few hours. The first filling experiments were realised using a pump with a maximum discharge of 70 m³/h. Because of different positions of the pump on the test site and the resulting differences in hydraulic resistance, the times to fill the polders varied.
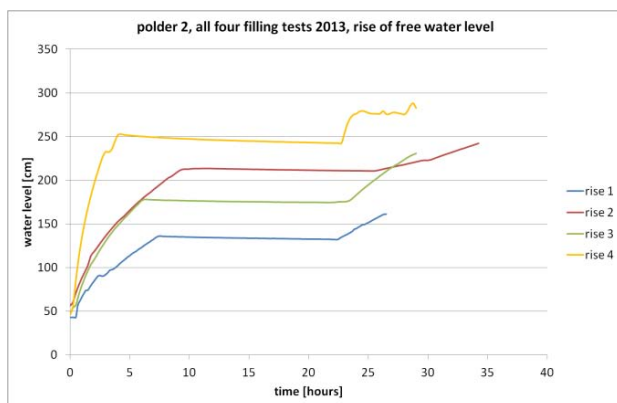
Figure AII.27 Polder 2 - all filling tests 2013 - rise of free water level.
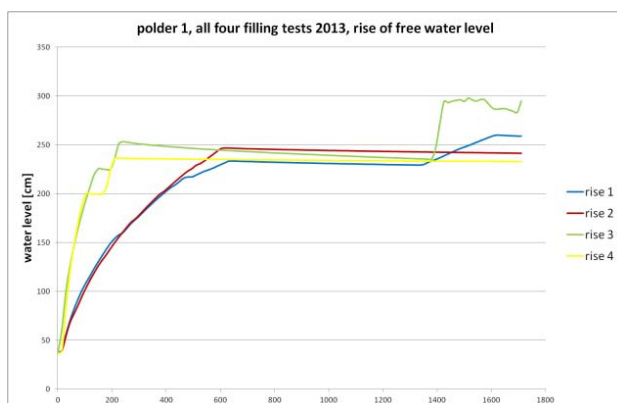
Figure AII.28 Polder 1 - all filling tests 2013 - rise of free water level.
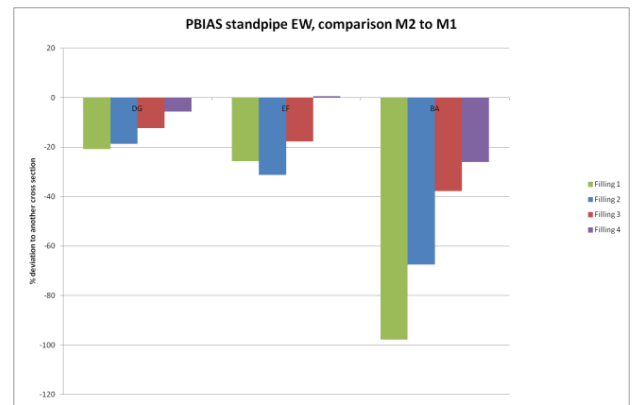
Figure AII.29. PBIAS standpipe EW, comparison M2 to M1
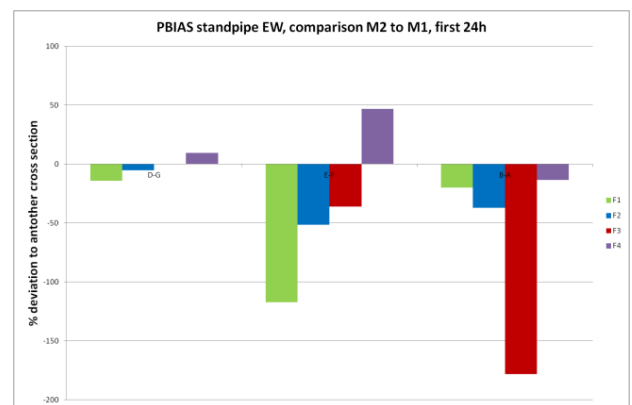
Figure AII.30. PBIAS standpipe EW, comparison M2 to M1, 24 h

For the overflowing tests, two pumps with a maximum discharge of 350 m³/h each were used. This allowed to fill the polder within three hours. This can be seen in the hydrographs in Figure AII.27and Figure AII.28.

To compare the materials and designs of the cross-sections, the PBIAS was used. Two different time periods of the filling experiments were used. At first, the whole filling test was regarded. Secondly, the first 24 hours of each filling test was analysed.

Material M2 (D, E, B) was compared with M1 (G, F, A) from both polder 2 (DG; EF) and polder 1 (BA). During the first filling test a deviation of about -20% occurred between the two materials in the first two examples (DG: without geogrid and EF: with geogrid). This deviation decreases in general with further filling tests (Figure AII.29). The comparison of materials in polder 1 (BA) resulted in a huge difference of nearly -100 %, however, significantly decreasing with further filling tests.

The same computation was performed for the first 24 hours of the filling tests (Figure AII.30). During the first filling tests in 2013 the deviations were in the range of +/-15 % between the two materials for the cross-sections without geogrid (DG). The deviations between the same

24

materials but with geogrid installed in the cover layer (EF) were larger than -100% during the first test, reducing (and finally changing the sign during the following three filling tests. The comparison of section B (M2) with A (M1) resulted in even larger differences of over -150 % during the third filling test while the deviations were in the range of -25 % for all other tests.

Figure AII.31 shows the comparison of the same materials in different cross-sections. It compares cross-sections with a geosynthetic solution (E; F; C) with cross sections without a geogrid or erosion control product (D; G; B). A geogrid is installed in section E and F and an RECP in section C. Sections D/E and B/C are built from M2, sections G/F with M1. The thickness of the cover layer is 1 m in polder 2 (DE; GF) and 1.5 m in polder1 (BC). The deviations between cross-sections with and without geogrid are very small (DE and GF).

The erosion control product, on the other hand, showed a significant influence during the first three experiments, however, without the possibility to define a trend. The deviations vary from 15 % to 400 %.
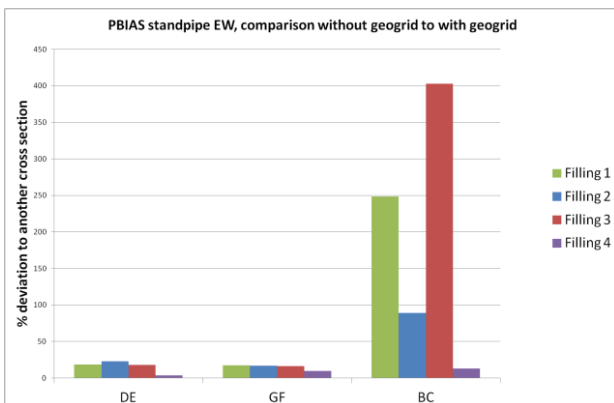
Figure AII.31 PBIAS - standpipe EW - comparison without/with geosynthetic solution.
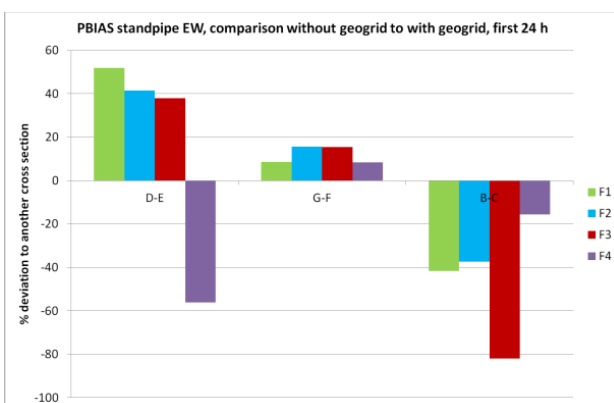
Figure AII.32. PBIAS standpipe EW, comparison of sections with and without geogrid reinforcement
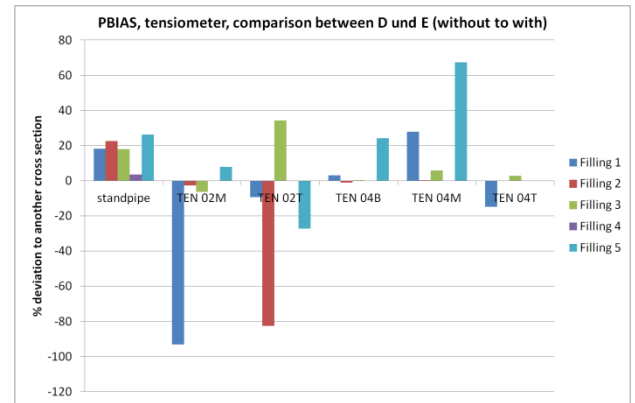
Figure AII.33. PBIAS tensiometers, comparison between D and E (without / with geosynthetic system)

Regarding the first 24 hours of a filling tests the deviation between the cross sections D and E vary from +50 % during the first test to -50 % in the fourth experiment. The comparisons between sections G and F show continuous deviations of 10 – 15 %. A deviation up to -80 % was computed during the third filling test comparing sections B and C (Figure AII.32).

Basically, it becomes obvious, that the computed differences highly depend on the chosen time interval. However, most of the differences that were computed with the PBIAS method are considerably below 50 %. Therefore, the different materials behave quite similar and the impact of the different geosynthetics solutions cannot clearly be defined.

Finally, the tensiometer data was compared using the PBIAS equation. Figure AII.33 shows an example for the comparison of sections D and E. The first five bars represent the standpipe results. The PBIAS deviation based on the standpipe values is around +20 % for all three filling tests. The following five bar charts (five bars each) show the results of the PBIAS computations based on the tensiometer data. There is no uniform trend for single tensiometers for different filling experiments and no trend for the PBIAS deviation for the five different tensiometers in the same filling test. The results are more or less scattered. Therefore, the tensiometer values were not used for the further PBIAS evaluation.

The PBIAS evaluation of M1 and M2 shows that the permeability of M2 is lower than that of, no matter whether a geogrid was used or not. The largest deviation was observed comparing sections A and B with the thicker cover layer. This may lead to the assumption that material differences are much more significant if the

cover layer is thicker. Impacts on the material like cracks, mouse holes and macro pores may have a larger influence on the upper 1 m of the dike cover. In deeper layers, the permeability may not be influenced as much by these impacts.

The analysis of the water permeability based on the measured data showed it to be higher than assumed for the initial modelling based on the laboratory values (see above). The tensiometer data showed considerable deviations in the tests which may be caused by aggregation processes, cracks and mouse holes in the upper 0.4 m of the cover layer where the tensiometers were installed. Hence, the tensiometer installation in the first 0.5 meters gave no representative results.

Therefore, the set up was changed in spring 2014 (Figure AII.34). The tensiometers were installed deeper inside of the cover layer to account for the quicker infiltration. At the locations D, 05 and PF two tensiometers were installed respectively for backup reasons in a horizontal distance of about 0.1 m along the dike axis.

The EC5 moisture sensors were originally planned to help detect the seepage line inside the dike core. However, due to settlements and the quick infiltration of the dike core, the sensors show the value "wet" most of the time, thus not really adding information to be analysed, and they were discarded. The free logger slots were used to install additional tensiometers. As the GCL seals the testing area against the underground, the dike toe of the outer slope dries very slowly. In the previous measurement set up the Theta Probe was installed 0.1 m above the GCL, also leading to a permanent "wet" signal. Therefore the moisture sensor is now installed in the upper third of the outer slope for in situ pF determination.

2.3.3. Filling tests in 2014 (F5 to F7/F8)

In 2014 three filling tests were performed in each polder. This time the filling process was set to fill a polder within 12 hours following a (quasi)linear hydrograph. Therefore, the polders were filled with approximately 0.1 m in a half hour. The water level was kept on the same level (+/- 0.15 m) for approx. ten days and emptied within a few hours (ground outlets completely opened).

This procedure was performed to be able to better compare the sections. Polders 1 and 2 have the same crest height while polder 3 is lower. To compare the cross-sections, the measurement set up was installed in the slope percentage to the height of the dike. All water level measurement data were corrected using this adjustment.

To compare the materials or designs of the cross-sections, the PBIAS was used. Materials M1 to M3 were compared as were cross-sections with the same materials, but different layout. For this experiment period the data evaluation was performed for the first 24 h of each filling test. The main differences are between the material M3 and the other two materials (up to -80 %).
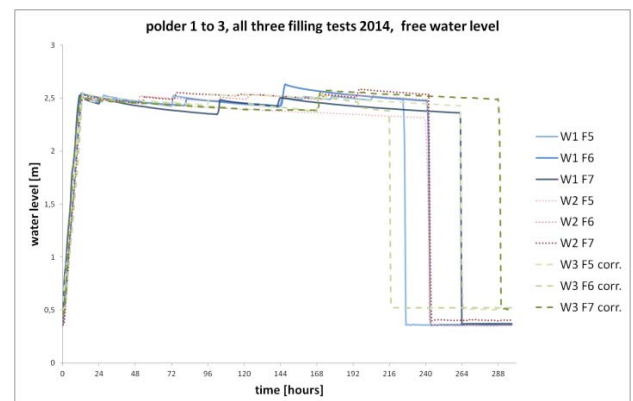
Figure AII.35 All polders, all filling tests 2014 - free water level.

Figure AII.34 Redesigned measurement set up 2014.
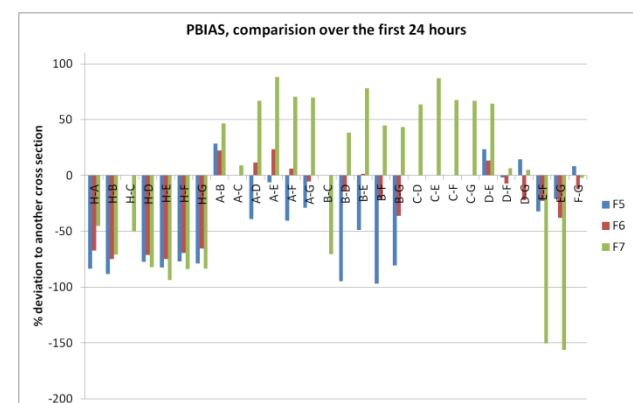
Figure AII.36. PBIAS, comparison of all sections, 24 h
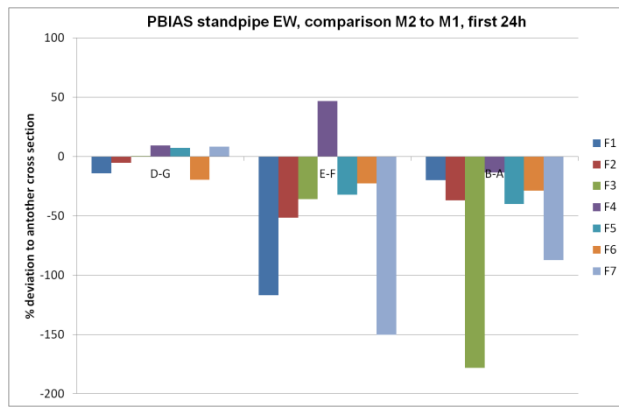
Figure AII.37. PBIAS standpipe EW, comparison M2 to M1, 24 h

The results of M1 and M2 are shown in Figure AII.37. Cross-sections D (M2) and G (M1) show less than 20 % deviation. Both cross-sections are built without geogrid. Sections E (M2) and F (M1) are built with a geogrid; the deviations vary between +50 % and -150 %. During the first four filling tests the derivation decreased and changed the sign, while looking at all seven tests it seems that there is just a large variation and there may be some outliers, such as tests 1, 4, 7. However, due to the small number of tests, this cannot be verified. The deviation between the cross section B (M2) and section A (M1) shows less than 50 %, except in filling tests 3 and 7.

Finally, the water levels inside the standpipes were analysed 150 hours after the start of the filling tests. In polder 2 all four cross-sections show the same tendency of generally decreasing water tables for each subsequent test. Polder 1 on the other hand, behaved differently, particularly in the last test which was performed at the end of the summer of 2014, after a considerable dry period. However, this data has not been readily evaluated regarding the possible causes.
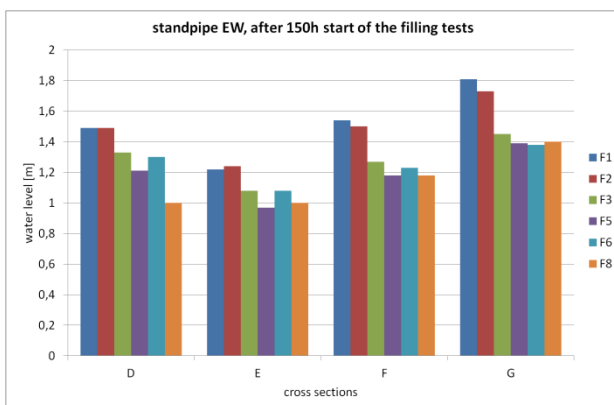
Figure AII.38. Standpipe EW, after 150 h, filling test, polder 2
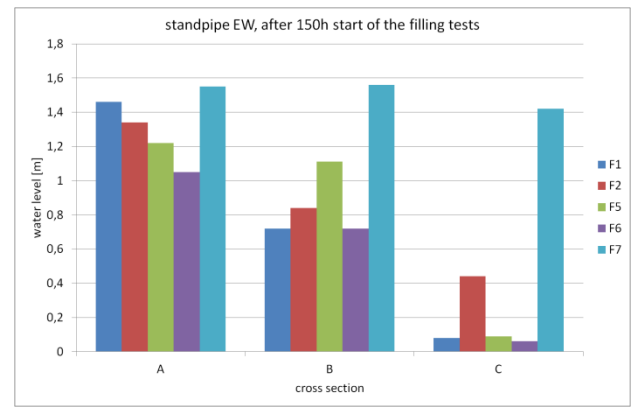
Figure AII.39. Standpipe EW, after 150 h, filling test, polder 1
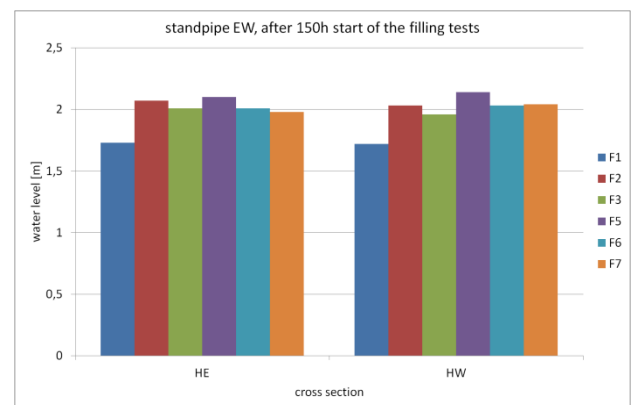
Figure AII.40. Standpipe EW, after 150 h, filling test, polder 3

Polder 3 shows different results to polders 1 and 2. The water level inside the standpipes increased with the first filling tests and resulted in a constant height after 150 h for the following tests. This allows the conclusion that the material did not change its characteristics during the two years of investigation.

2.4. In-situ saturated shear strength analysis

Before and after selected filling tests, the undrained shear strength was determined on the outer slope (inside the polder) with a vane shear tester to determine the change in strength during in-situ saturation. Figure AII.41 and Figure AII.42 show results of measurements on the outer slope of the western dike (overflowing dike). Only in section G, in which this particular slope was not well compacted in the upper 20 cm, because during the profiling of the dike surface the contractor removed too much DM and afterwards placed additional material on the embankment, a reduction in shear strength after saturation for at least 10 days can be seen. All other results show that the saturation rather leads to an
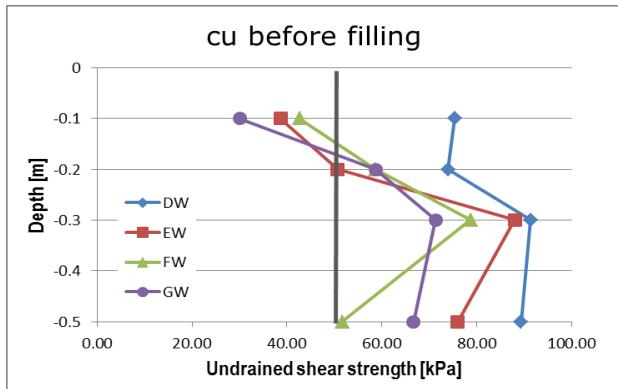
Figure AII.41. Field vane shear test, cu values before filling, polder 2
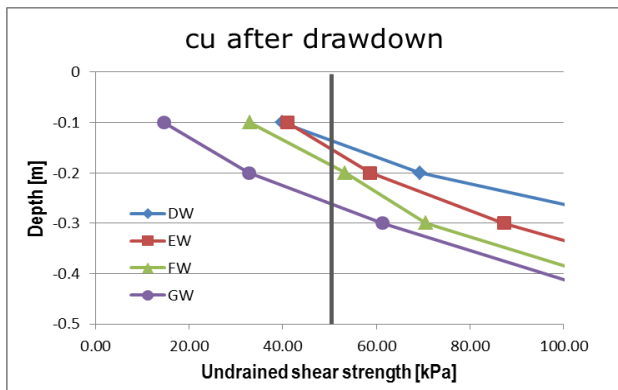
Figure AII.42. Field vane shear test, cu after drawdown, polder 2

improvement of the shear strength. Also, it can be seen that even after an initial greening which had died back at the time of measurements after several weeks of filling with brackish water, after permanent walking on the embankments for instrumentation and maintenance and soil genesis processes, only the upper 20 cm showed cu-values below the desired value of 50 kPa. However, even on the slopes with lower shear strength measured, no erosion through rainfall was observed. Finally, it has to be noted, that usually the upper 10-20 cm are well rooted, providing additional stability to the system.

2.5. Deformation analysis

One week after completion of the test dike, aluminium rods with a diameter of 0.01 m and a length of 0.5 m were installed on the crests of the research dike as well as on the slopes and along the toe as measurement points for geodetic settlement control. In the DredgDikes project, settlements were not the main focus and thus no electronic settlement gauges were used. At the beginning, 58 measurement points were installed across the whole construction (Figure AII.43).

Since the initial measurement on 06 June 2012 five control measurements were performed until 27 June 2013. Settlements of up to s = 0.2 m at the crest and usually s < 0.1 m at the toe were measured. A selection of results is provided in (Figure AII.43).
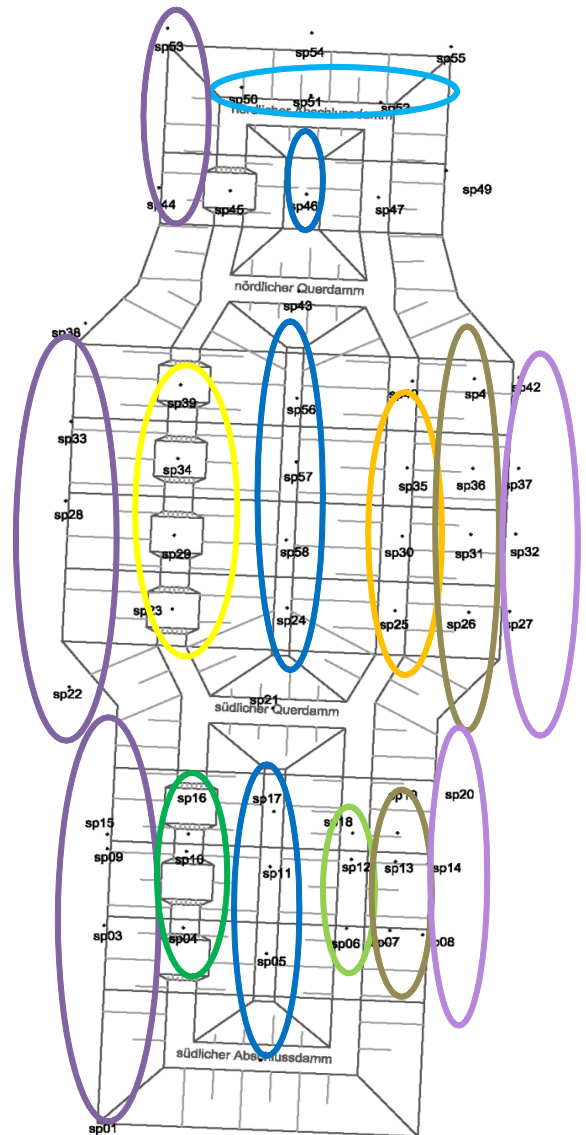
Average settlements [m]	6 June to 16 Oct 2012	6 June 2012 to 16 April 2013	6 June 2012 to 27 June 2013
Polder 1 west crest	0.05	0.08	0.09
Polder 1 east crest	0.09	0.13	0.15
Polder 2 west crest	0.08	0.14	0.15
Polder 2 east crest	0.14	0.22	0.23
Polder 3 crest	0.08	0.14	0.15
North dam crest	0.10	0.16	0.17
Underground west	0.01	0.02	0.01
Slope east	0.06	0.10	0.11
Underground middle	0.01	0.04	0.01
Underground east		0.01	0.00

Figure AII.43. Results of the geodetic settlement measurements
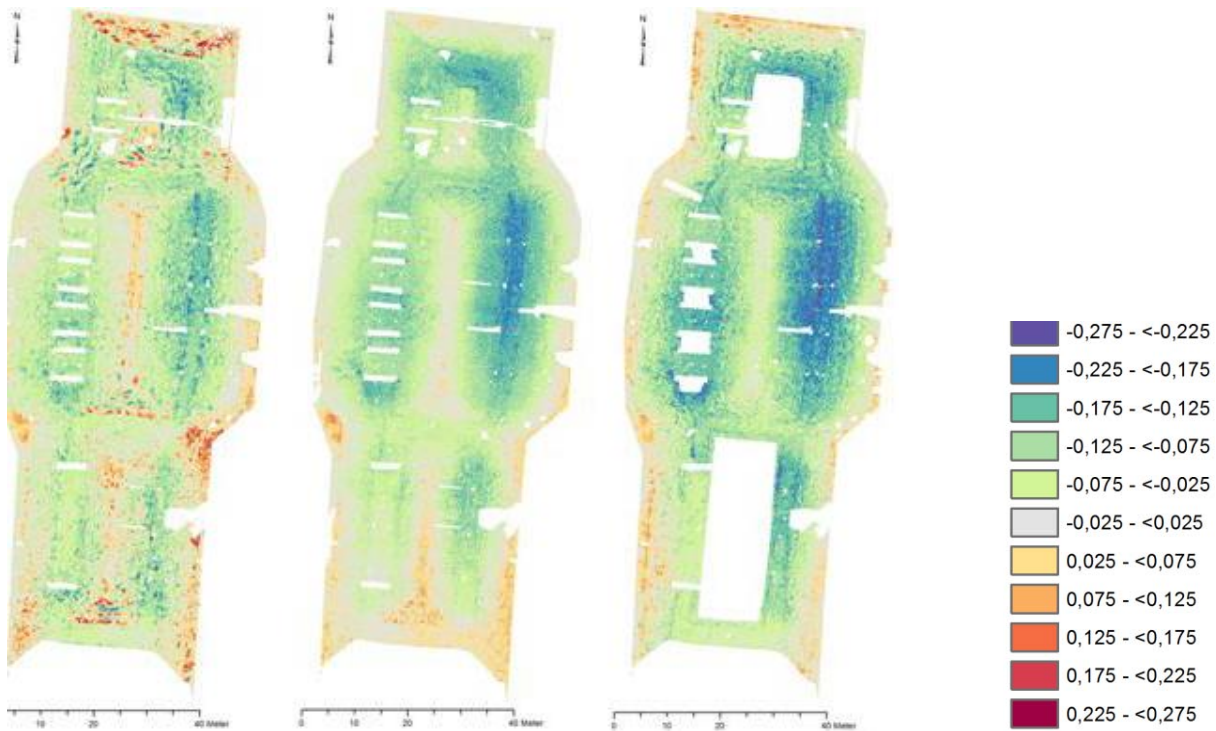
Figure AII.44. UAS (unmanned aerial system) photogrammetric measurements of the Rostock research dike – deformations

During this time period, also measurements with UAS (unmanned aerial systems) were performed. The analysis of the settlements over the time (6, 10 and 12 month) showed settlements on the crest between 0.23 m and 0.28 m (Figure AII.44), comparable to the geodetic point measurements. More information on this technology and on results regarding the research dike can be found in [32], [33], [34], [35], [36].

2.6. Installation tests

2.6.1. Dike construction technology

In 2011 a compaction testing field was built to test the installation of the materials M1 and M2. The soil was installed in layers of 30 cm using a bulldozer and a 12.5 ton sheep's foot roller for the compaction. The bulldozer installation was unproblematic and thus focus was set to the compaction technology to reach a demanded degree of compaction (DOC) of 90% (Proctor density). In the wet summer of 2011 none of the materials was dry enough to reach this value. The variation of crossing counts did not show a significant effect and the vibration seemed to have no effect either (Figure AII.45, Figure AII.46).

In spring 2012 the actual dike construction started. Due to the different slope inclinations and cross-section designs the construction technology was adjusted several times. Usually, the sand core would be hydraulically installed and then profiled. However, due to the size of the research construction the sand core was built dry and compacted with a roller compactor with vibration.

The homogenous dike of polder 3 was built in horizontal layers of 30 cm. The bottom half was compactted with the standard roller compactor. The upper part was built up with the bulldozer only using the material removed during the profiling of the lower part.

The installation of the cover layer in polder 1 on the steep slopes with a 1V:2H inclination was not trivial. Usually the cover layer on a dike would be installed in layers across the sand core surface (see guideline Chapter 5). However, the slope was too steep for this technology. The cover layer on the western dike was installed by putting considerably more material in front of the sand core. However, the proposed layer thickness of 30 cm could not be realised, because the profiled sand core would have been destroyed during compaction. The thicker layers on the other hand may not be as well compacted in the lower parts, however, this was not controlled in the actual compaction test (cf. Figure AII.47b and guideline Chapter 5).
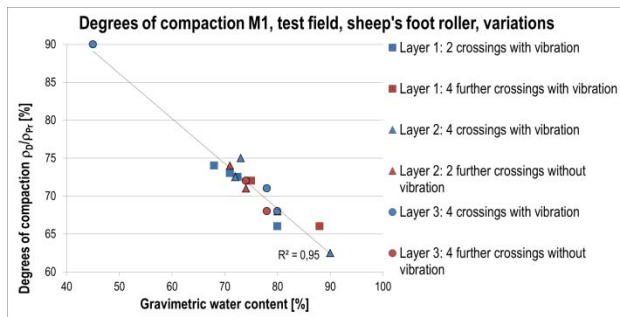
Figure AII.45. DOC for M1 and different installation and compaction modes with/ without vibration, variation of crossings
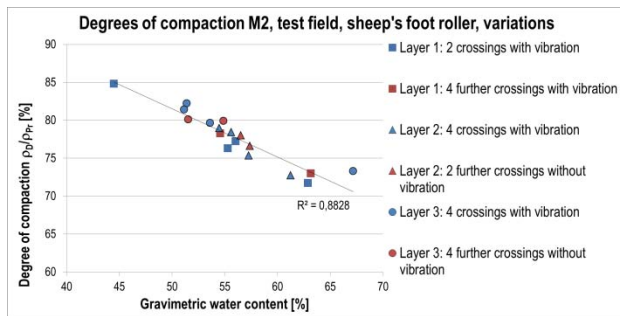
Figure AII.46. DOC for M2 and different installation and compaction modes with/ without vibration, variation of crossings

On the eastern dike of polder 1 a different technology was chosen: The sand core was only built up to 1 m height and the cover material was placed on both sides in horizontal layers of 30 cm (cf. guideline Chapter 5). This method was repeated until the crest was reached.

In polder 2 the cover material was installed in layers of max. 30 cm on top of the sand core. The installation with a bulldozer and the compaction with a roller compactor were easily possible.

2.6.2. Comparison of different compactors

Three different compaction methods were used in the installation tests (Figure AII.47): a sheep's foot roller compactor with vibrator (12.5 t), a standard roller compactor with vibrator (12.5 t), and a standard bulldozer (13.0 t). The evaluation of all compaction data showed only small differences between the compaction results (Table AII.17, Figure AII.48, Figure AII.49 and Figure AII.50).

Initially it was supposed that the compaction after bulldozer compaction would be considerably lower than after compaction with roller compactors. Data evaluation shows a 6 % lower DOC (mean values) for M1 when compacting with the bulldozer only, which is significant. For M2 a 2.5 % lower DOC was observed, which is not significant with respect to the data population.

Figure AII.47. Compactors used for the technology comparison

Table AII.17. Results of the DOC analysis from the test dike

	Roller compactor	Bulldozer
M1		
Number of values	23	27
Mean value	78.6%	72.4%
Standard deviation	6.33%	4.61%
M2		
Number of values	28	27
Mean value	84.2%	81.7%
Standard deviation	6.35%	8.27%

Also, a higher risk of non-uniform compaction was assumed for the bulldozer compaction, which would result in larger standard deviations. However, there is a lower spread of the respective data for M1 and a slightly higher spread for M2. Both are not significant. Thus the assumption could not be verified in this test.

As a result the bulldozer compaction was chosen for installation efficiency in polder 2, particularly due to the crumbly state of the ripened DM. For material with larger loam or clay clots the method would have to be revised.
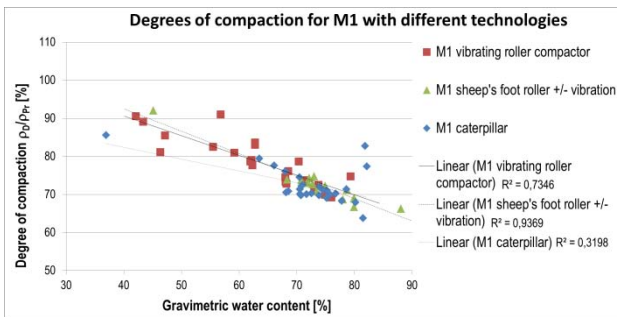
Figure AII.48. DOC for M1 and different compaction technologies
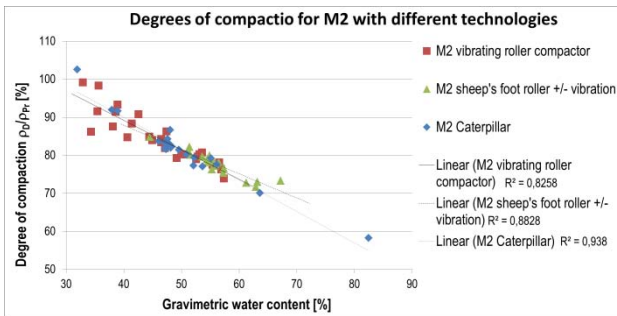
Figure AII.49. DOC for M2 and different compaction technologies
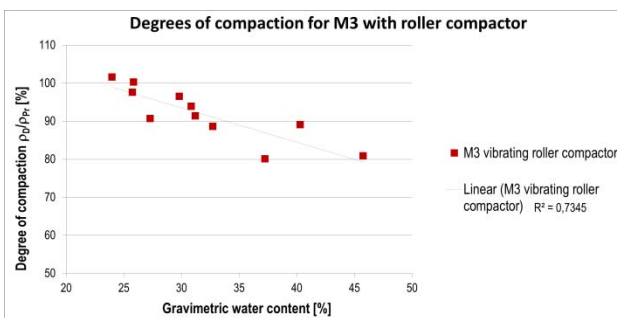
Figure AII.50. DOC for M3 with roller compactor

Finally, it could be seen that a real decision about a best technology could not be made, because the data showed a distinct dependency of the DOC on the water contents (Figure AII.48, Figure AII.49, Figure AII.50) rather than significant differences between the technologies. Therefore, an additional installation and compaction test was planned (cf. Chapter 8).

2.7.　Vegetation tests

The turf development both on the dike and on especially prepared testing plots with different DMs and in different weather conditions has been investigated during the projects lifetime.

In preparation of the test dike sowing a standard dike seeding mixture (variation 1) was tested on all chosen materials directly on the storage heaps on the municipal DM processing plant in Rostock. In addition, the mixture was tested with added legumes (variation 2).

Variation 2 was also tested on a compaction testing field (that was installed in 2011 before the dike construction) and based on this experience it was selected for the research dike seeding also. The mixture with added legumes should provide a deeper root reinforcement and thus additional strength to the dike surface as well as a fast greening. Moreover, the white clover and the lucerne both provide an additional nitrogen source and ensure the turf conservation through fertilizing effects. Therefore, the root depth needed to be investigated.

On the research dike embankments the seeding mixture (variation 2) was tested in 27 small testing fields with different surface conditions, irrigation and wind protection on all chosen DMs for seeding and germination issues. Table AII.18 gives an overview of the different seeding tests.

2.7.1.　Test set-up and measurement techniques

Two different seed mixture variations were investigated in the seeding pre-tests. Variation 1 is a standard seed mixture for dikes. In variation 2 a portion of legumes was added: White Clover (*Trifolium repens*) and Lucerne (*Medicago sativa*). The composition of the seeding mixtures is presented in

Table AII.19. The seed was applied with 30 g/m² according to the manufacturer's instruction. In variation 2 the portion of the principal constituents was reduced accordingly.

Table AII.18. Overview of seeding tests with number of test fields, material and reference period

Seeding pre-test 9 test fields M1/2/3 2011	Sowing in spring on fine, crumbly surface, initial irrigation directly after sowing.
Compaction testing field 2 test fields M1/2 2011 - 2013	Sowing in autumn on compacted surface, surface was roughened / loosened before the seeding.
Research dike M1/2/3 2012 - 2013	Sowing in summer on compacted surface, partly roughened; fine crumbly DM on erosion control mats. Hydroseeding technology.
Seeding test on research dike embankment 27 test fields M1/2/3 2012 - 2013	Sowing in autumn 2012 on different surfaces: compacted, roughened and with additional crumbly topsoil applied.

Table AII.19. Seed mixtures for the test fields and the test dike

Component	Variation 1	variation 2
	[%]	[%]
Festuca rubra	60	54.6
Lolium perenne	30	27.3
Poa pratensis	10	9.1
Trifolium repens		6
Medicago sativa		3
sum	100	100

Figure AII.51. Prepared compaction testing field

The seeding pre-tests confirmed the assumption of a fast germination and robust growth of grasses and grass-legume mixtures on DMs, which adds to a long-term research experience in Rostock [37].

The compaction testing field was built up of three sections (only DM; with geosynthetic reinforcement installed to reduce cracking in 60 cm below the surface; with reinforcement in two layers, 30 cm and 60 cm below the surface as planned for the research dike). The sowing was realised in Sept. 2011 using seed mixture variation 2. Therefore, the surface of the two DMs was roughened about 2 cm deep. The seed was spread evenly, raked in and fixed with a hand roller (Figure AII.51).

In Oct. 2013 the root penetration at the compaction testing field was determined. For this purpose, profiles of 60 cm depth were dug and the root penetration in the excavated material as well as on the profile walls was investigated. In addition, cracks were detected and documented photographically to assess the functionality of the reinforcement solution.

2.7.2. Test procedure and analysis on the dike

Two weeks after construction of the research dike the sowing was realized in June 2012 by hydro-seeding. Therefore, the seed mixture including the legumes (variation 2) was mixed with water and a binder. Through the binder the seeds stick to the soil surface, however, on the steeper dike slopes (1V:2H) a slight slipping of seeds was noticed. The seeding could not be realised in conformity with the requirements of the EAK [38] (cf. guideline Chapter 5). Both the geometry of the research dike and the time factor demanded a different procedure. An initial fertilizer donation was avoided intentionally.

On the research dike, mechanical mowing was chosen and realized as tending strategy. This made sure that a thick and closed vegetation cover was established. The mowing was performed more often than usual on dikes in Mecklenburg-Vorpommern twice to four times a year because of the technical specifications of the available mowing machine.

In the initial phase after seeding, there was a dry period of 3 months in which the seeds did not germinate on the weather prone dike embankments where both wind and sun quickly dry out the surface. On identical DM on the flat grounds around the dike germination started quickly after the seeding. On the dike embankments, an irrigation trial, including the covering of one cross-section with a translucent plastic sheet to retain the moisture, did not help the germination. Only in October, when precipitation returned, the germination on the dike started quickly and a comparably dense vegetation developed even before the winter. At some places, however, a re-seeding was needed, because the binder from the hydroseeding had worn off over time and both wind and birds removed parts of the seeds from the DM surfaces.

2.7.2.1. Additional seeding test on the embankments

Since there were critics connecting the "negative" germination result during the summer with the salts contained in the DMs or the general composition of the DMs, an additional seeding test (seeding test on research dike embankments) was developed which included a good fertile top soil from the agricultural research fields of the University of Rostock's agricultural departments. 27 plots of 1 m² with different boundary conditions were prepared to re-investigate the suitability of the DMs for greening on exposed dike embankments. The test fields were realized on the eastern slopes of polders 2 and 3 on materials M1, M2, and M3 with different soil preparation, with and without initial irrigation, with and without wind protection and on one plot per material a 5 cm cover with standard fertile topsoil was placed for comparison.

2.7.2.2. Vegetation coverage analysis

In 2013 the vegetation cover of the research dike was checked twice with the help of aerial photography from a UAS (unmanned aerial system, see Paragraph 2.3). The cover ratio and vitality were estimated and compared. Therefore, the aerial photographs were converted into raster images and a vegetation index was calculated in ArcGIS [39]. The determined values were converted into qualitative values and then classified. The 10 obtained classes (single colour values in the raster) were summarised in 3 groups for interpretation of the vegetation cover. Colour values 1 to 5 mean very good to good cover ratio, colour value 6 means less covered areas and turf vitality not in a good state and colour values 7 to 10 labels the almost or totally bare areas on the dike. By counting the single pixels and knowing the pixel size the cover ratio of the different groups can be calculated.

Through the classification the development status of the test dike between April and June 2013 could be compared. However, when comparing the images it has to be considered, that the lighting conditions as well as the mowing situation on the respective days were not congruent. In addition, some installations were set up on the research dike between April and June which were not removed from the raster images. Additional restrictions are related to the composition of the vegetation cover (leaves, stalks, branches, trunks etc.) and the reflection properties of the individual components. The background properties (reflection of the soil, leaf-litter covering), solar altitude angle and solar azimuth also play a role. Thus, the results should be regarded as an approximation.

2.7.2.3. Sampling and root analysis

At the end of the vegetation period (early Nov. 2013) and after performing the overflowing tests, 48 topsoil samples (down to 20 cm) were taken from all embankments to evaluate the roots. Samples were taken from the dike crest and from the upper and lower embankment. The samples had a size of 5 x 5 x 15 cm³ (Figure AII.52a). The vegetation (grass cover) was cut ($\leq$ 2 mm) and the sample was watered. Afterwards the sample was wet sieved (1 mm sieve). The relatively intact root body (partly with the erosion control product stuck to it) was carefully washed out (Figure AII.52b) and fine roots with more than 1 cm length were collected and separated. The

Figure AII.52. a) Prepared sample for watering, b) Connected root system for further preparation

Figure AII.53. a) Soil and stones, rests of roots and organic material in the sieve, b) Washed out root system with rooted RECP

strongly clotted soil residues were wet sieved [40] to remove organic residues (woody roots and debris) and gravel (Figure AII.53).

The samples were dried to mass constancy at room temperature, weighed and stored for future treatment. A further step was incineration at 500°C in the muffle furnace to determine the root mass.

2.7.2.4. Grass cover during the overflowing tests

Eventual grass cover damages during the overflowing tests on the research dike were documented. A comparison between the cross-sections (DM, RECP) and the overflowing events (intensity, duration) combined with the data of the root penetration analysis and the erosion rate measurements (cf. 2.2.3) should enable a differentiation between the different materials and sections with erosion protection. The test sections (60 x 60 cm²) of each flume were documented with a measurement frame. The pictures were rectified and the concavity was eliminated by calibration with a special programme [41]. With the double correction the pictures can be overlaid and the erosion can be highlighted.

The problem of comparing the different sections is to estimate the damages of the initial situation and after overflowing events (Figure AII.54 and Figure AII.55). A digitalization that will enable the estimation of damages is always a subjective procedure because there are no clearly visible edges. There are also problems with the mowing residues at the beginning and the bending grass due to the flowing water, partly covering damages.

Figure AII.54. Cross section D (52 x 38 cm), flume 1, section 6, initial situation (l) and after the fourth test (r)

Figure AII.55. Cross section E (52 x 38 cm) with erosion mat, flume 1, section 6, initial situation (l) after the fourth test (r)

2.7.3. Typical results and evaluation

2.7.3.1. Results from the compaction testing field

The autumn sowing on the compaction test field verified the spring results from the seeding pre-test. A fast sprout of the variation 2 mixture was observed. An adequate pre-winter growth provided a development of a vital and compact vegetation cover in the following vegetation period (Figure AII.56). The increased growth of the cultivars was documented by 4 necessary cuts in 2012. Between the two substrates M1 and M2 no significant growth differences could be observed. The amount of legumes was broadly similar in the first year after seeding, but in 2013 the amount of legumes was significantly higher in M2 than in M1. This was also confirmed by [21].

The excavation on the compaction testing field in Oct. 2013 showed a rooting of the whole horizon (0.6 m). In material M1 the rooting clearly decreased below the first 30 cm depth. In the top layer 0 to 30 cm of depth only few legume roots were found. This may be due to the fact of a low proportion of legumes (leaf area density) at the surface of M1. However, fine roots were also found in the layer of 60 cm. The root penetration in the topmost soil horizon of M2 was denser and more intensive than in M1. The legumes roots reached a depth of more than 50 cm.

The geosynthetic reinforcement to reduce cracking showed no negative effects on the root penetration. On the contrary, more roots were found on the geogrid, since

roots may use the grid for water supply. Apparently the cracking did not seem to be reduced by the reinforcement product in this test. Above and beneath product cracks penetrated with branched roots could be observed. The width of the observed cracks differs from few mm to 2 cm.

Figure AII.56. Turf in September 2013 of the compaction testing fields materials M1 (l) and M2 (r)

Figure AII.57. Soil layer 20 to 30 cm, materials M1 (l) and M2 (r)

Figure AII.58. Rooted 3D-RM in material M2 (l), legume roots in depth of 50 cm in material M2 (r)

Figure AII.59. Material M1 soil horizon depth 60 cm (3D-RM) (l), Material M2 3D-RM in 30 cm depth (visible rooting and cracking) (r)

2.7.3.2. Results from the research dike

On the research dike the hydro-seeding failed at the beginning. After a first slight growth of grass an extensive saltbush (Atriplex) vegetation cover developed on parts of the test dike. The continuous aridity led to a loss of germinating seed during the summer, covering only 20 % to 50 % of the area (Figure AII.60). The seeding and re-seeding of blank areas by hand in Aug. 2012 did not result in a complete vegetation cover before Sept. Only with significant higher precipitation at the beginning of Oct. and the reduced evaporation the growth of the grasses and legumes improved considerably (Figure AII.61a). The vegetation development in spring 2013 was delayed by a long strong winter. After the snow had melted in April the young grasses in the re-sewn areas were visible. The grasses endured the winter well. In some areas the protective snow had been blown away, and the vegetation was frozen to death. The soil surface was dried by the dry freeze and the topsoil felt like fine grained powder (the same situation was found at the compaction testing field). The vegetation recovered with increasing temperatures in May and within only few weeks a close vegetation cover was established (Figure AII.61r). With increasing temperatures the activity of voles started to become visible (Figure AII.62l).

2.7.3.3. Test fields on the research dike embankments

The test fields were installed in mid-Sept. 2012 resulting in a fast and regular greening. Only marginal differences between the variations could be observed: the vegetation cover in the variations with standard topsoil germinated 1-2 days earlier and looked a bit more compact initially. The fields were monitored through 2013. The differences in compactness levelled quickly and only the amount of legumes stayed higher in the topsoil variation (Figure AII.63).

Figure AII.60. Surface of test dike two weeks after hydro-seeding; decomposed binder (l), beginning saltbush growth (r)

Figure AII.61. Turf development at the test dike; polder 2 in 2012 (l), polder 1 in 2013 freshly mowed (r)

Figure AII.62. Activity of voles (l) and crack on the research dike (r)

Figure AII.63. Two different variations of the seeding test on the dike embankment – compacted surface, M1 with initial irrigation (l) and variation with topsoil (2 cm) above M2 (r)

The whole vegetation cover of the research dike was checked twice using aerial images (cf. above). The cover ratio and vitality were estimated and compared. In April 2013 after the winter up to 64 % of the areas were covered with vegetation in a good state. In June 2013 with recovered vegetation 80 % of the areas achieved a good cover ratio. Some areas were still not completely covered until June, so e.g. the eastern slope of polder 1. This slope had little vegetation from the seeding and was covered very fast by the saltbush (Atriplex). In winter the saltbush died back. Despite of re-sowing some areas were still bare in June (Figure AII.64).

Figure AII.64. Comparison of cover ratio of the test dike after winter season in April (l) and mid-June (r) 2013 (aerial images from [42])

2.7.3.4. *Turf evaluation during overflowing tests*

The evaluation of the erosion damages by overflowing is shown for two samples exemplarily. The turf and the network of roots of the different embankments (cross sections B to H) have borne up against the overflowing experiments. A complete functional failure of the slope could not be detected. Very few individual grass blades of the turf were pulled out due to the high traction from the overflowing water. Apart from that, areas without vegetation cover showed minor erosion. In some cases, some fine-grained soil particles at the surface were eroded by the overflowing water until the network of roots lay open and then the erosion process stopped. If the highly branched root system of young fine elastic roots remains intact than it will remain the high erosion resistance. After the first overtopping almost only the bare areas were visible when the mowing rests and dry grass were washed away. Figure AII.65l shows a vole hole surrounded by a nearly intact vegetation cover. Not even the highest load increment during the overflowing showed any severe damages (Figure AII.65r).

Figure AII.66r shows very pronounced surface erosion in cross section E, on the erosion control geomat GMA. The turf was damaged before the experiments started,

Figure AII.65. Detail cross-section D; Initial situation (bare areas and vole hole)(l), state after fourth overflowing (r)

Figure AII.66. Detail E (initial situation with dry vegetation) (l), fourth overflowing (fine networking roots visible in RECP) (r)

dry grass blades can be seen (Figure AII.66a). The loose soil above the GMA (no compaction) was washed out in spite of the branched root system. Already after the first overflowing increment the cover showed damages. With further overflowing the area eroded until the GMA with contained roots lay bare. This effect is issue for further investigations, e.g. in a direct shear test, to gain more knowledge about the maximum thickness of soil cover on top of a GMA.

2.8. Crack detection

The crests and embankments showed intensive shrinkage cracking, starting on the parts finished in April 2012 and particularly developing during the three very dry summer months after dike completion at the end of May 2012. At first, visual observations on the surfaces were made. While materials M1 and M2 showed intensive cracking, on material M3 no cracks were observed. However, due to the manifold tasks during and after the dike construction, such as sensor installation, compaction control, etc., the crack development was only poorly documented. As soon as the vegetation started to grow, visual methods (including aerial photography) were not possible any more. Therefore, the infiltration / seepage tests were hoped to provide data with considerable differences of surfaces with different crack intensities. However, since the reinforcement as yet showed a minor effect, the measured differences in seepage flow are too

small to decide about different cracking formation and crack sizes in the materials.

Therefore, a geoelectric method (electric resistivity tomography) was performed in September 2014 on three slopes (M2 with and without reinforcement and M3) to distinguish cracked and non-cracked areas in the dike covers. The measurements and evaluation were performed by Dr. Marcin Zielinsky, formerly Strathclyde University Glasgow [43]. Selected results are shown in the following figures. The analysis was performed after the summer with more than four weeks distance to the previous polder filling experiments. As can be seen in Figure AII.67, the surface of the crest and inner (eastern) slope show high resistivities while the resistivities on the outer slope are lower. In 60 cm depth the material M2 shows comparably uniform resistivities. This can be judged to be a homogenous moisture distribution, in the same magnitude as on the outer slope surface. The higher resistivities on crest and eastern slope surface can have different reasons: It may be cracks, intensive vole activity or just dryer material. Since the polders had been filled for several weeks before the summer of 2014 during the infiltration and seepage tests, the material on the outer slope (facing west) was still nearly saturated, while the inner slopes (facing east) had dried out for several months. Thus, a clear distinction regarding cracking zones is still not possible.

Figure AII.68 shows three selected vertical cross-sections of ERT evaluation for cross-section D. They

Figure AII.68. ERT evaluation Sept. 2014 [43] for cross-section D, measured 4 m wide strip across the section; 0 = outer embankment toe (inside polder); diagram of vertical cross-section 5 of 11.
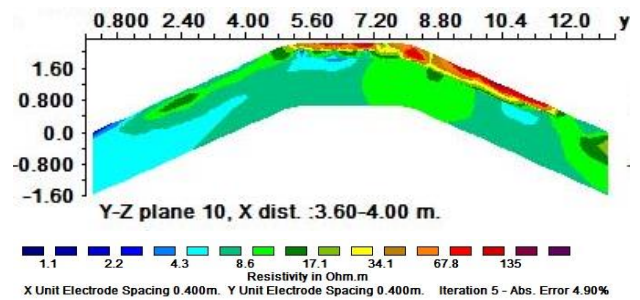
Figure AII.69. ERT evaluation Sept. 2014 [43] for cross-section H, measured 4 m wide strip across the section; 0 = outer embankment toe (inside polder); diagram of vertical cross-section 10 of 11.

show an identical picture with the dry / high resistivity zone on the upper 60 cm of the crest and inner slope. Even with the high electrode resolution of 40 x 40 cm single cracks are not clearly visible. Also, the comparison to polder 3, cross-section H (Figure AII.69) in which no cracks have been visible at the surface at any time since the construction and which also shows the high resistivities at the crest and inner slope supports the assumption that the higher resistivities do not particularly show cracks but rather dry zones. However, areas of potential concern can be identified which will be looked at more closely in the future, e.g. by digging up these areas to actually look inside the cross-sections.

3. MODELLING AND COMPUTATIONS - GERMAN RESEARCH DIKE

The modelling and computations of the German research dike, both regarding flow conditions and stability, have not been completed yet. First results can be found in [44] and [45]. Further results will be published on the project website when available.

Figure AII.67. ERT evaluation Sept. 2014 [43] for cross-section D, measured 4 m wide strip across the section; 0 = outer embankment toe (inside polder); diagram of horizontal layers 1 & 4 of 8.

4. LABORATORY TESTS FOR CCPS AND COMPOSITE MATERIALS

4.1. Materials used in the Polish DredgDikes investigations

In the Polish DredgDikes research dike near Gdansk two basically different types of Ash were used: A bottom ash mixed with dredged sand from the Vistula river mouth was used in the dike core and a mixture of different ashes (fluid ash, fly ash) and other binders (Tefra®) was used in parts of the dike cover while in the rest of the cover a clay was used. The grading curves of the bottom ash and sand are provided in Figure AII.70 and Figure AII.71.

The goal of the preliminary laboratory investigation was to choose the optimum ash - sand mixture of a composite to be applied at the test site. The tests were performed to determine basic soil properties, compressibility and soil strength, compaction and permeability parameters. The tests were made on sand and ash itself as well as on the mixtures with different ash content. The mixtures were prepared using volumetric ratios. In the first stage properties of ash and sand were investigated, (Table AII.20). Table AII.21 shows a compilation of the properties of the materials investigated in Gdansk.
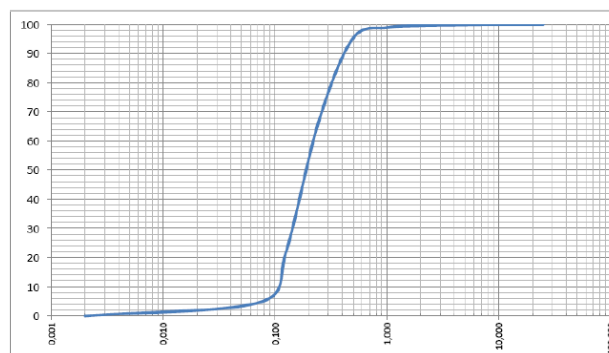
Figure AII.70. Grading curve of bottom ash
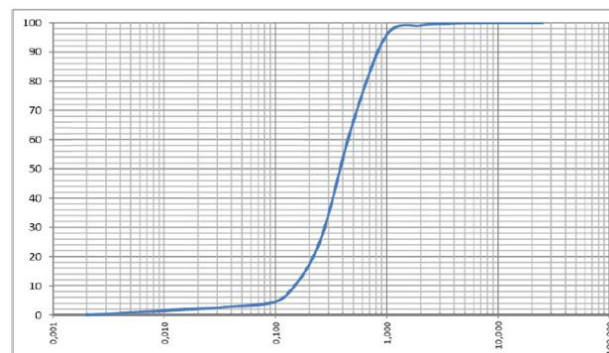
Figure AII.71. Grading curve of dredged sand

Table AII.20. Granulometry and specific gravity of the bottom ash and dredged material [46]

Parameter	Bottom ash	Dredged sand
Uniformity coefficient U	2.00	3.14
Curvature coefficient Cc	0.87	1.30
Mean grain diameter d50 [mm]	0.20	0.40
Specific gravity ρs [g/cm3]	1.87	2.67

Table AII.21. Properties of the materials investigated in Gdansk

Material		Clay	Ash & Silt	Ash & Sand
		Upstream cover layer	Downstream cover layer	Dike core
Strength type	-	Mohr-Coulomb	Mohr-Coulomb	Mohr-Coulomb
Total unit weight	$\gamma\ [kN/m^3]$	18	16	13
Saturated unit weight	$\gamma_{sat}\ [kN/m^3]$	21	20	16.3
Hydraulic conductivity	$k\ [m/s]$	1 e -7	1 e -7	1 e -5
Void ratio	$e[-]$	0.79	0.64	0.69
Porosity	$n[-]$	0.44	0.39	0.41
Cohesion	$c\ [kN/m^2]$	30	50	5
Angle of internal friction	$\varphi\ [°]$	25	20	37
Dilatancy	$\psi\ [°]$	0	0	0
Young's modulus	$E[kN/m^2]$	15,000	30,000	22,500
Poisson's ratio	$\nu[-]$	0.35	0.30	0.25

4.2. Composites from CCPs and dredged sand

The proportion of components in the test dike was chosen based on initial tests on the dredged materials: it was examined, how the properties of the mixture are influenced by the variation of the percentage of ash. The following mixtures of bottom ash and dredged sand were analysed for the application in the sand core (Table AII.22).

The following results were obtained in the laboratory tests. Figure AII.72 and Figure AII.73 show the maximum dry density and optimum water content derived from the Proctor test.

Table AII.22. Mixtures of bottom ash and dredged sand

Investigated mixtures of bottom ash and dredged sand			
Percentages (% ash / % sand)			
0 / 100	40 / 60	50 / 50	60 / 40
70 / 30	80 / 20	90 / 10	100 / 0
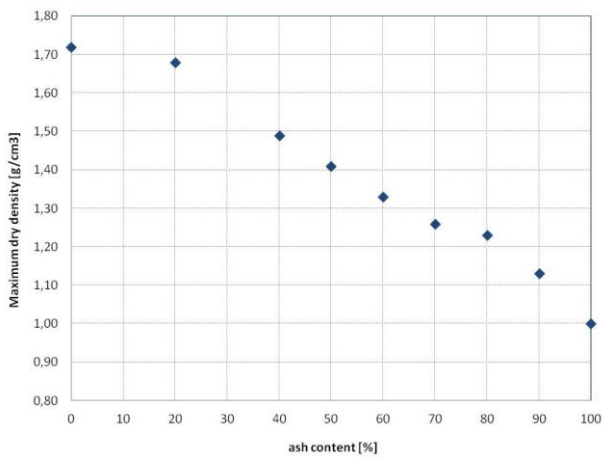
Figure AII.72. Maximum dry density for the different composites
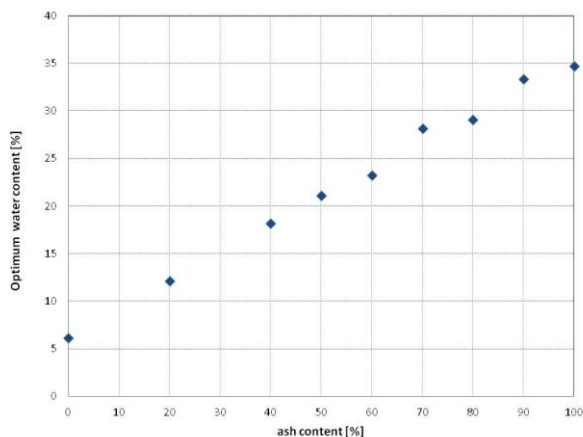
Figure AII.73. Optimal water content for the different composites
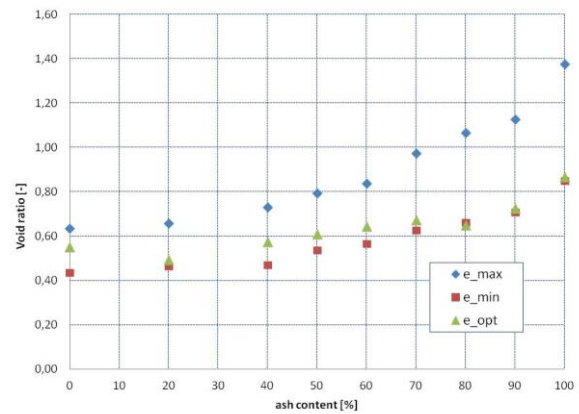
Figure AII.74. Void ratio as determined from the oedometric test
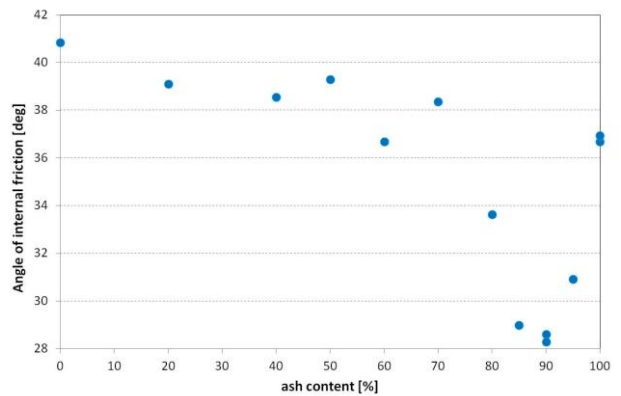
Figure AII.75. Angle of internal friction – direct shear test
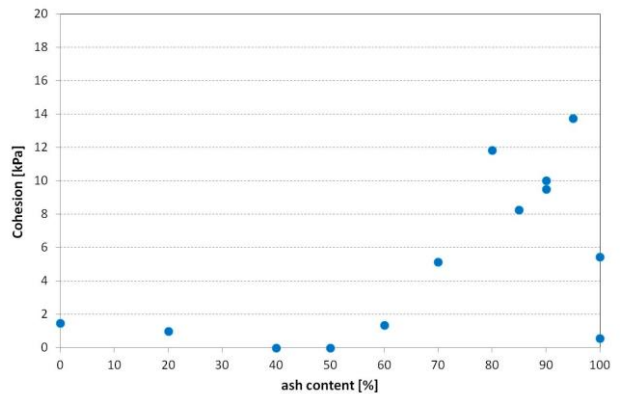
Figure AII.76. Cohesion – direct shear test

The void ratio was determined in the oedometric test (Figure AII.74). The angle of internal friction and cohesion were derived from direct shear tests (shear box). The results for the investigated composites are summarised in (Figure AII.75 and Figure AII.76).

At the end of the tests, an optimum mixture of 70/30 (ash/sand) was chosen for the research dike construction. Figure AII.77 and Figure AII.78 show the results from the direct shear test and the oedometric test for this mixture.
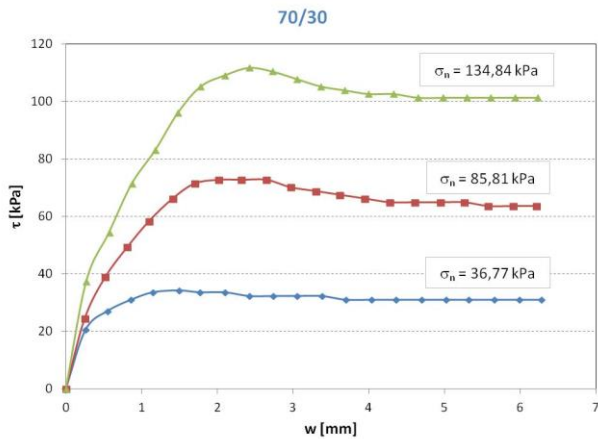
70/30

Figure AII.77. 70/30 mixture of ash and sand – direct shear test
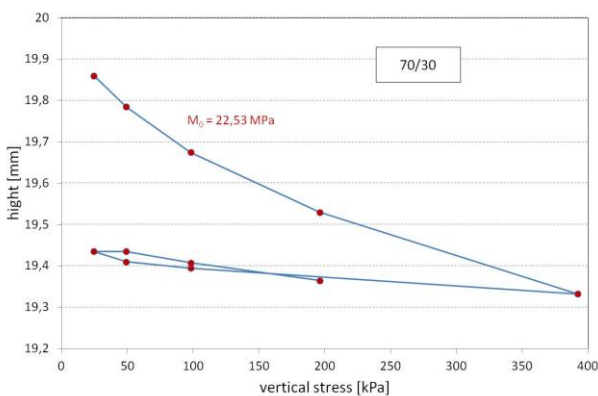
Figure AII.78. 70/30 mixture of ash and sand – oedometric test

The mixture has a relatively high permeability coefficient (k = 1·10⁻⁵ m/s). However, it is assumed that will decrease over time because of the cementation due to the pozzolanic properties of the coal ashes.

4.3. Triaxial compression tests

The triaxial compression test is a common method to determine the strength and stiffness parameters of soils. In comparison to other standard tests, e.g. direct shear test, the boundary effects disturbing homogeneity of the stress/strain field are minimised in the triaxial sample during the test. In the DredgDikes project the program of triaxial investigations involved tests on organic DM from Rostock and bottom ash-dredged sands mixtures. Generally the test procedures on DMs can simply follow the standard national specifications.

One of the major problems relating to the laboratory testing of DMs is to obtain undisturbed samples with homogeneous structure. In case of harbour DM there is a frequent problem of solid waste material inclusions which in the most cases trigger a failure mechanism in the

sample. Another problem is related to the differences of mechanical characteristics between the samples constituted and consolidated in the laboratory and in the field. In a case of the fine-grained DMs from Rostock only undisturbed samples obtained in situ were tested.

The bottom ash - dredged sand mixtures were tested initially only in the laboratory to choose the best proportions of ash and sand in the compound. The selected volumetric 70 % ash and 30 % dredged sand mixture was applied to build the test dike in Gdańsk. Undisturbed samples were obtained from excavation at the research dike (Figure AII.79).

The triaxial results on the samples obtained in situ have shown significantly better mechanical characteristics than their equivalents constituted in the laboratory. The tests were repeated and it was observed that this phenomenon is gained by the time. This is attributed to the strong influence of ageing in the ash-sand mixtures. Natural cementing of the mixture skeleton which was developed during ageing has increased both effective friction angle and cohesion.

In the case of less permeable and cohesive DMs from harbour undrained triaxial tests should be performed. Example results are shown in Figure AII.80. It allows to determine effective and undrained strength parameters (effective friction angle ϕ', effective cohesion c' and undrained cohesion c_u respectively). The effective stiffness parameters should be obtained from other tests, preferably oedometric compression.

Figure AII.79. Obtaining undisturbed samples of bottom ash-dredged sand mixture from the excavation at the test dike in Gdańsk.
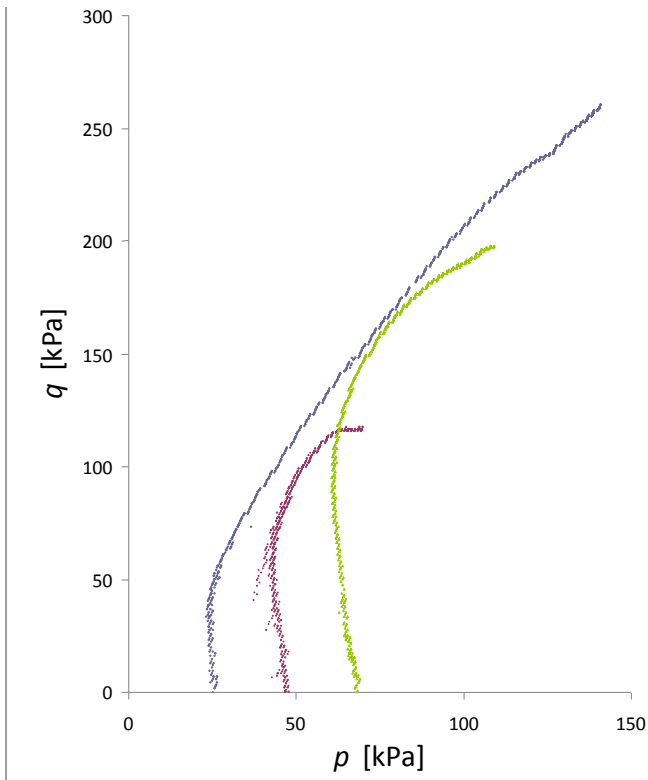
Figure AII.80. Example results of undrained triaxial tests on undisturbed samples of DMs from Rostock harbour (stress paths on p-q plane).
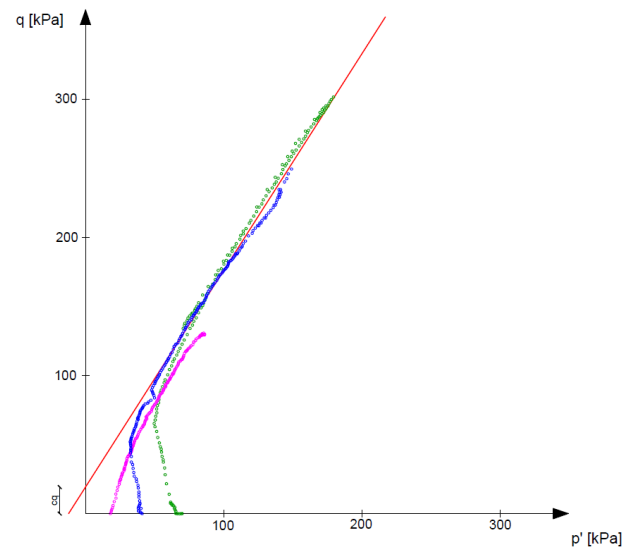
Figure AII.81. Example results of undrained triaxial tests on undisturbed samples of bottom ash-dredged sand mixture (stress paths on p-q plane).

The triaxial tests on mixtures with dredged granular soils should be performed both as drained and undrained. In the case of drained tests unloading is important which allow to determine unloading/reloading stiffness.

As in the body of dikes the effective stress level is not high it should be also taken in to account when selecting the initial consolidation pressures in the triaxial tests (both drained and undrained). In the triaxial tests performed in the DredgDikes project initial isotropic consolidation stress states were chosen to be not higher than 50% of the effective vertical stress at the bottom of the analysed dike. Example undrained test results on bottom ash-dredged sand mixtures are shown in Figure AII.81.

5. EXPERIMENTS ON THE POLISH FULL-SCALE RESEARCH DIKE

5.1. The Polish research dike

The 3 m high test dike located in Wiślinka/ Trzcińsko on the bank of Vistula River ca. 20 km outside the City of Gdańsk (Figure AII.82) was completed in the summer of 2012. The 4 m wide test segment of the 24 m long dike has been separated by sheet pile walls to obtain 2D plane conditions for seepage and overtopping tests with a controlled water level (Figure AII.84).

The ground underneath the test dike was extensively explored with the use of CPTU penetrometer. Under a shallow sandy crust, some fine-grained soft deposits interbedded by sandy layers were probed. Due to good drainage conditions the consolidation of the soft deposits under additional loading was quite fast and occurred almost entirely during the earth works.

To focus the attention on the seepage within the dike, its bottom was sealed against the permeable ground by a 0.5 m thick clay liner. A high water level of 2.5 m could be maintained until steady flow within the dike body was achieved. The greening was realized with rolled sod placed directly on the dike cover made of Tefra® and clay, a solution that cannot be recommended because of the poor water and nutrient supply in the thin soil layer of the rolled sod.

Figure AII.82. Location of the Polish research dike
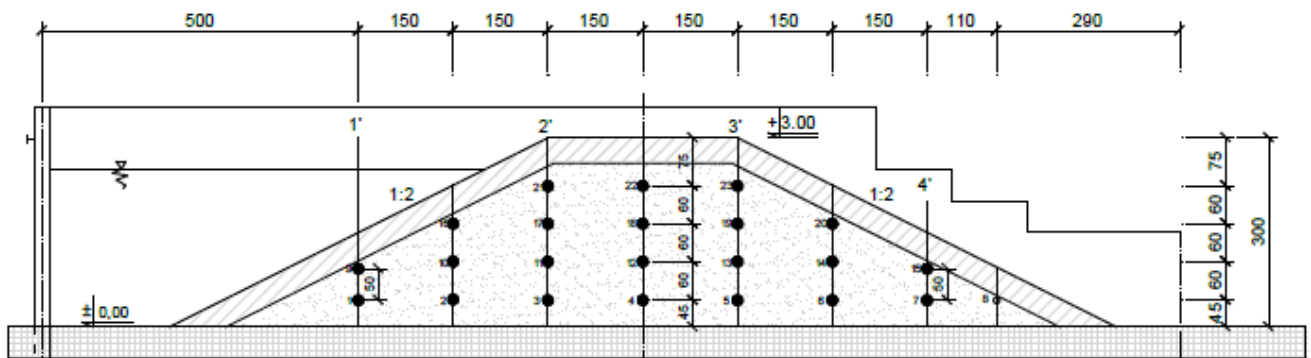
Figure AII.83. Geometry of the Polish research dike section and position of moisture probes and piezometers

Figure AII.84. Polish research dike with sheet pile basin
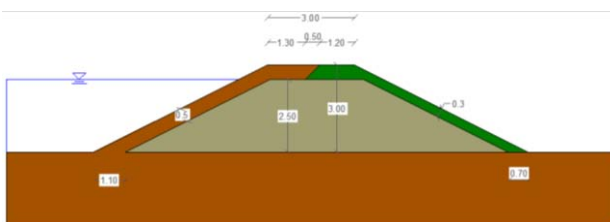
Figure AII.85. Materials and geometry of the Polish research dike
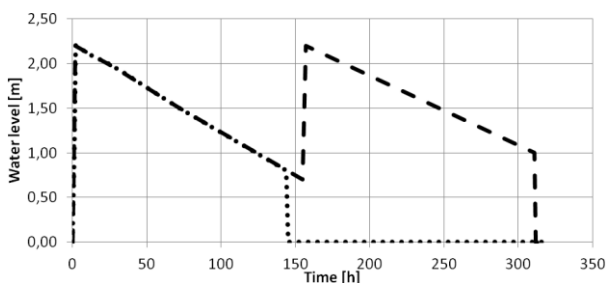
Figure AII.86. Flood wave shape: one-week experiment (dotted line) and two-week wave (dashed line)

The research dike is composed from three different materials (cf. Table AII.21):

1. the dike core is made of a mixture of bottom ash and dredged sand;
2. the cover layer is divided into two materials:

- clay in 50 cm layer thickness on the upstream side;
- a mixture of Tefra® (a special fluid ash mixture) and dredged sand in a 30 cm layer downstream.

Figure AII.85 shows the geometry and the position of the different materials. Both slopes have an inclination of 1V:2H and the dike is 3.0 m high with a 3.0 m wide crest.

In the dike core 24 soil moisture probes have been installed to measure the seepage line. The dense sensor raster allows the comparison with numerical simulations. Four piezometers are used to verify the sensor data (Figure AII.83). Additionally, sampling and laboratory testing of the physical and mechanical parameters of the applied sand-ash mixture were carried out during the test.

5.2. Seepage measurements

The described test dike was completed in autumn 2012 and instrumented in the end of 2012. First large-scale experiments started in spring of 2013. There were two lowland flood scenarios investigated, namely: a short flood wave (one-week experiment) and a long flood wave (two-weeks, double peak experiment). The experiments were conducted in 2 repetitions each to observe the mechanical and hydraulic behaviour under cyclic saturation/desaturation process.

Figure AII.86 presents the hydraulic loading water level in the upper basin for the mentioned two flood scenarios. The rather steep curve in the beginning of each scenario was caused by a small volume in the upper basin and resulting fast filling by the pump (1 h to fill the basin to 2.5 m). Although in nature the uplift of the water table takes more time, this case was considered to be more dangerous to the dike structure compared to slower filling (due to higher gradient of pressures inside dike core).

43

The water was held in the upper basin, slowly infiltrating the dike core and subsequently:

- in a first (one-week) scenario, water was released from the upper basin after 6 days,
- in a second (two-weeks) scenario, a second flood peak was simulated and, finally, the water was released from the upper basin after 13 days.

The measurements of soil moisture were performed using dielectric moisture sensors EC-5. The sensors measure the volumetric water content (VWC) in the soil in order to obtain geotechnical parameters, such as the degree of saturation (S_r), which is calculated according to equation 5:

$$S_r = VWC/n \qquad\qquad (5)$$

with   VWC = volumetric water content

        n = porosity

Despite the controlling during the construction phase, it is impossible to have perfectly homogenous compaction in the dike core; as a result, a slight variation of porosity in the dike core is expected. The mean value of porosity in the dike was estimated to be n = 0.4 and this value was used to calculate S_r in the general case. The value n was adjusted for the lower moisture sensors when completely saturated by measuring the maximum value of VWC.

The moisture development in the one-week scenario is presented Figure AII.87 to Figure AII.90 in chosen time steps. The artefacts result from the linear interpolation between measurement points.

Although there is not much visual difference between pairs of graphs, one can notice a little higher line of the fully saturated region in the second experiment. Similar results were observed in the two-week scenarios of the experiments. This effect gets clearer if the water levels in the piezometers are compared at the same time in subsequent experiments as shown in Table AII.23.
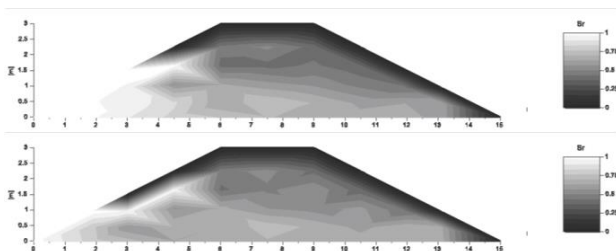
Figure AII.87. Maps of S_r at t=1h; experiment: No.1 (upper graph) and No.2 (lower graph)
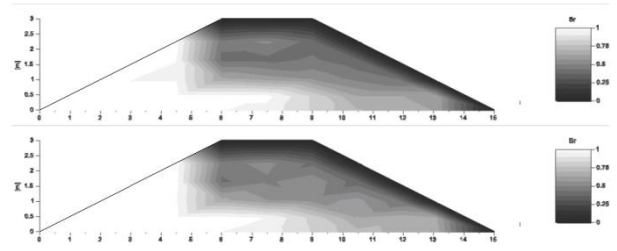
Figure AII.88. Maps of S_r at t=4h; experiment: No.1 (upper graph) and No.2 (lower graph)
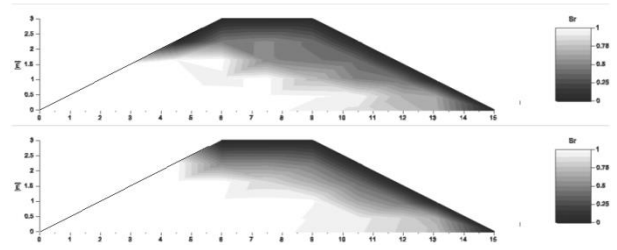
Figure AII.89. Maps of S_r at t=24h; experiment: No.1 (upper graph) and No.2 (lower graph)
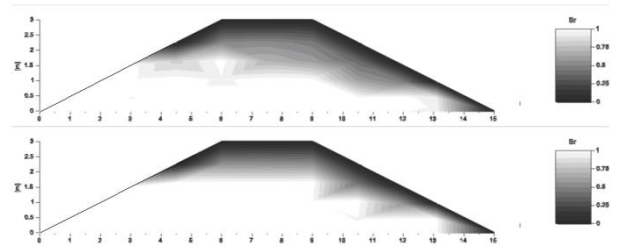
Figure AII.90. Maps of S_r at t=72h; experiment: No.1 (upper graph) and No.2 (lower graph)
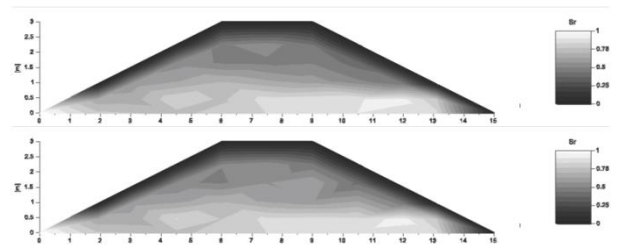
Figure AII.91. Maps of residual S_r at t=96h after water release in experiment: No.1 (upper graph) and No.2 (lower graph)

Table AII.23 shows the results of five experiments: two one-week series (No1, No2) and three two-week series (No3-No5) with the same first phase characteristics as the previous two experiments (Figure AII.86). There is not much difference after 6 hours between the all the waves. The variations in the first piezometer (P1) are caused by a different infiltration rate due to weather conditions in the upper basin at the beginning of the experiment. However, there are differences visible after 36 hours, especially in piezometer P4, where there is an increase in water level with each repetition of experiment. This behaviour may

Table AII.23. Water levels measured in piezometers in chosen experiments at given time

t = 6h				
Exp. No	P1 [m]	P2 [m]	P3 [m]	P4 [m]
No1	2.11	0.48	0.15	0.00
No2	2.26	0.51	0.21	0.00
No3	2.15	0.48	0.21	0.00
No4	2.03	0.32	0.10	0.00
No5	2.25	0.43	0.15	0.00
t = 36h				
Exp. No	P1 [m]	P2 [m]	P3 [m]	P4 [m]
No1	1.90	1.54	0.95	0.00
No2	2.10	1.77	1.19	0.18
No3	2.00	1.62	1.04	0.23
No4	2.01	1.73	1.28	0.44
No5	1.91	1.62	1.18	0.35

be an indicator of flushing out of small particles resulting in an increase of hydraulic conductivity of the dike core, but the study showed this is not the case. The reason of comparatively faster flow is residual moisture, which was generally higher after several repetitions of flooding; e.g. compare the residual moisture in experiments No1 and No2 on Figure AII.91. This effect results in a higher relative permeability in unsaturated flow and a relatively faster flow through the dike.

5.3. Overflowing experiments

Figure AII.92 illustrates the Polish research dike including the areas relevant for the overflowing experiments. A compilation of information about the sections used for the overflowing tests is given in Table AII.24.

Like in Rostock, the Gdansk experiments have been planned resembling a test series of the US National Transportation Product Evaluation Program NTPEP [25], (cf. Paragraph 2.2). Additionally, overflowing experiments were carried out on the unvegetated surface. Therefore, the top layer including vegetation was removed.

5.3.1. Test set-up and measurement techniques

Based on a modified NTPEP test set-up two parallel flume channels were installed on the embankment. Figure AII.93 shows the basic experimental set-up. Each flume has an inner width of 0.6 m and is separated into

Figure AII.92. Overflowing sections of the experiments in Gdansk, September 2014

Table AII.24. Information about the cross-section used for overflowing in Gdansk, September 2014

	Test section
Material	?
RECP	no
Slope (V:H)	1:2
Length [m]	6.7
No. test sections*	9
No. short term tests – vegetated	10
No. short term tests – unvegetated	8
No. long-term tests	-

* No. of test sections resp. measuring areas each flume is divided into

Figure AII.93. Basic experimental set-up of the Gdansk flume system

10 test sections. The flumes were made of form boards and each of these was fixed onto the slope surface and sealed with construction foam. Wooden slats serve as markings for the individual test sections.

On the dike crest the water inlets for discharge control were placed. The water delivery system included the Vistula (as reservoir), a large pump and flexible tubes (Figure AII.94), the sheet pile basin (Figure AII.95), steel shutters at the inlets (Figure AII.96) and a large runoff channel (Figure AII.97).

Figure AII.94. The pump delivers water into the sheet pile basin

Figure AII.95. Filled sheet pile basin

Figure AII.96. Closed water inlets

Figure AII.97. Runoff channel to lead the water back to the Vistula

The discharge for the overflowing experiments was regulated on the dike crest with steel shutters. Depending on the polder filling height and the opening width of the gate a flume target discharge could be adjusted. For peak discharges the pump delivered up to 750 m^3h^{-1}.

Figure AII.98. Runoff channel to lead the water back to the Vistula

Table AII.25. Grades to describe the slope surface reg. erosion [29]

Grade	Condition of test section
1	non-failure
2	initial failure
3	various damage
4	failure

Both the flow velocity and runoff depth were determined during the experiments. To measure the flow velocity a portable magnetic-inductive sensor was used on the dike crest and in every test section on the slope (Figure AII.98). The run-off depth on the dike crest and on the slope was measured using a ruler.

The erosion on the slope surface was determined with a pin-profiler (cf. Paragraph 2.2). Additionally, each test section was evaluated with grades between 1 and 4 (Table AII.25) before and after each overflowing test according to [29].

Photographic images of each test section were made before and after each test stage, which have been used to compare the slope surface conditions, e.g. regarding the vegetation coverage.

5.3.2. Test procedure and analysis

The experiments were carried out as follows:

- the initial state of the embankment was recorded (pin-profiling, marking, image & written documentation),
- the discharge was slowly increased by opening the shutters within approx. five minutes, to minimise the shock load on the soil surface,
- 45 minutes (vegetated) respectively 6 to 10 minutes (unvegetated) overflow with the target discharge,
- the flow velocity and discharge depth were measured in each test section and on the dike crest

- the shutters were closed, the residual water drained,
- the final state of the dike embankment was recorded including pin-profiling, marking, image and written documentation (also used as initial recording for the subsequent flow level or final recording for the whole test series) and
- the measured data was transferred to a record sheet.

The target discharges had to be chosen before the start of the test series. The limiting factors are the performance of the pump and the sizes of the sheet pile basin. Table AII.26 and Table AII.27 contain compilations of the mean discharge rates and the dependent variables measured and computed in September 2014.

The test record sheets had to be analysed afterwards. Therefore several values had to be calculated or recalculated to control the target values: (i) soil loss per test-section and cumulated for the whole flume, (ii) discharge, and (iii) shear stress.

5.3.2.1. Results and evaluation

Four large-scale field test series with a total of 18 individual overflowing tests were carried out at the Gdansk research dike in September 2014, including 10 short-term tests on the vegetated slope and 8 short-term tests on the unvegetated slope. The following tables show the final results of all short-term overflowing experiments in Gdansk, both vegetated and unvegetated (Table AII.28, Table AII.29).

During the overflowing experiments it was determined, that the clay layer also was built on the landward slope from the dike crest in direction to the dike toe for approximately 2.5 m, in contrast to the planned composition of the dike top layers (cf. chapter 6.1). Due to this structure big differences of the cumulated soil loss values between the upper and lower parts of the flumes

Table AII.26. Mean unit discharges (q), measured and computed hydraulic values (flow velocity (v), discharge depth (h), shear stress (τ)), Froude and Reynolds numbers, vegetated, Gdansk Sept. 2014

Stage	Ø q [ls⁻¹m⁻¹]	Ø v [ms⁻¹]	Ø h [m]	Ø τ [Pa]	Fr[1] [-]	Re[2] [-]
1	52	1.3	0.041	199	2.05	40,653
2/3	97	1.86	0.053	260	2.57	73,255
4	200	2.9	0.071	350	3.46	146,736
5	233	3.38	0.076	373	3.91	180,231

[1] *Fr* < 1: subcritical, *Fr* > 1: supercritical
[2] *Re* ≤ 2320: laminar, *Re* ≥ 2320: turbulent

Table AII.27. Mean unit discharges (q), measured and computed hydraulic values (flow velocity (v), discharge depth (h), shear stress (τ)), Froude and Reynolds numbers, unvegetated, Gdansk Sept. 2014

Stage	Ø q [ls⁻¹m⁻¹]	Ø v[1] [ms⁻¹]	Ø h [m]	Ø τ [Pa]	Fr[2] [-]	Re[3] [-]
1	41	n.m. [1]	0,020	98	n.c. [1]	n.c. [1]
2	116	n.m. [1]	0,050	245	n.c. [1]	n.c. [1]
3	153	n.m. [1]	0,053	261	n.c. [1]	n.c. [1]
4	172	2.89	0,051	250	4.08	110,868
5	204	n.m. [1]	0,066	321	n.c. [1]	n.c. [1]
6	500	6.67	0,077	378	7.66	359,417

[1] not measurable / not computable
[2] *Fr* < 1: subcritical, *Fr* > 1: supercritical
[3] *Re* ≤ 2320: laminar, *Re* ≥ 2320: turbulent

Table AII.28. Max. cumulative soil loss (CSL) and hydraulic forces, short-term tests series, vegetated, Sept. 2014

Flume	Max. CSL [cm]	Max. q [ls⁻¹m⁻¹]	Max. v [ms⁻¹]	Max. h [m]	Max. τ [Pa]
1	3.1	249	3.27	0.079	386
2	2.8	217	3.49	0.073	359

Table AII.29. Max. cumulative soil loss (CSL) and hydraulic forces, short-term tests series, unvegetated, Sept. 2014

Flume	Max. CSL [cm]	Max. q [ls⁻¹m⁻¹]	Max. v [ms⁻¹]	Max. h [m]	Max. τ [Pa]
1[1]	2.7	115	n.m. [2]	0.050	245
2	3.0	500	6.67	0.077	378

[1] Only two discharge stages
[2] Not measurable

Table AII.30. Max. cumulative soil loss (CSL) and hydraulic forces, short-term tests series with focus on the upper ("1 - 3") and lower ("4 - 9") test sections, vegetated, Sept. 2014

Flume	Max. CSL [cm]	Max. q [ls⁻¹m⁻¹]	Max. v [ms⁻¹]	Max. h [m]	Max. τ [Pa]
1 - "1 to 3"	1.3	249	2.74	0.097	474
1 - "4 to 9"	4.0	249	3.49	0.070	343
2 - "1 to 3"	2.3	217	2.61	0.093	457
2 - "4 to 9"	2.8	217	3.64	0.064	313

Table AII.31. Max. cumulative soil loss (CSL) and hydraulic forces, short-term tests series with focus on the upper ("1 - 3") and lower ("4 - 9") test sections, unvegetated, Sept. 2014

Flume	Max. CSL [cm]	Max. q [ls⁻¹m⁻¹]	Max. v [ms⁻¹]	Max. h [m]	Max. τ [Pa]
1 - "1 to 3"	3.3	115	n.m. [1]	0.050	245
1 - "4 to 9"	2.0	115	n.m. [1]	0.050	245
2 - "1 to 3"	3.0	500	6.92	0.098	482
2 - "4 to 9"	2.8	500	7.00	0.068	333

[1] not measurable

were measured. Thus, the results of these single flume parts will be presented separately. Hence, the focus lies on the upper test sections "1 to 3" and the lower test sections "4 to 9" (Table AII.30, Table AII.31).

The soil loss rates were compared with the shear stresses and the flow velocities from each flume, with focus on the upper and the lower parts of the flumes, for both vegetated (Figure AII.99, Figure AII.101, Figure AII.102, Figure AII.103) and unvegetated conditions (Figure AII.100, Figure AII.104, Figure AII.105, Figure AII.106). Due to the large amount of data, only the results regarding the shear stress are presented here. In addition, Figure AII.107 shows the image documentation of the slope surface development of flume no. 1. Because of the scattering of the measurement results, it was not possible to define a "best fit" trend line through the data points. Instead, a linear trend line was chosen for all charts to define the flume specific soil loss functions. The slopes of the trend lines describe the magnitude of the erosion rates (cf. 2.2.3): the steeper the trend line, the higher is the erosion rate.

The results for the vegetated slopes show during the discharge stages 3 to 4 ($q_{max} \approx 200$ ls^{-1}m^{-1}) low values of cumulated soil loss (CSL). Particularly in flume no. 1 a CSL of approximately 2 mm at a shear stress of τ ≈ 350 Pa is a very good result. But at the highest discharge level 5 the total failure of the slope surface suddenly occurred: the entire top layer including vegetation slipped away in test sections 4 to 9 on top of the Tefra cover (Figure AII.107). This explains the sudden and steep rise of the regression lines in Figure AII.99, Figure AII.101 and Figure AII.103. It also leads to the assumption that the connection between the vegetation layer and the dike cover is insufficient or even missing. In the contrary, the slope surface in flume no. 2 withstood the high forces. Here, a CSL of approximately 1.6 cm occurred at a shear stress of τ ≈ 360 Pa. Still, this value is higher than recommended in [26] (CSL$_{max}$ = 1.27 cm). Both test series show the initiation of erosion at a shear stress of about 200 Pa.

After the failure in flume no. 1, the vegetation layer was removed in the flumes and overflowing experiments were carried out directly on the clay (test sections 1 to 3) and on the Tefra mixture (test sections 4 to 9). In both flumes erosion started at shear stress of τ ≈ 100 Pa (Figure

AII.100). After two discharge levels in flume no. 1 a big amount of the clay layer slipped away and this test series was cancelled. Causes for the big amount of soil loss were the installed instrumentation for seepage measuring at exactly this location, the related wiring and only slightly compacted soil coverage. The material in flume no. 2 withstood 6 discharge stages, although CSL ≈ 3 cm was higher than the ASTM recommendation. Particularly in flume no. 2 it can be noticed that after the first discharge level a relatively large amount of soil was removed, but in the course of the following discharge levels the amount of cumulated soil loss rises moderately. This illustrates the modest slope of the regression lines in Figure AII.100 and Figure AII.105.

A major disadvantage of erosion measuring with the pin profiler is that the erosion is measured only at five points in the upstream part of a test sections but is valid as an average value for the whole test section. Therefore, every test section was rated with erosion grades (Table AII.25) before and after each flow event. Although no quantitative amounts of soil loss are determined, this method has the
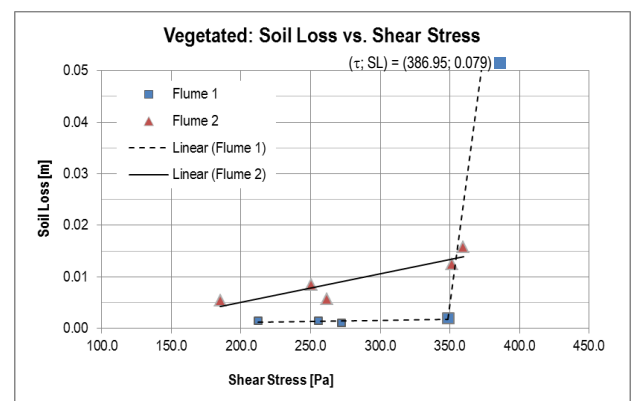
Figure AII.99. Erosion rates flumes 1 & 2 (vegetated); soil loss and shear stress, steep trend line = high erosion rate, Sept. 2014
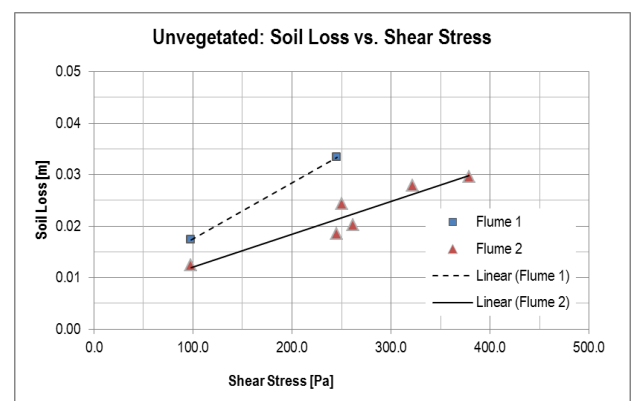
Figure AII.100. Erosion rates flumes 1 & 2 (unvegetated); soil loss and shear stress, steep trend line = high erosion rate, Sept. 2014
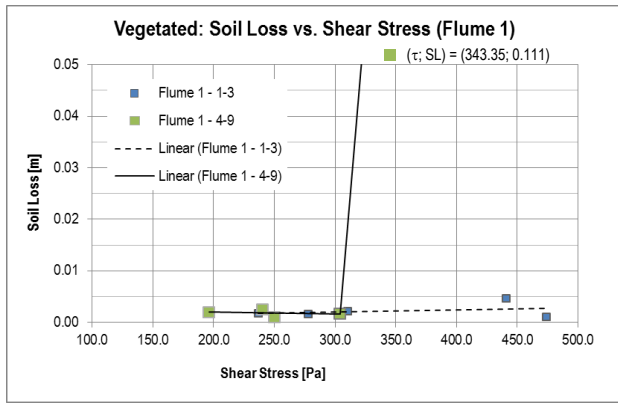
Figure AII.101. Erosion rates flume 1 (vegetated); soil loss and shear stress, steep trend line = high erosion rate, focus on the upper ("1-3") and lower ("4-9") flume parts, Sept. 2014
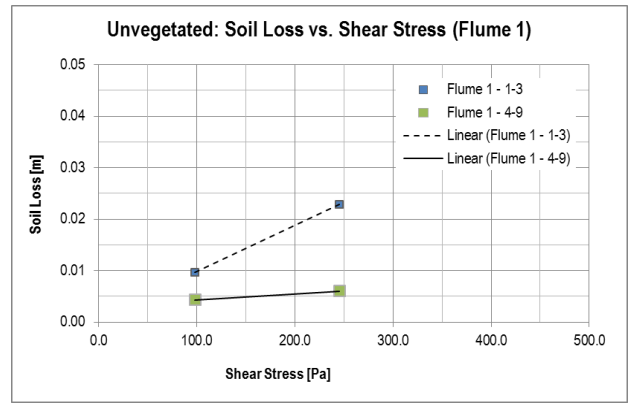
Figure AII.104. Erosion rates flume 1 (unvegetated); soil loss and shear stress, steep trend line = high erosion rate, focus on the upper ("1-3") and lower ("4-9") flume parts, Sept. 2014
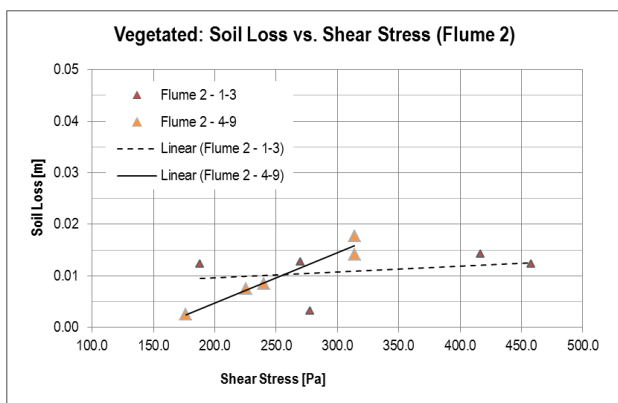
Figure AII.102. Erosion rates flume 2 (vegetated); soil loss and shear stress, steep trend line = high erosion rate, focus on the upper ("1-3") and lower ("4-9") flume parts, Sept. 2014
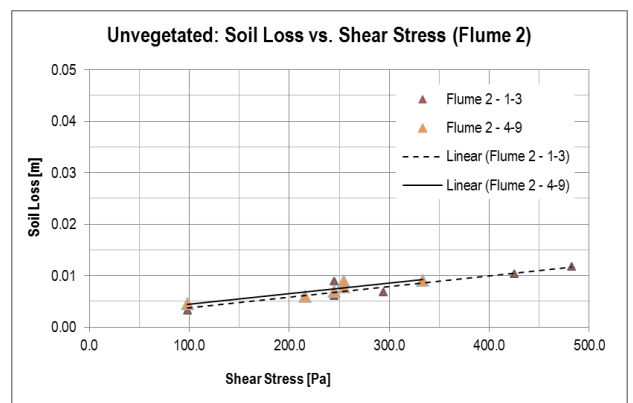
Figure AII.105. Erosion rates flume 2 (unvegetated); soil loss and shear stress, steep trend line = high erosion rate, focus on the upper ("1-3") and lower ("4-9") flume parts, Sept. 2014
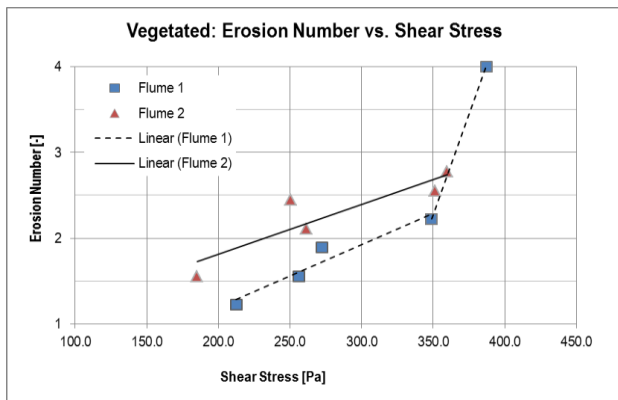
Figure AII.103. Erosion rates flumes 1 and 2 (vegetated); Erosion number (grade) and shear stress, steep trend line = high erosion rate
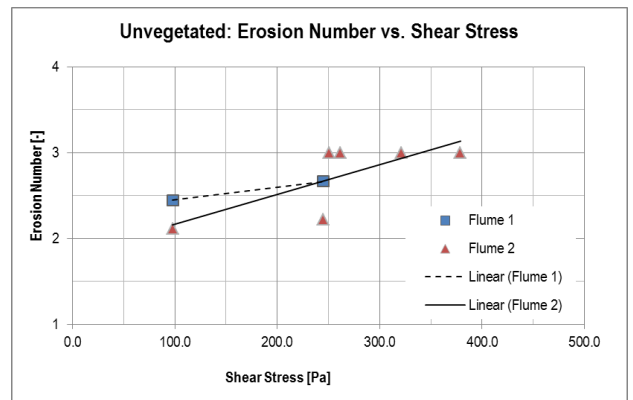
Figure AII.106. Erosion rates flumes 1 and 2 (unvegetated); Erosion number (grade) and shear stress, steep trend line = high erosion rate

advantage that the surface condition can be described fully with the grades "1" (non-failure) to "4" (failure). The erosion numbers were compared with the shear stresses for vegetated and unvegetated slope conditions (Figure AII.103; Figure AII.106).

The reasons for the high amounts of soil loss in both flumes and to the failure of the vegetation layer in flume no. 1 can be summarized as follows:

- Insufficient or no connection between the vegetation layer and the dike cover due to insufficient friction between the layers or missing root penetration.
- The use of rolled turf is inappropriate to construct a slope surface with a high resistance against erosion (weak connection of the soil layers, artificial rills etc.).
- Insufficient compaction of soil or layer parts increase instability and the removal of soil particles.

Flume No. 1
vegetated

| Original slope condition (Flume 1) | 1st load level (F1) $q \approx 54{,}4\ ls^{-1}h^{-1}$ $\varnothing v \approx 1{,}26\ ms{-1}$ $\varnothing h \approx 0{,}043\ m$ $\varnothing \tau \approx 212{,}55\ Pa$ | 2nd load level (F1) $q \approx 100{,}7\ ls^{-1}h^{-1}$ $\varnothing v \approx 1{,}95\ ms{-1}$ $\varnothing h \approx 0{,}052\ m$ $\varnothing \tau \approx 256{,}15\ Pa$ | 3rd load level (F1) $q \approx 109{,}0\ ls^{-1}h^{-1}$ $\varnothing v \approx 1{,}99\ ms{-1}$ $\varnothing h \approx 0{,}053\ m$ $\varnothing \tau \approx 272{,}50\ Pa$ | 4th load level (F1) $q \approx 187{,}1\ ls^{-1}h^{-1}$ $\varnothing v \approx 2{,}71\ ms{-1}$ $\varnothing h \approx 0{,}071\ m$ $\varnothing \tau \approx 348{,}80\ Pa$ | 5th load level (F1) $q \approx 249{,}3\ ls^{-1}h^{-1}$ $\varnothing v \approx 3{,}27\ ms{-1}$ $\varnothing h \approx 0{,}079\ m$ $\varnothing \tau \approx 386{,}95\ Pa$ |
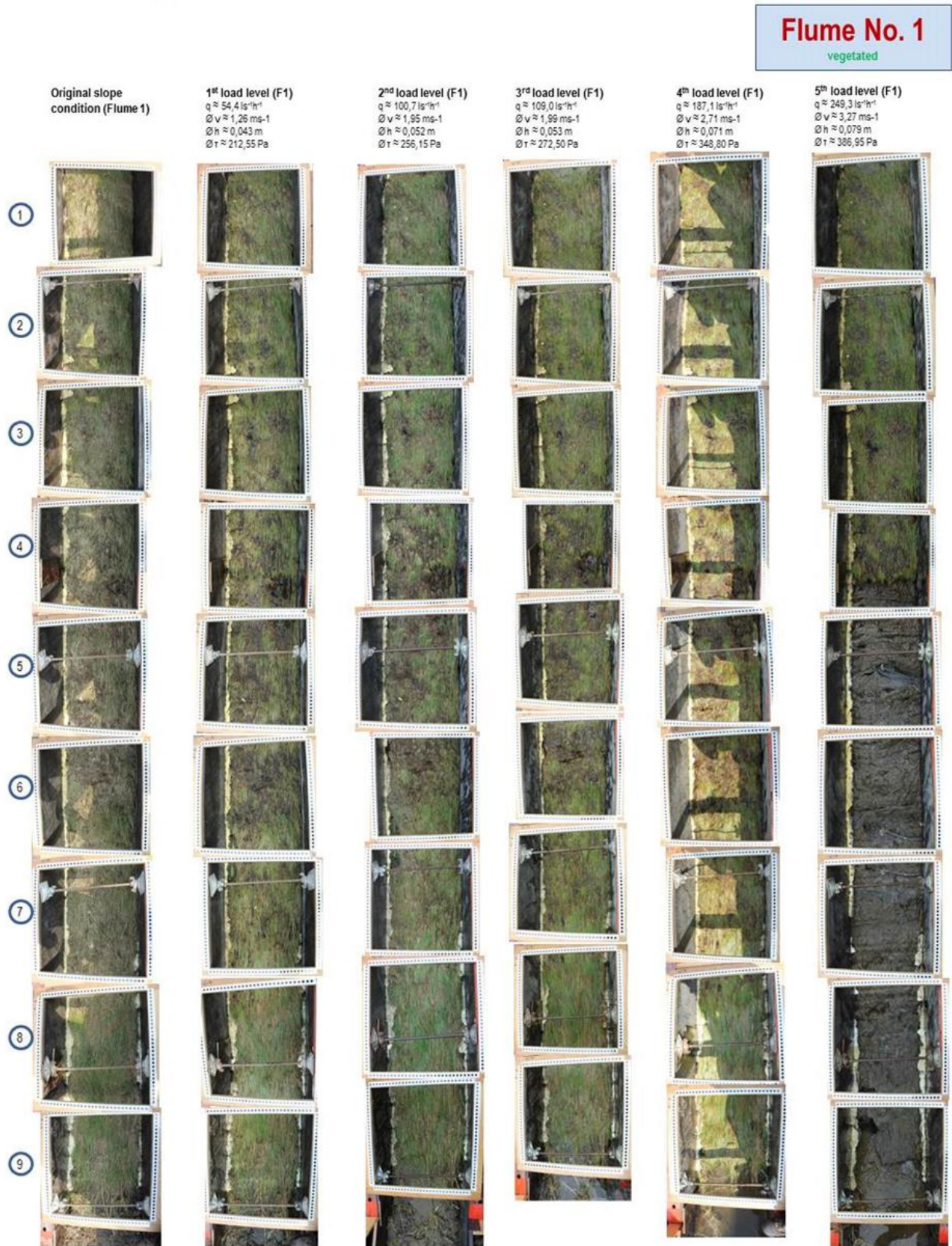
Figure AII.107. Development of the slope surface condition of flume no. 1. From left to right: initial state, after 1st target discharge, after 2nd target discharge, after 3rd target discharge, after 4th target discharge, after 5th target discharge. From toe to the crest: flow direction / numbered test sections.

5.4. Environmental analysis

There are numerous concerns on environmental aspects of using ashes in earth constructions. Some ecologists are suspicious to all CCPs, indicating high concentration of heavy metals and other toxic materials, increased radiation etc. In order to repel such speculations, ECOBA (European Coal Combustion Products Association) deputed environmental analyses to get the REACH certificate for ash-based products (cf. guideline Paragraph 3.2).

To address these issues within the DredgDikes project, several chemical analyses were made, both for components of the composite materials and for the filtrate water during seepage analysis. The samples of dredged sand and ash were tested on a chosen set of chemical properties closely related to environmental indicators and water purity indictors. Some results, related to heavy metal content in sand and ash, are presented in Table AII.32. Additionally, a sample of the sand ash composite was taken from the test dike and placed in the triaxial apparatus to obtain a leachate sample. The leachate was produced by saturating the probe and slowly circulate pure water through the sample. The Polish values of acceptable content (occupational exposure limit) are presented in Table AII.32 as a reference. These reference values are mandatory for most strict requirements of soil subjected to environmental protection and drinkable water resources, and it is mostly fulfilled by a margin of safety for this material. Moreover, one can observe much lower values of heavy metal concentration in leachate, compared to constituents; it confirms wide opinions of forming so-called ash matrix, as a result of developing cementation, which traps heavy metal molecules in the skeleton, thus not allowing them to be freely dissolved.

Table AII.32. Results of the chemical analysis of heavy metals in leachate from composite soil

		Sand	Ash	Leachate water	Reference value*
Pb	[mg/kg]	16.0	23.0	<0.2	50.0
Cd	[mg/kg]	<0.5	<0.5	<0.01	1.0
Cu	[mg/kg]	<2.0	30.0	<0.05	30.0
Hg	[mg/kg]	0.0018	0.0140	0.0009	0.5
pH	[-]	7.98	8.90	7.52	-

*Reference values taken from [47] - highest requirements for soils in protected areas and drinking water intakes

6. MODELLING AND COMPUTATIONS - POLISH RESEARCH DIKE

6.1. Seepage analysis

6.1.1. Steady state analysis

The research dike in this study was numerically modelled in the two-dimensional space (Figure AII.108) using the software Slide in version 5.0 [48]. With this program, it is possible to carry out a finite element based groundwater seepage analysis for saturated / unsaturated, steady state flow conditions.

Finite element numerical methods are based on the concept of subdividing a continuum into small pieces, describing the behaviour or actions of the individual pieces and then reconnecting all the pieces to represent the behaviour of the continuum as a whole. This process of subdividing the continuum into smaller pieces is known as discretisation or meshing. The pieces are known as finite elements. Discretization or meshing is one of the three fundamental aspects of finite element modelling (the other two are defining material properties and boundary conditions). Discretization involves defining geometry, distance, area, and volume. It is the component that deals with the physical dimensions of the domain.

The groundwater analysis in Slide is a finite element analysis, and therefore a finite element mesh is required in order to solve the problem. A three-noded triangles mesh is used to analyse the flow in the embankment, as shown in Figure AII.109.

After the finite element mesh has been generated, it is necessary to define the boundary conditions describing the groundwater problem. The boundary condition used in the model is *Total Head* (Figure AII.110). The total
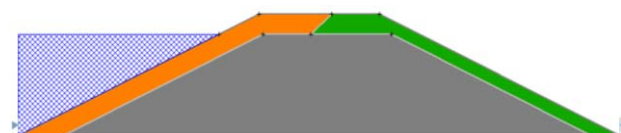
Figure AII.108. Model for groundwater analysis in Slide 5:0
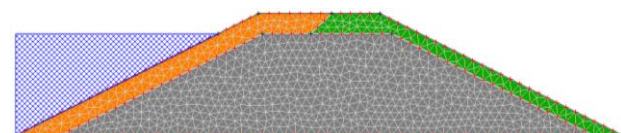
Figure AII.109. Mesh and discretization of the model

hydraulic head is made up of pressure head and elevation. The elevation represents the gravitational component. In equation form the total head is defined as:

$$H = \frac{u}{\gamma_w} + z \qquad (6)$$

Where:

H = the total head (m);

u = the pore-water pressure (Pa);

γ_w = the unit weight of water (kN/m^3);

z = the elevation (m).

$\frac{u}{\gamma_w}$ is referred to as the pressure head in units of length.

The total head hydraulic boundary condition defines the conditions that exist along the bottom of a reservoir: it is simply the elevation head at the top of the reservoir. For the test dike the maximum water level is 2.5 m.
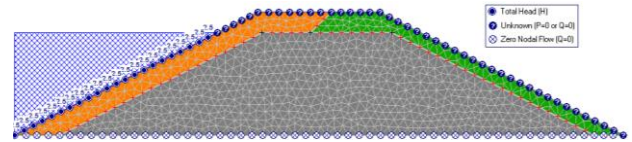
Figure AII.110. Boundary conditions

The slope surface on the right is given an unknown boundary condition; the bottom of the external boundary is given the *Zero Nodal Flow* boundary condition. The boundary flux Q = 0 indicates that no additional flux is going to be added or removed at these nodes. The Q = 0 condition does not allow the water to exit.

The hydraulic properties (permeability characteristics) previously specified for the materials were entered in the programme and the groundwater analysis was performed. Figure AII.111 shows the results.
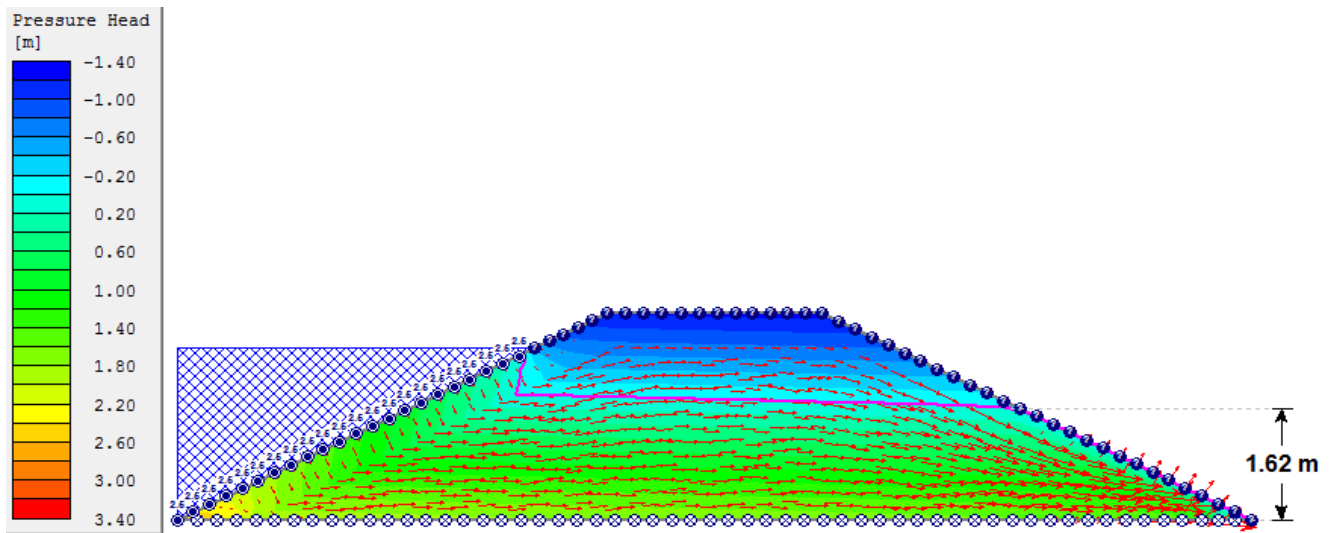
Figure AII.111. Groundwater analysis. Slope 1:2
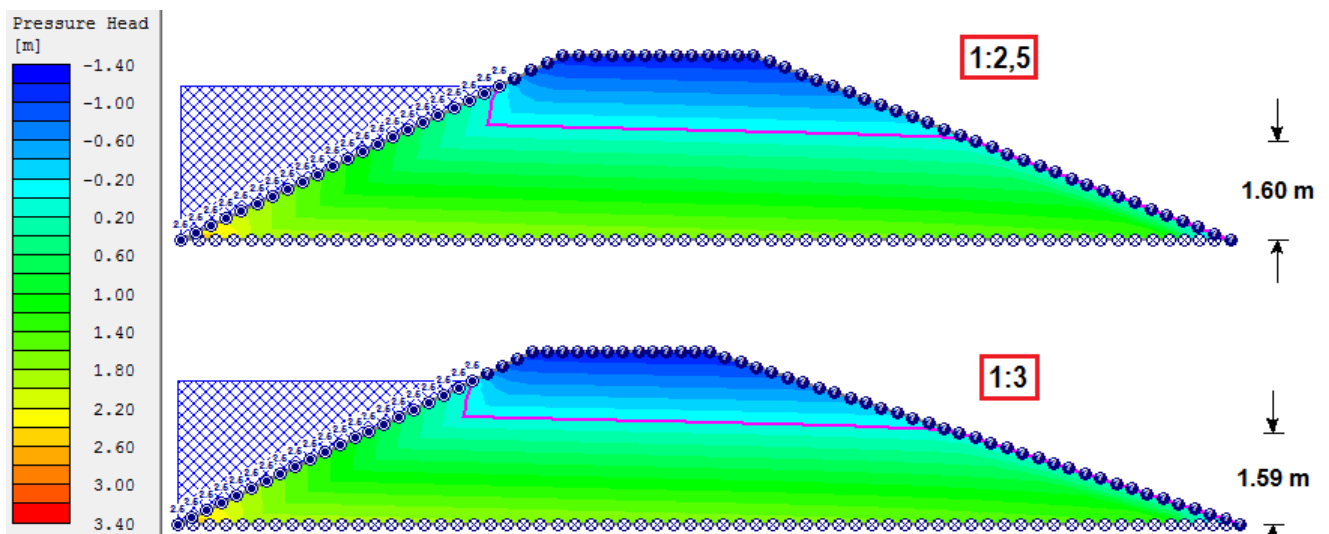
Figure AII.112. Groundwater analysis. Slopes 1:2.5 and 1:3
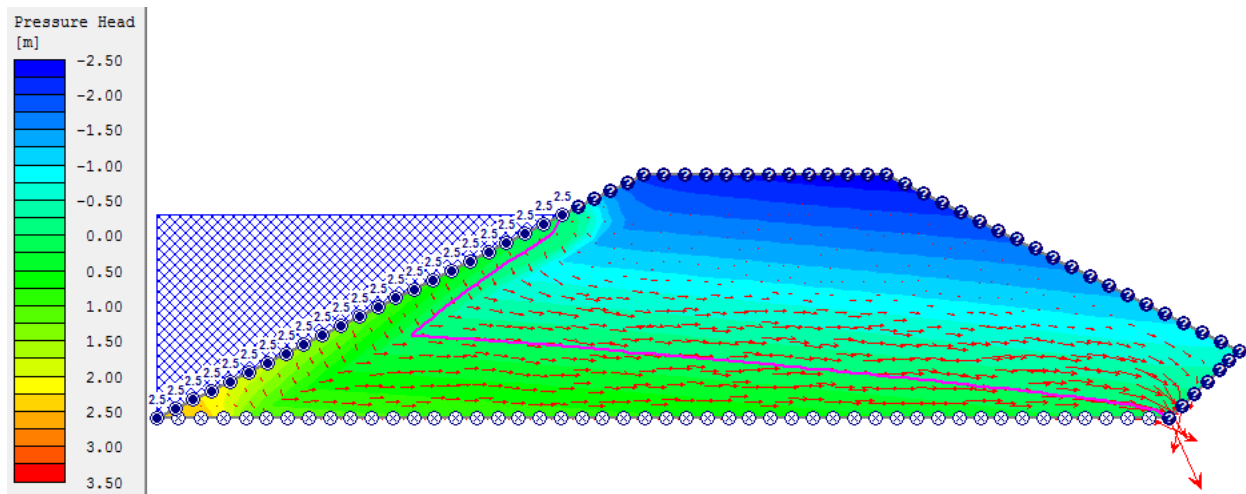
Figure AII.113. Groundwater analysis with toe-drain

The pink line is on the model charts highlights the location of the pressure head H = 0 contour boundary. For a slope model, this line represents the position of the water table (phreatic surface) determined from the finite element analysis. In the initial analysis the water table touches the external facing 1.62 m above the dike toe. Due to the high permeability of the material in the most central part of the embankment, the hydraulic load is not dissipated.

The toe of the embankment is under a high pressure, and if this is not dissipated, it may cause the removal of the external layer by uplift failure. The seepage coming through the dike above the ground surface (through seepage) is very detrimental: when seepage velocity is sufficient to move materials, internal erosion such as piping may be the result.

The analysis was performed again, to find a way to avoid the water spillage.

At first, the slope of the downstream side was changed: from 1V:2H, to 1V:2.5H and 1V:3H. As it is shown in Figure AII.112, this modification did not lead to acceptable results. The height of the water escape on the downstream slope could not be reduced considerably (1.62 m on the 1V:2H slope to 1.59 m with 1V:3H).

The second modification is the introduction of a downstream toe-drain in the embankment (Figure AII.114). The drain is so permeable compared to the other embankment materials that it does not contribute to the dissipation of the head (potential energy) loss through the structure. It is assume that the drain will be capable of removing all the seepage that arrives at the drain,

meaning that the drain will not be under positive pressure at any time (water pressure in the drain will be zero). Physically, the drain needs to exist in the embankment, but it does not need to be present in a numerical model. Only if the drain would clog with fines so that it begins to impede the seepage flow, the drain would need to be included in the numerical model.

The main boundary condition was again *Total Head.* The right slope surface and the drain were given the *Unknown* boundary condition; the *Zero Nodal Flow* boundary condition was defined for the bottom and the external boundary. The results using the same material permeabilities as in the above examples are presented in Figure AII.113. Obviously, this time the water table does not cross the external facing, but there is an important spill of water through the drain. This means that the system cannot achieve steady state conditions, or a seepage problem will occur.
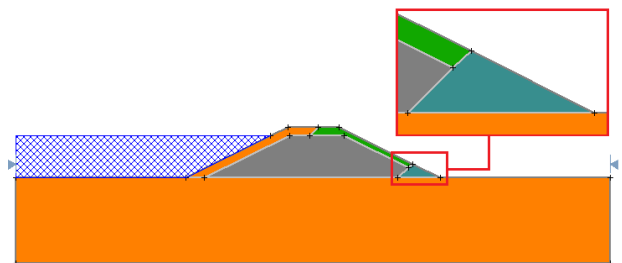
Figure AII.114. Toe-drain in the embankment
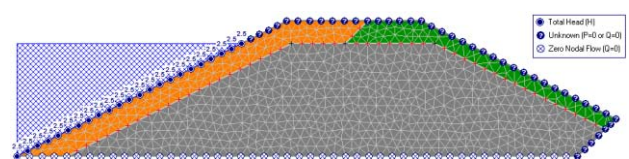
Figure AII.115. Modelling of the drain. Meshing & boundary conditions

6.2. Stability analysis – theoretical background

In the limit state analysis of stability, which is the conventionally used method to estimate safety factors for geotechnical problems, the failure mechanism is chosen by trials. Typically circular slip lines are assumed with different radii and centres. In the more advanced procedures the slip line can be combined from several arbitrary shaped segments reflecting the specific geometry of the analysed problem. However, the slip line is not chosen according to geomechanical equations; they are adopted on the base of intuition and experience of an engineer. It is also a problem of posing conditions of groundwater flow which influences the pore pressure distribution in the dike body and hence the effective stress state and shear strength of soils. The seepage line can be introduced directly or it can be obtained from numerical simulations of the groundwater flow through the dike.

In FE analyses the equilibrium of internal and external forces is controlled in every calculation step to not overshoot a specified error. If a failure mechanism occurs it is a result of overloading in the analysed system. For the dike structure we need, however, it is a quantitative estimation of the safety, i.e. a safety factor. In contrary to the limit state analysis, in FE simulations both deformation and stress states can be simultaneously taken into account. The methods of stability analysis proposed in the commercial geotechnical FE systems include:

- $\tan(\phi')$-c' reduction method, commonly known as ϕ'-c' reduction method; instead of increasing an external loading, the $\tan \phi'$ and c' are reduced incrementally in several calculation steps up to the loss of equilibrium. Then the following ratio is calculated as the safety factor: $F = (\tan(\phi') + c') / (\tan(\phi')_r + c_r')$
- c'/c_u reduction method, where only effective cohesion c' or undrained cohesion c_u is reduced up to the loss of equilibrium. This method can be applied for highly cohesive soils or in the undrained analysis of stability respectively.
- stress level method, where the safety factor is defined as a multiplier of a deviatoric stress invariant q which causes the loss of equilibrium when increased increamenttally.

Stability of dikes can be considered separately for the dike body and the global stability, including the soil ground conditions underneath the dike. An important issue in the FE stability analysis is the possibility of coupling between effective stress and seepage. This is possible with the use of the so-called pore pressure elements, sometimes denoted as u-p elements (u = displacement; p = pore pressure). In these elements additionally to the displacement degrees of freedom also pore pressures are stored. Generally u-p elements allow taking into account loading, effective stress changes and the consolidation process at the same time. They are also capable to be applied in the undrained analysis with the use of effective or total stresses.

Stability analyses of dikes should be performed at the critical stages for the equilibrium for the following cases:

- steady state flow through the dike under high water level with crest loading.
- transient flow through the dike after rapid drawdown of high water level with crest loading.
- two above cases without crest loading.

In the advanced FE analysis a realistic deformation and effective stress field in the dike cross-section can be obtained when using the appropriate constitutive model of soil behaviour and a suitable seepage model. In the constitutive model properly specified primary loading and unloading conditions are important. This allows applying a suitable stiffness which is highly dependent on the strain history, stress level and consolidation state (i.e. normal consolidation or overconsolidation). Among the models available in the commercial FE systems, the so-called cap-models assure at least that loading and unloading conditions during compression are taken into account. The elastic-plastic isotropic hardening cap models are usually implemented with nonlinear elastic stiffness based on the logarithmic or exponential compression laws (e.g. Hardening Soil Model).

Considering groundwater flow it is important to include partly saturated flow in the analysis. To this end the Soil Water Characteristic Curve (SWCC) is needed to describe hydraulic parameters of the groundwater flow in unsaturated zones. The most common model of partly saturated flow, where SWCC is used, is the model proposed by Van Genuchten. When analysing the dike behaviour taking into account partly saturated flow

usually pore water suction in the unsaturated zones occurs. Since it increases the effective stress level and hence shear strength it should be ignored when estimating the safety factor.

6.3. Slope stability analysis for the research dike

The slope stability was analysed using different methods. Let us assume the model made of bottom ash – (dredged) sand mixture with the same size as the test dike and consider the inner slope stability. Three different slopes (1V:2H, 1V:3H, 1V:3.5H) and effective cohesion of the mixture varying from 5 to 20 kPa are taken into account.

6.3.1. Analytical solution

It can be shown [49] that the equilibrium condition of a sliding mass can be expressed in terms of slope geometry parameters and effective shear strength parameters of the soil on the slope (Eq. 7):

$$\sin\beta + i\frac{\gamma_w}{\gamma'}\sin\lambda \leq \frac{c'}{\gamma'D\cos\beta} + \left(\cos\beta - i\frac{\gamma_w}{\gamma'}\cos\lambda\right)\tan\phi' \quad (7)$$

Let us consider the water flow parallel to the slope. In this case hydraulic gradient is equal:

$$i = \sin\beta \quad (8)$$

An infinite slope model is considered. One should notice the advantage of the equilibrium condition in Eq. 7, which takes into account granular soil with some effective cohesion. Such approach enables the analysis of the bottom ash – (dredged) sand composite, with a small effective cohesion increasing with time due to the cementation effect. The left side of Eq. 7 can be formulated as follows

$$L = \sin\beta \cdot \left(1 + \frac{\gamma_w}{\gamma'}\right) \quad (9)$$

while the right side of the Eq. 7 can be rewritten to

$$R = \frac{c'}{\gamma'D\cos\beta} + \cos\beta \cdot \tan\phi' \quad (10).$$

For cohesionless soils (c' = 0 kPa) Eq. 7 reduces to the well-known solution:

$$\tan\beta \leq \frac{\tan\phi'}{1 + \frac{\gamma_w}{\gamma'}} \quad (11)$$

Table AII.33. R/L ratio in cohesive soils for D = 1 m

Effective cohesion	1V:2H	1V:3H	1V:3.5H
c' = 5 kPa	1.37	1.93	2.22
c' = 10 kPa	2.12	2.93	3.36
c' = 20 kPa	3.63	4.94	5.64

The effective cohesion significantly contributes to the slope stability [49]. Left and right sides of the Eq. 7 were calculated for different slope inclination and effective cohesion for a given vertical soil depth D = 1 m. One should mention that the choice of the vertical soil depth, where the slippage occurs, is important for the slope stability in cohesive soils. It is assumed that the ratio length of the slope over D should exceed 20 in order to consider infinite slope length. The calculated ratio right to left side (R/L) is given in Table AII.33.

The results indicate a good stability of the considered slopes, assuming flow parallel to the slope. Additional analysis should needs to be performed for the water exit zone, where the flow lines are less inclined (more dangerous situation) and the requirements should be stricter.

6.3.2. Numerical analysis

The numerical analyses of the steady state flow through the dike were performed using the SLIDE 5.0 [48] and PLAXIS 8.2 [50] programs for FEM analysis. Calculations were made for a homogeneous dike built from ash-sand composite and for the covers on the slope. These analyses were performed with the soil parameters from above. The phreatic line (cf Figure AII.111) exits on the slope at elevation 1.62 m for the 1V:2H inclination. Similar results were obtained for 1V:3H and 1V:3.5H slopes. The slope stability was checked using the traditional Bishop method. For a given slope inclination the shape of the phreatic line obtained in FEM calculation was introduced to the model analysed with Discontinuity Layout Optimization (DLO) [51]. The latter is a new numerical method [52] which automatically identifies the critical configuration of sliding soil blocks at failure. It finds the true critical slip-line failure mechanism for any geotechnical problem. The calculation can be performed for and adequacy factor on load or an adequacy factor on strength. The latter approach was used for slope stability calculation. Here, both effective angle of internal friction

and effective cohesion are divided by the strength adequacy factor F to identify the critical slip line – failure mechanism.

The results of the DLO analysis with sliding blocks at failure for different slope inclination and effective cohesion are given in Figure AII.116 to Figure AII.123. General failure conditions are observed when the overall stability is satisfied (e.g. Figure AII.117, Figure AII.119). When an unstable slope is detected (adequacy strength factor F less than or close to 1) an unrealistic bloc sliding mechanism is observed (Figure AII.116, Figure AII.118, Figure AII.121).

The sliding block pattern does not enter the compacted clay substratum due to its high strength resistance. The sliding occurs on top of the clay layer. The DLO analysis confirms the influence of the effective cohesion within the dike body on the failure mechanism and the dike safety. The influence of the inner slope inclination is also important. For a small cohesion, i.e. c' = 5 kPa, the dike models present unstable behaviour, regardless of the considered slope inclination. This finding is contradictory to the analytical solutions for an unconstrained slope (cf. Table AII.33). Similar levels of safety are obtained for higher cohesion, however with different failure mechanisms.

Figure AII.116. Strength adequacy factor F, 1V:2H, c' = 5 kPa, F = 0.692 (unstable)
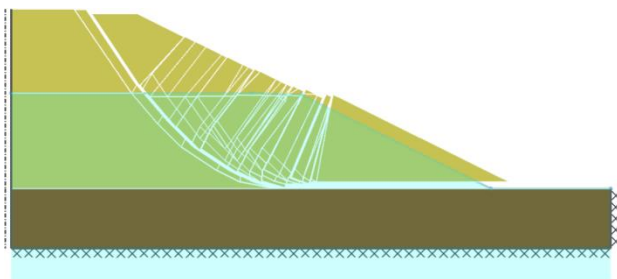
Figure AII.117. Strength adequacy factor F, 1V:2H, c' = 10 kPa, F = 2.309
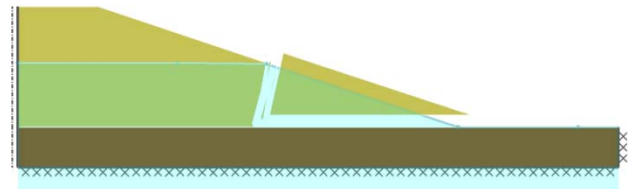
Figure AII.118. Strength adequacy factor F, 1V:3H, c' = 5 kPa, F = 0.955 (unstable)
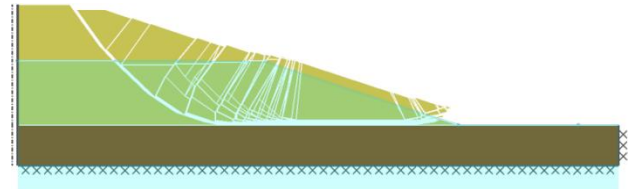
Figure AII.119. Strength adequacy factor F, 1V:3H, c' = 10 kPa, F = 2.606
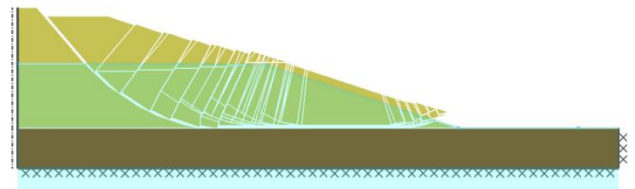
Figure AII.120. Strength adequacy factor F, 1V:3H, c' = 20 kPa, F = 5.162

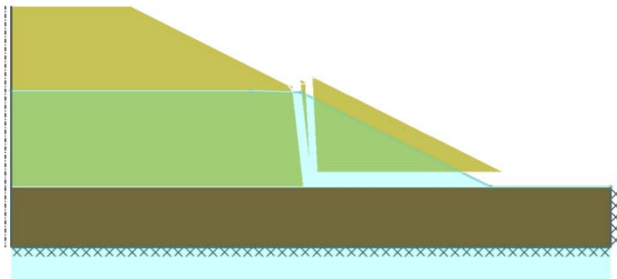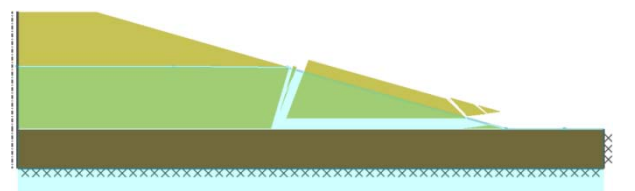*Figure AII.121. Strength adequacy factor F, 1V:3.5H, c' = 5 kPa, F = 1.073 (unstable)*
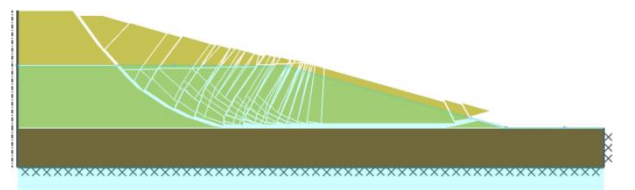
Figure AII.122. Strength adequacy factor F, 1V:3.5H, c' = 10 kPa, F = 2.856
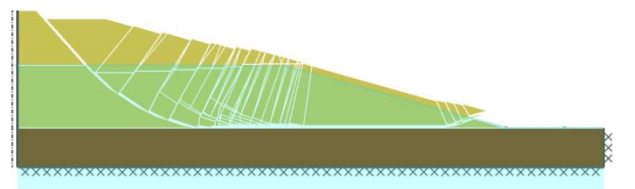
Figure AII.123. Strength adequacy factor F, 1V:3.5H, c' = 20 kPa, F = 6.055

7. INVESTIGATIONS AT THE PILOT DIKE

7.1. The pilot dike

The DredgDikes pilot dike is located at the stream "Körkwitzer Bach" in Neuheide, approximately 30 km north-east of Rostock. The dikes along the stream should protect the villages of Neuheide and Klockenhagen as well as the agricultural land in the proximity from flooding, both resulting from high water levels of the lagoon "Saaler Bodden / Ribnitzer See" and from upstream. However, it had deteriorated during the past decades and at some places the flood embankment is still nearly level with the surrounding areas as a result of major settlements caused by the soft peat ground. Therefore, the municipalities are in favour of a reconstruction of the whole dike system, which is, however, very expensive. On the other hand, the banks of the stream are FFH protected areas (Figure AII.124) which is why the nature protection authorities would rather keep the dike low and permeable and which made the planning particularly difficult. Finally, the authorities approved the proposal of the reconstruction of 500 m of the old dike, protecting the village of Neuheide, at the north-western corner of the stream on the western bank. This pilot investment should prove that the construction with a suitable ripened dredged material is possible and also cost effective.

There is a comprehensive study for the reconstruction of the whole dike length on both banks of the stream prepared by the local planning bureau WastraPlan [53] on which the plans for the pilot section are based. Together with the DredgDikes lead partner and the water and soil association "Untere Warnow – Küste" the standard cross-section was developed (Figure AII.125). The same
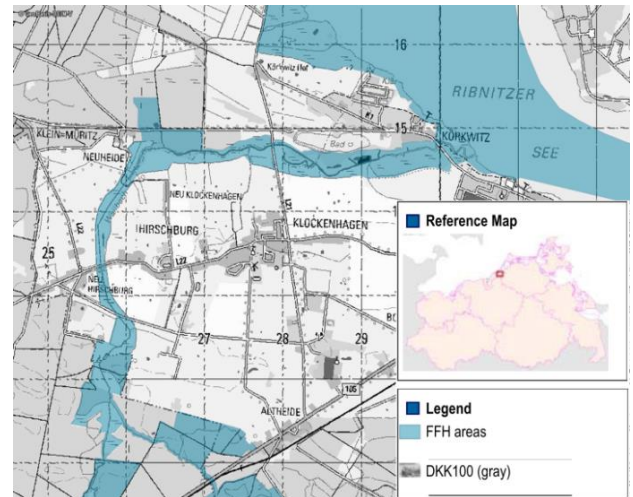
Figure AII.124. Location of the Körkwitzer Bach and FFH areas along its banks (GeoBasis-DE/M-V)

planners were subcontracted to prepare the permission documents and execution plans and to supervise the actual construction works.

On 27 November 2013 the construction of the pilot dike started. At first the drainage trench parallel to the dike was relocated because the reconstructed dike partly rests on top of the old trench filled with soil from the old dike. Then the old dike was removed in sections and the construction road was built on top of the woven geotextile placed on the formation. Since the sandy gravel material used for the construction road has a low erosion resistance, part of the cover material was placed at the banks for erosion protection. Both the sand and DM were compacted using a sheep's foot roller compactor. The construction road was finished by 20 December 2013.

Works were resumed on 13 January after a particularly warm and wet period; however, high water and ice impeded further construction until the end of March (Figure AII.126, Figure AII.127). The construction was completed at the end of April 2014 (Figure AII.128).
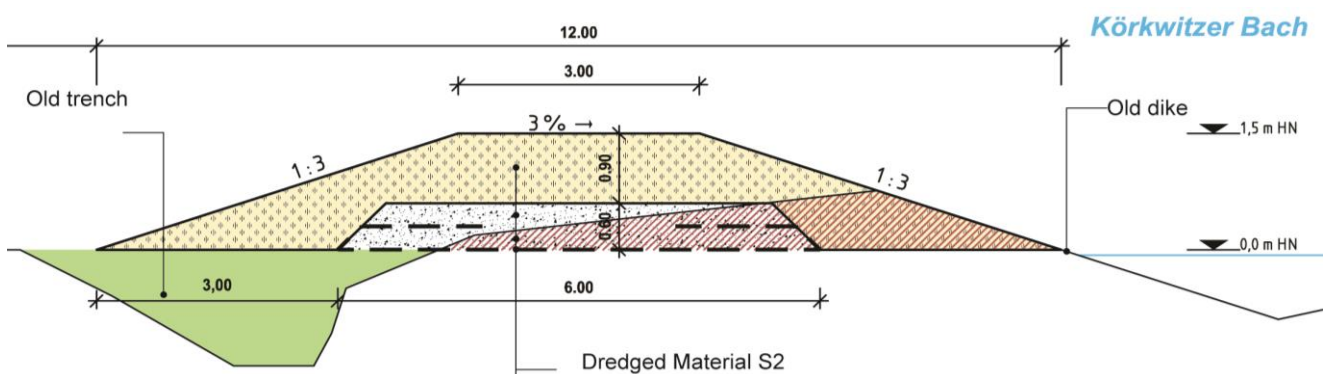
Figure AII.125. Standard cross-section for the reconstruction of the dike at the Körkwitzer Bach (WastraPlan 2013)

Figure AII.126. Flooded construction site 01-2014

Figure AII.127. Frozen construction site 02-2014

Figure AII.128. Completed pilot dike 05-2014

Figure AII.129. Compaction control in the cover layer made of dredged material 04-2014

The investigation at the pilot dike include the installation technology and the installed material quality, seepage through the dike by means of both logged and manually measured standpipes, vegetation monitoring and deformation monitoring. Therefore, a variety of instruments and standpipes were installed, together with a data logger that can be accessed from distance.

7.2. Installation monitoring

During the construction, the installation quality of the cover material was controlled. Therefore, the degree of compaction, the vane shear strength and the uniaxial compression resistance (using a pocket penetrometer) were determined and dynamic plate load tests were performed (Figure AII.129).

The installation quality was generally good and in conformity with the recommendations in the guideline. The degree of compaction was generally above the thresholds recommended in the guideline, Chapter 5 (Figure AII.130, Figure AII.131) and the initial shear strength determined with the field vane tester was above 50 kN/m² with a median value of 115 kN/m² (Figure AII.132). According on DIN 19712 material S2 would not be suitable as dike core material because of the organic matter content of OM > 4 %, although it has been proven that the OM is stable in the long term according to the AT_4 test [54]. However, it is in line with the guideline recommendations (cf. above). The water permeability is also sufficiently low.

The dredged material S2 is similarly fine-grained as material M2, thus there is a risk of shrinkage and surface cracking during dry periods. On the pilot dike there was some cracking visible before the vegetation established. However, the cracking was not as severe as on the research dike (cf. above). Initially, technological measures were planned to mitigate the cracking problem, e.g. by tilling and re-compacting the surface according to [38]. This was not necessary to the date of publication of this document.

The pilot dike will be subject to long-term monitoring and investigations. In the frame of the monitoring programme samples from the dike will be analysed in the geotechnical laboratory of Rostock University, Chair of Geotechnics and Coastal Engineering.
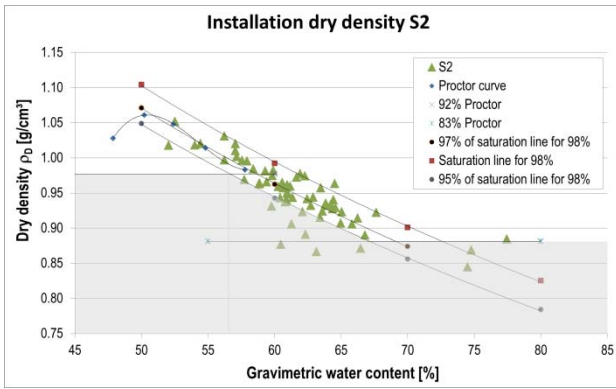
Figure AII.130. Installation dry density of material S2 on the pilot dike compared with the proposed quality control method from the guideline
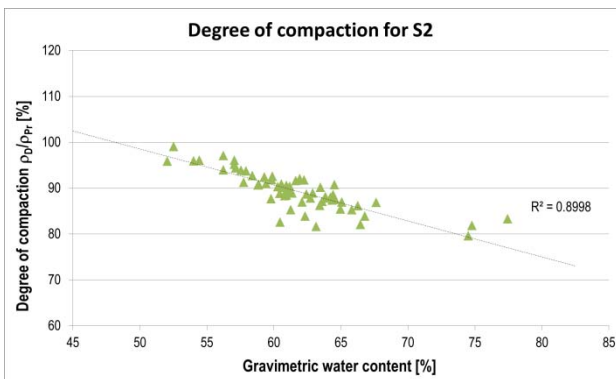
Figure AII.131. Evaluation of the degree of compaction of S2 on the pilot dike with ρ_{Pr} = 1.062 g/cm³
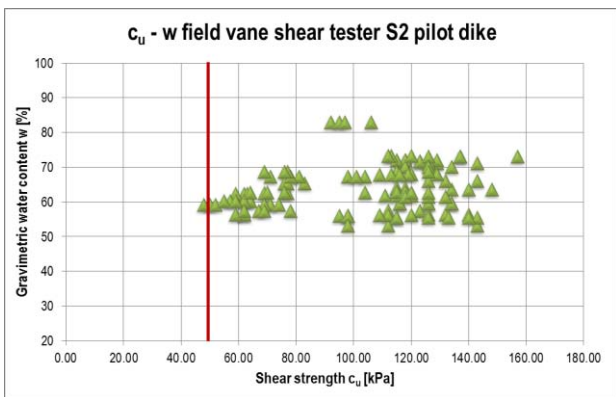
Figure AII.132. Shear strength as determined with a vane shear tester and associated water content during installation of S2 on the pilot dike

7.3. Instrumentation and measurements

The pilot dike has been instrumented with a variety of sensors. Wires and aluminium strips were placed underneath the dike (Figure AII.133) and between the sand core and the DM cover. In this way the thickness of the different layers can be determined using a cable detection device and the georadar method. Additionally, the surface deformation is recorded with geodetic methods.

Figure AII.133. Construction of the dike core with geosynthetic reinforcement and wire placement underneath the dike 12-2013

To control the seepage through the dike body standpipes have been installed every 50 m from the crest down to the gravel core of the dike. Also, a representative section has been equipped with tensiometers in the cover layer to receive information about the saturation of the dredged material. Together with water level gauges on both sides of the dike (water level of the *Körkwitzer Bach* and of the drainage trench on the western side) as well as precipitation and temperature sensors (both air and soil temperatures) the instrumentation generates data that can be used for future modelling of the system.

7.4. Vegetation monitoring

The vegetation monitoring is comprehensively covered in a project report [55] about the environmental and vegetation assessment for the pilot dike. The main results are that the greening developed quicker on the dike crest than on the embankments, due to seed dislocation on the slopes as well as other factors, such as wind and a long dry period following the seeding in mid-April 2014, which is more problematic on slopes than on a horizontal surface. During the first summer, the intrinsic seeds (salt bush etc.) grew intensively. Only after they were cut and some bare areas were re-seeded the actual grass cover was established in autumn 2014. Then, the vegetation closed quickly, providing a good erosion protection cover before the winter.

In an additional seeding test on the pilot dike embankments with variations in surface preparation and different initial fertilizer donations it could be shown that with a well-chosen seeding date the grass develops quickly and well and a fertilizer donation is not necessary on the investigated DMs.

8. ADDITIONAL INSTALLATION TEST FIELD IN ROSTOCK

In July 2014 an additional installation test field was built on Rostock's municipal DM processing plant to add to the knowledge of the earlier installation test field from 2011 and the installation tests on the research dike. In the previous tests, the installation water contents varied extremely which is why the determination of differences between the technologies was difficult. Therefore, materials with a low range of water contents were used (S2 and MB12). The test field consists of 15 test plots with 5 x 5 m² each. Material S2 was installed as it was delivered from the storage heaps and both materials were installed after homogenisation with a screener shovel (SH, MB12) – both to reach a more reliable average water content and to investigate the effectiveness of homogenisation regarding installation, stability, etc. Four different compaction technologies were used (excavator shovel only, excavator tracks only and roller compactors with 1.5 t and 16 t respectively). In the fifth variation the upper 30 cm were mixed with coconut fibre to investigate the reinforcement effect of the fibres in situ after the positive results from the lab investigations (Chapter 1). The plan can be seen in Figure AII.134.

8.1. Compaction technology

8.1.1. Compaction with the excavator shovel [S]

The compaction with an excavator shovel is sometimes used on steep slopes when an embankment cannot be accessed with other compaction machinery without danger. At some points on the Rostock DredgDikes research dike this technology was used, particularly at the crest when the excavator used the surplus material from slope profiling to be installed at the top of the dike where it was difficult to drive with the roller compactor. Therefore, this technology was investigated regarding its effectiveness. It was assumed that the compaction would always be too low and that the desired cu values would not be reached. In the field test the compaction with the shovel was realized by pressing it vertically to the ground (min. 5 times), while the small compacted areas were overlapped to reduce the possibility of lower compaction areas (Figure AII.135). The applied compaction pressure was approx. 39 kN/m².
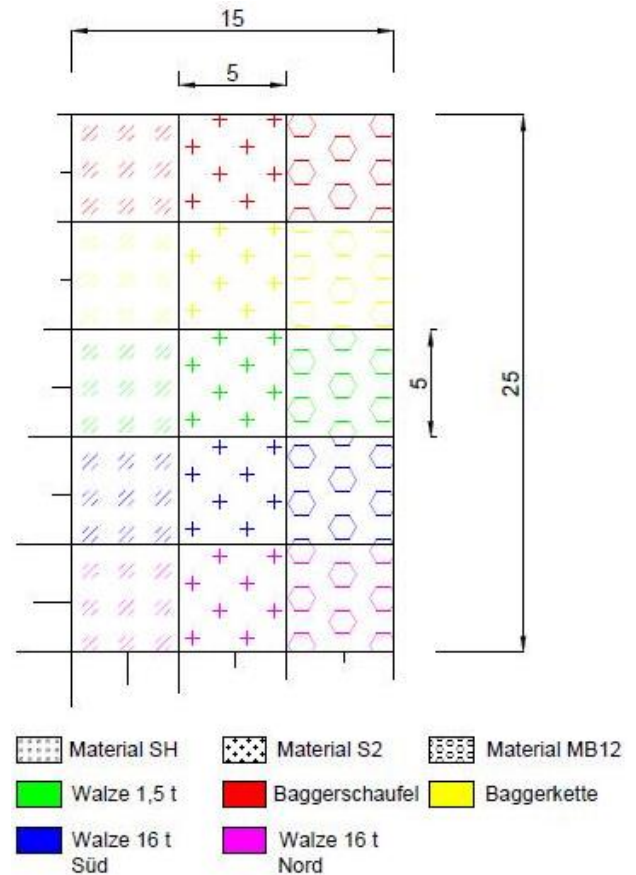
Figure AII.134. Plan of the installation testing field 2014

Figure AII.135. Compaction with the excavator shovel only

8.1.2. Compaction with the excavator track [BK]

A second compaction method was performed with the excavator as a replacement for a bulldozer track (to save cost on the test field). The compaction energy was introduced by the self-weight of the excavator via the tracks. The pressure underneath the tracks was approx. 54 kN/m². Six crossings were realised with an overlapping of the already compacted areas of 15 cm. This method should stand for the bulldozer compaction on the research dike (Figure AII.136).

Figure AII.136. Compaction with the excavator tracks only

Figure AII.137. Sheep's foot compactors 16 t and 1.5 t

8.1.3. Compaction with sheep's foot compactors

The use of vibrating compactors is the standard method for the installation of earth materials in geotechnical engineering. The important factors for a successful compaction are the weight of the machine, the oscillating mass which is separated from the machine, its frequency and amplitude, and the working speed of the machine. Roller compactors without vibration often have an effective compaction depth of only 20 cm while the vibration increases this depth to approx. 50 cm.

For the DM used the compaction with vibration only is not possible since the cohesion is considerable. Therefore, a kneading device is needed (Figure AII.137).

Two different sheep's foot roller compactors were chosen: a small hand operated machine of 1.5 t with a continuous speed and vibration control and a working width of 1.0 m. The maximum working pressure is 61 kN/m². The large compactor is a 16 t machine with a working width of 2.5 m and a working pressure of 167 kN/m². For both types of compactors, 6 crossings were defined with an overlapping of 15 cm to the respective previous course.

8.2. Homogenisation

Both the homogenisation and the mixing with fibres to reinforce the DMs were realised with ALLU screener crusher attachments for excavators. Part of the material S2 was homogenised, stones and large clay clots were removed. The screener crusher has a weight of 1,600 kg and a volume of ca. 1.2 m³. The screener crusher has two rotating drums with fixed blades (Figure AII.138) which can crush clay clots and smaller stones. All material that is not crushed is held back in the screener shovel to be separately deposited. The 250 m³ of homogenised DM needed for the tests were produced in half a day (Figure AII.139).

Figure AII.138. Drum with blades of the screener crusher

Figure AII.139. Soil homogenisation with screener crusher

8.3. Stabilisation with coconut fibres

Based on the laboratory experiments in which the fibre reinforcement of the DMs was investigated in the uniaxial compression test to find a suitable mixture of DM and fibres, the production of the mixture was planned for the field tests.

Figure AII.140. Drums of the screener bucket for fine screening

Figure AII.141. Mixing of fibres and DM with the screener bucket

Figure AII.142. Good fibre distribution in the DM

The coconut fibre that was chosen for the initial reinforcement of the DM with respect to the workability, compactibility and particularly regarding an initial effect to reduce shrinkage cracking, was delivered in large bales. The fibre length was 20-50 mm. The bales were difficult to break up on the construction site. The screener crusher used for homogenisation of the DMs could not break up the clots and thus the fibre distribution in the DM was insufficient. Therefore, a second screener shovel

(screening bucket) for fine screening was delivered with a volume of 0.6-0.7 m³ (Figure AII.140). However, this did not improve the process much. Then, the fibre bales were manually broken up by hand before the screening bucket was used to mix them into the homogenised DM (Figure AII.141). However, the maximum achieved degree of fibres in the mixture was below 1.0 %, while 1.5 % were planned based on the laboratory results. The fibre-DM mixture showed a good fibre distribution (Figure AII.142) but with additional fibres formed clots and blocked the screener bucket.

8.4. Laboratory analyses

The field test was supported by a laboratory analysis programme as presented in Table AII.34. For the determination of the fibre concentration there is no standardised method. The coconut fibres are organic matter that could be determined as a loss on ignition (LoI). However, since the organic matter and lime content

Table AII.34. Overview of the used test methods

Laboratory testing	Field investigation
Proctor density and optimal water content DIN 18127	Density with undisturbed samples DIN 18125-1
Plasticity parameters / Atterbert limits DIN 18122	Shear resistance with vane shear tester DIN 4094-4
Shear parameters – direct shear test DIN 18137-3	Shear resistance with pocket penetrometer DIN 18136-2
Grain size analysis DIN ISO 11277	Ev2-value with dynamic plate load test DIN 18196
Water content DIN 18121-2	Water content DIN 18121-2
Loss on ignition DIN 18128	
Lime content DIN 18129	
Fibre concentration*	

* not standardised

Figure AII.143. Dried fibre and soil mixture during sieving

in the DMs is considerable and the fibre concentration is comparably small (< 1 % grav.) this method which was not possible. The standard deviations of the LoI are often larger than the fibre content. Therefore, the samples were sieved using four different sieves (4 mm, 2 mm, 1 mm, 0,4 mm) to separate the soil from the fibres (Figure AII.143) after drying in the oven for 2 days at 60°C.

8.5. Results

The shear strength was measured in situ with a vane shear tester and a pocket penetrometer. Both methods show comparable results (Figure AII.144 and Figure AII.145; Figure AII.146 and Figure AII.147). T Figure AII.148 shows that the achievable compaction was independent on the existing water content (mainly between 25 % and 40 % for material MB12). Therefore, the strong dependency on the installation method as shown in the previous four figures is reliably. Based on this data, the compaction with an excavator shovel

showed considerably lower shear strength values than the other methods. The investigations show that the compaction with a heavy sheep's foot compactor is the best solution, however, depending on the material, the compaction with a hand held compactor or the tracks of a heavy machine (bulldozer, excavator) can be nearly as good. Thus, the technology needs to be chosen in a test field (cf. guideline Chapter 5).

Figure AII.146. Shear strength of material MB12 determined with a vane shear tester (median, 1st and 3rd quartile, min and max)

Figure AII.147. Shear strength of material MB12 determined with a pocket penetrometer (median, 1st and 3rd quartile, min and max)
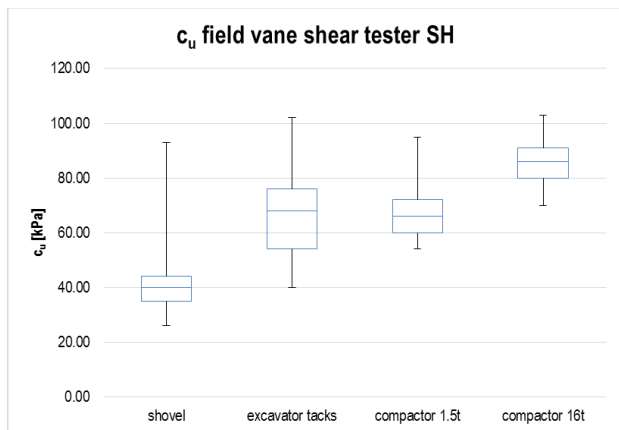

Figure AII.144. Shear strength of material SH determined with a vane shear tester (median, 1st and 3rd quartile, min and max)
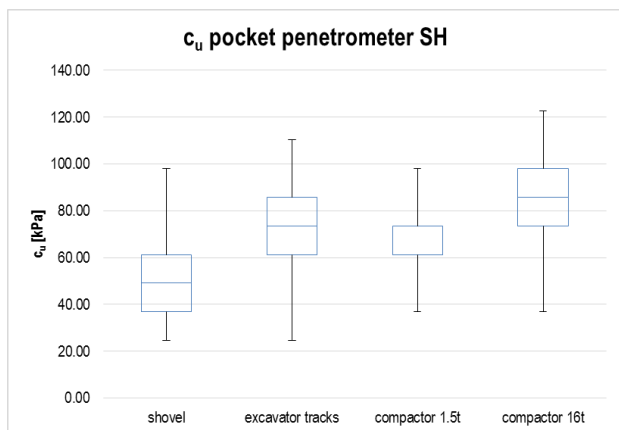

Figure AII.145. Shear strength of material SH determined with a pocket penetrometer (median, 1st and 3rd quartile, min and max)
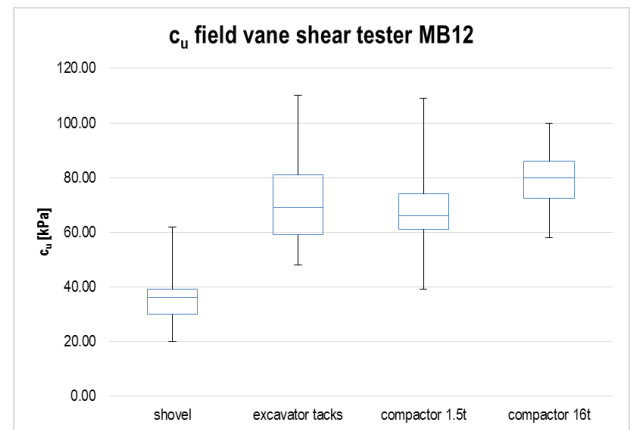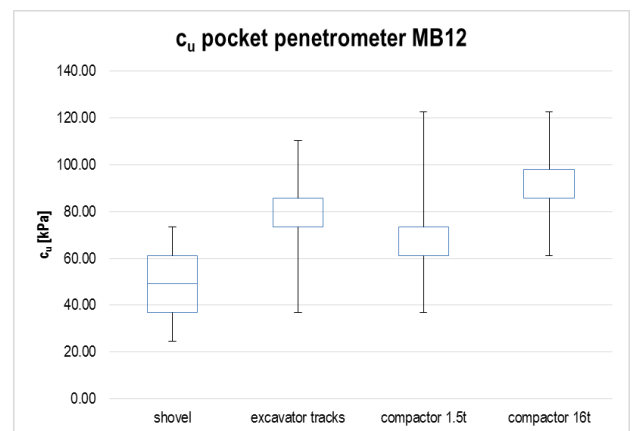

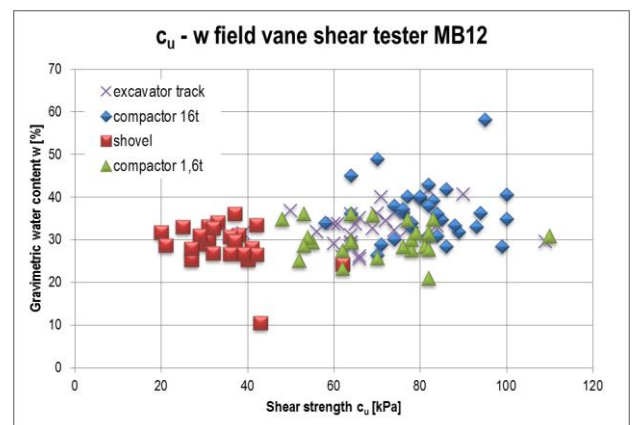*Figure AII.148. Shear strength and water content for material MB12*

REFERENCES

[1] Henneberg, M. & Neumann, R. 2014 Environmental and vegetation assessment report, DredgDikes component 4. Project report.

[2] Große, A.-K. & Saathoff, F. 2014: Geotechnical characterization of different fine-grained, organic dredged material batches from the Baltic Sea area - Peculiarities and adaptations, *Proceedings of the South Baltic Conference on Dredged Materials in Dike Constructions*, 10.-11. April 2014, Rostock, 12 pp.

[3] RPW 2006. Guidelines for the Testing of Mineral Liners in Waterways Engineering, EU-Notifizierung Nr. 2006/370/D vom 23.10.2006.

[4] Weißmann 2003. Die Widerstandsfähigkeit von Seedeichbinnenböschungen gegenüber ablaufendem Wasser [The resistance capacity of landside sea dike embankments against overflowing water], Mitteilungen aus dem Fachgebiet Grundbau und Bodenmechanik. University Duisburg-Essen. 147 pp.

[5] Große, A.-K., Cantré, S. & Saathoff, F. 2015. The applicability of disintegration tests for cohesive organic soils. Journal of Environmental Engineering and Landscape Management 23(1):1-14.

[6] DIN 19683-16 Soil quality – Physical laboratory tests – Part 16: Determination of aggregate stability using the method of wet-sieving.

[7] Chenu C., Le Bissonnais, Y. & Arrouays, D. 2000. Organic matter influence on clay wettability and soil aggregate stability, Soil Sciences Society of America 64(4): 1479–1486.

[8] Ametzketa, E. 1999. Soil aggregate stability: a review. Journal of Sustainable Agriculture 14(2-3): 83-151.

[9] Dal Ferro, A., Berti, A., Francioso, O., Ferrari, E., Matthews, G. P. & Morari, F. 2012. Investigating the effects of wettability and pore size distribution on aggregate stability: the role of soil organic matter and the humic fraction, European Journal of Soil Science 63(2): 152–164.

[10] DIN 18130-1 1999. Baugrund, Untersuchung von Bodenproben. Bestimmung des Wasserdurchlässigkeitsbeiwerts. Teil 1: Laborversuche.

[11] Campbell D.J., Stafford, J.V. & Blackwell, P.S. 1980. The plastic limit, as determined by the drop-cone test, in relation to the mechanical behaviour of soil, Journal of Soil Science, 31, 11-24.

[12] ISO/TS 17892-12. Geotechnical investigation and testing – Laboratory testing of soil -- Part 12: Determination of Atterberg limits.

[13] Wang D.K., Zentar, R, Abriak, N.E. & Xu, W.Y. 2013. Shear Strength Behavior of Cement/ Lime-Solidified Dunkirk Sediments by Fall Cone Tests and Vane Shear Tests, Geotechnical Testing Journal 36(1), 155-162.

[14] Nagaraj H.B., Sridharan, A. & Mallikarjuna, H.M. 2012a. Re-examination of Undrained Strength at Atterberg Limits Water Contents, J. Geotech. Geoenviron. Eng. 30(4), 727-736.

[15] Haigh S.K., Vardanega, P.J. & Bolton, M.D. 2013. The plastic limit of clays, Géotechnique 63(6), 435-440.

[16] Nagaraj H.B., Sridharan, A. & Mallikarjuna, H.M. 2012b. Reply to the Discussion on „Re-examination of Undrained Strength at Atterberg Limits Water Contents", Geotech. Geol. Eng. 30(6), 1393-1395.

[17] Prakash K. & Sridharan, A. 2006. Critical appraisal of the cone penetration method of determining soil plasticity, Can. Geotech. J. 43(5):884–888.

[18] Feng T.W. 2004. Using a small ring and a fall-cone to determine the plastic limit, J. Geotech. Geoenviron. Eng. 130(6), 630-635.

[19] Wood D.M. & Wroth, C.P. 1978. The use of the cone penetrometer to determine the plastic limit of soils, Ground Engineering 11(3), 37.

[20] Lee L.T. & Freeman, R.B. 2009. Dual-Weight Cone Method for Simultaneous Liquid and Plastic Limit Determination, J. Geotech. Geoenviron. Eng. 134(1), 158-161.

[21] Lesch, S. 2012. Projekt DredgDikes - Ermittlung der Erosionsstabilität gegen Überströmen von begrüntem Baggergut in einer kleinmaßstäblichen Strömungsrinne. Diploma thesis Universität Rostock.

[22] Olschewski J., Cantré, S. & Saathoff, F. 2014. Overflowing Tests on the Rostock DredgDikes Research Dike, Proceedings, South Baltic Conference on Dredged Materials in Dike Construction (Eds. Saathoff, F. & Cantré, S.), 67-74. Universität Rostock.

[23] Cantré, S., Große, A.-K., Neumann, R., Nitschke, E., Henneberg, M. & Saathoff, F. 2013. Fine-grained organic dredged materials for dike cover layers : Material characterisation and experimental results. Proceedings WODCON XX World Dredging Congress and Exibition : 3-7 June 2013, Brussels: 1-14.

[24] Cantré, S., Saathoff, F., Große, A.-K. & Just, H. 2014. Two Research Dikes Made of Fine-Grained Organic Dredged Materials. Proceedings of the South Baltic Conference on New Technologies and Recent Technologies in Flood Protection. Gdansk: 1 - 8.

[25] NTPEP 2013. National Transportation Product Evaluation Program - Erosion Control products (ECP), Reports. Online: www.ntpep.org/Pages/ECP.aspx.

[26] ASTM D-6460 2008. Standard Test Method for Determination of Rolled Erosion Control Product (RECP) Performance in Protecting Earthen Channels from Stormwater-Induced Erosion. ASTM International. West Conshohocken, 2008. 9 pp.

[27] Neumann R. & Henneberg M. 2014. The Project DredgDikes: Characterization of chemical properties of the dredged material and first results on vegetation monitoring. South Baltic Conference on Dredged Materials in Dike Construction, 8 pp.

[28] EurOtop 2007. Wave Overtopping of Sea Defences and Related Structures: Assessment Manual, Boyens Medien GmbH & Co. KG, Heide i. Holstein, 178 p.

[29] Van der Meer, JW., Hardeman, B., Steendam, GJ., Schttrumpf, H. & Verheij H. 2010. Flow depths and velocities at crest and inner slope of a dike, in theory and with the Wave Overtopping Simulator, 30th Int. Conference on Coastal Engineering, 15 p.

[30] Moriasi, D.N., Arnold, J.G., Van liew, M.W., Bingner, R.L., Harmel, R.D. & Veith, T.L. 2007, Model Evaluation Guidlines for Systematic quantification of accurancy in watershed simulations, American Society of Agricultural and Biological Engineers.

[31] Kumar R., Naja, M., Pfister, G.G., Barth, M.C., Wiedinmyer, C. & Brasseur, G.P., 2012, Simulation over South Asia using the weather research and forecastung model with Chemistry (WRF-Chem): chemistry evaluation and initial results, Geoscientific Model development, 5.

[32] Naumann M., Bill R. & Niemeyer F. 2014. Untersuchungen zur Eignung von Unmanned Aerial Systems (UAS) zur Deformations-analyse von Deichbauwerken. Photogrammetrie, Laserscanning, optische 3D-Messtechnik, Beiträge der Oldenburger 3D-Tage 2014. Wichmann Berlin, Offenbach: 146 - 155.

[33] Naumann, M., Bill, R., Niemeyer, F. & Nitschke, E. 2014. Defor-mation Analysis of Dikes Using Unmanned Aerial Systems (UAS). Proceedings of the South Baltic Conference on dredged materials in dike construction: 119 – 126.

[34] Naumann, M. & Bill, R. 2014. Deformation analysis of a test dike. GIM International 2014: 22 – 25.

[35] Naumann, M., Bill, R. & Niemeyer, F. 2014. Generierung Digitaler Geländemodelle mittels Bilddaten von unbemannten Flugsyste-men zum Monitoring von Küstenschutzbauwerken. gis.Science. 2014(1): 30 – 37.

[36] Naumann, M.; Geist, M.; Bill, R.; Niemeyer, F. & Grenzdörffer, G. 2013: Accuracy comparison of digital surface models created by aerial systems imagery and terrestrial laser scanner. ISPRS - International Archives of the Photogrammetry, Remote Sensing and Spatial Information Sciences, XL-1/W2: 281 - 283. .

[37] Henneberg, M. 1992. Untersuchungen zur landwirtschaftlichen Nutzung von Schlickspülfeldern am Beispiel des Spülfeldes Radelsee Rostock, Doctoral Thesis, Universität Rostock, 116 pp..

[38] EAK 2002/2007. Empfehlungen für die Ausführung von Küsten-schutzwerken durch den Ausschuss für Küstenschutzwerke der Deutschen Gesellschaft für Geotechnik e.V. und der Hafenbau-technischen Gesellschaft e.V. [German recommendations for the design of coastal protection constructions], Westholsteinsche Verlagsanstalt Boyens & Co., Heide i. Holstein, 589 pp.

[39] ArcGIS. Geoinformation software. www.arcgis.com.

[40] DIN 52098:2005-06. Aggregates test methods - Determination of particle size distribution by wet sieving.

[41] ImageIron. Software zur automatischen Messung und Korrektur von Abbildungsfehlern in Digitalkameras.

[42] Chair of Geodesy and Geoinformatics, Universität Rostock – Aerial images.

[43] Zielinsky, M. 2014. ERT analysis on the DredgDikes research dike. Dr. Zielinsky performed the measurements in Sept. 2014 and provided the evaluation diagrams.

[44] Meyer, C. 2013. Projekt DredgDikes - Untersuchung von Sicker-vorgängen im Rostocker Versuchsdeich durch Feldversuche und numerische Berechnungen. M.Sc. thesis Universität Rostock.

[45] Jurisch, T. 2015. Auswertung von Durchsickerungsversuchen am DredgDikes-Versuchsdeich durch inverse Modellierung mit FeFlow. M.Sc. thesis, Universität Rostock.

[46] Bałachowski, L; Sikora, Z. 2013. Mechanical properties of fly ash - dredged material mixtures on laboratory test, Studia Geotechnica et Mechanica, Vol. XXXV, No. 3, 2013.

[47] The ordinance of the Minister of Environment of 9th September 2002 on soil quality standards. (Journal of Laws 2002 No. 165 item 1359)

[48] Slide 5.0 software. Online: www.rocscience.com.

[49] CIRIA 2013. International Levee Handbook, Report C731, Online: www.ciria.org.

[50] Plaxis 8.2 manual. Geotechnical FEM analysis software. Online: www.plaxis.nl.

[51] Smith, C.C. & Gilbert, M. 2007. Application of discontinuity layout optimization to plane plasticity problems. Proceedings of the Royal Society A: Mathematical, Physical and Engineering Sciences, 463 (2086): 2461-2484.

[52] LimitState 3.0 manual. www.limitstate.com/geo.

[53] WastraPlan 2010. Study on the reconstruction of the Körkwitzer Bach.

[54] Morscheck, G., Lemke, A. & Henneberg, M. 2014. Matured dredged material as restoration substrate in landfill surface sealing systems. Proceedings of the South Baltic Conference on Dredged Materials in Dike Construction, Rostock: 155-162.

[55] Neumann, R. & Henneberg, M. 2014. Environmental and vegeta-tion assessment report, DredgDikes component 4. Project report, 33 p. Online: www.dredgdikes.eu.